The Thesis Committee for Sungmoon Hwang
Certifies that this is the approved version of the following thesis:

Experimental Investigation of Near-Field Effects on the SASW Dispersion Curve

APPROVED BY
SUPERVISING COMMITTEE:

Supervisor:

Kenneth H. Stokoe II

Brady R Cox

Experimental Investigation of Near-Field Effects on the SASW Dispersion Curve

by

Sungmoon Hwang, B.S.

THESIS

Presented to the Faculty of the Graduate School of

The University of Texas at Austin

in Partial Fulfillment

of the Requirements

for the Degree of

MASTER OF SCIENCE IN ENGINEERING

The University of Texas at Austin

August, 2014

Abstract

Experimental Investigation of Near-Field Effects on the SASW Dispersion Curve

Sungmoon Hwang, M.S.E.

The University of Texas at Austin, 2014

Supervisor: Kenneth H. Stokoe II

When any method of surface wave testing that involves Rayleigh waves is performed, one important assumption is that plane Rayleigh waves are being measured. In the forward modeling or inversion procedure that is used to analyze the field dispersion curve to determine the field V_s profile, the analysis is based on the wave field consisting of plane Rayleigh waves. Therefore, field dispersion curves that contain near-field data could adversely distort the field V_s profile. To minimize the influence of near-field effects, several criteria have been recommended in the past. However, most of the criteria were based on empirical equations that implicitly assumed zones of influence, or numerical simulations. There is a lack of experimental investigation, particularly full-scale field investigations. Even, the numerical solutions have been based on simple soil profiles without significant velocity contrasts between soil layers and/or varying thicknesses of soil layers which can significantly influence near-field effects. Data from full-scale field test using the Spectral-Analysis-of-Surface-Waves (SASW) method was used in this thesis research. SASW tests performed at two stages in the construction of a deep, 90-ft thick

backfill were studied. The V_s profiles were normally dispersive, with a substantial increase in the velocity of the layer beneath the backfill. The study shows the adverse distortions that can occur in the field dispersion curve from near-field effects when the spacing of the receiver pair is: (1) above the zone of rapidly increasing V_s near the surface and (2) less than the depth to the stiffer layer in deeper measurements. Other factors that affect the results are discussed and recommendations are presented to minimize the introduction of near-field effects, at least in these relatively simple V_s profiles.

TABLE OF CONTENTS

List of Tables

List of Figures

CHAPTER 1 : INTRODUCTION

1.1 BACKGROUND

Plane Rayleigh wave motion, in the fundamental and higher modes, is an important assumption in the Spectral-Analysis-of-Surface-Waves (SASW) method. This assumption of plane wave motion is valid when the active seismic source is located far enough from each receiver pair used in field testing. In this case, typically called far-field case, the cylindrical wavefront near the source is well approximated by a plane wavefront. Much of the body wave energy is dissipated since body waves attenuate faster with distance than the Rayleigh wave and the additional near-field wave energy has also been highly attenuated (Aki and Richards, 1980). However, sometimes the active sources are closer than desired to the receiver pair, resulting in two issues for the measurements; (1) cylindrically propagating waves and additional near-field energy and (2) significant body wave energy (Zywicki 1999). The area where the body waves and the cylindrical wavefront impact the measurement is called the near-field, and the effects cause by the invalid assumption is called near-field effects (Yoon and Rix 2009).

Extensive research was conducted (Heisey et al. (1982); Sanchez-Salineero et al. (1987), Roesset et al. (1990), Hiltunen and Woods (1990), Gucunski and Woods (1992), and Al-Hunaidi (1993)), but the most of them were established on numerical simulation with lack of experimental data. Even the numerical solution was based on simple soil profiles which did not have large velocity contrasts between soil layers and varying thicknesses in the soil layers. To minimize the near-field effects, several recommendations for filtering criteria have been proposed as listed in the Table 1.1

(Yoon and Rix 2009). As seen in the Table 1.1, the recommendations differ from each other, probably due to different site conditions (shear wave velocity profiles). And only Hiltunen and Woods (1990) recommendation was based on experimental data.

Table 1.1 Summary of Filtering Criteria for Near-Field Effects in the SASW Method (Yoon and Rix, 2009)

Reference	Filtering criterion	Receiver configuration	Method of study
Heisey et al. (1982)	$x_1/\lambda_R > 1/3$	$\Delta x/x_1 = 1$	Numerical
Sánchez-Salinero et al. (1987)	$x_1/\lambda_R > 2^a$	$\Delta x/x_1 = 1$	Numerical
Roesset et al. (1990)	$x_1/\lambda_R > 1/2$	$\Delta x/x_1 = 0.2-2$	Numerical
Hiltunen and Woods (1990)	$x_1/\lambda_R > 1/2$	$\Delta x/x_1 = 1$	Experimental
Gucunski and Woods (1992)	$x_1/\lambda_R > 1$	$\Delta x/x_1 = 1$	Numerical
Al-Hunaidi (1993)	N/A	$\Delta x/x_1 = 1$	Numerical

Hiltuene and Woods (1990) investigated the near-field effect using experimental testing to find appropriate filtering criteria. The test was performed on the pavement on the G. G Brown parking lot (asphaltic concrete pavement site) with constant ratio of X (receiver spacing) to L_R(Rayleigh wavelength) as the ratio of S (source-to-near-receiver distance) to X changes from 0.5 to 3.0, trying to find the X/ L_R value when all values of S/X became nearly the same. As the value of X/ L_R became larger, the probability of measuring plane Rayleigh wave motion without near-field effects increases. The result of these tests is shown in Figures 1.1 and 1.2 (Hiltunen and Woods 1990).

As shown in the Figures 1.1 and 1.2, as wavelengths (L_R) become longer than 5 ft, the plane velocity became independent of the S/X value, indicating there are no significant near-field effects contaminating the measurement.

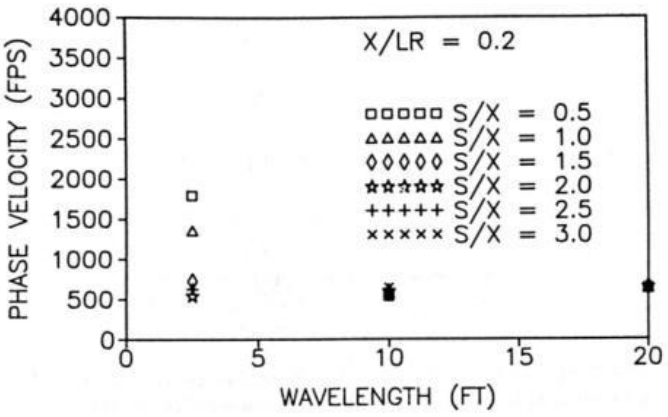

Figure 1.1 Experimental Dispersion Curves for X/ L_R = 0.2 at G.G Brown Parking Lot Site (Hiltunen and Woods,1990)

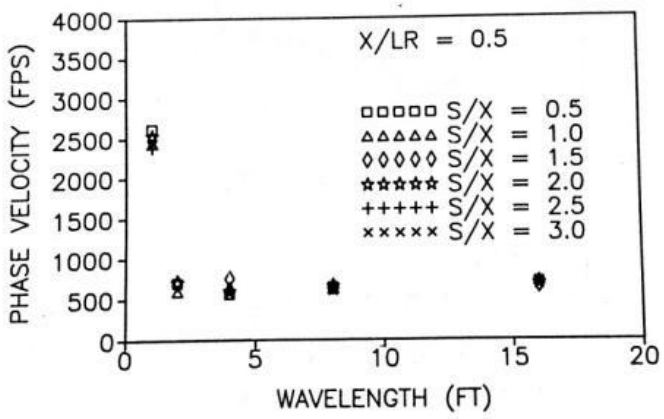

Figure 1.2 Experimental Dispersion Curves for X/ L_R = 0.5 at G.G Brown Parking Lot Site (Hiltunen and Woods, 1990)

On the other hand, for wavelengths less than 5 ft, the phase velocity depends on the S/X value. When the X/ L_R was 0.2, only the shallow layers were influenced by near-field effects (Hiltunen and Woods 1990). However, this conclusion was made with few comparisons. Therefore, more, longer-wavelength data are required to investigate near-field effects in terms of typical SASW arrays.

1.2 OBJECTIVES OF THIS RESEARCH

A significant amount of field SASW testing has been performed by personnel associated with the Geotechnical Engineering Center (GEC) at the University of Texas. AS part of this thesis, the writer has participated in multiple SASW field projects. The overall object of the thesis research is to select and analyze field data for comprehensive sets of SASW tests at one or more "simple" sites, where the soil conditions are well documented. The comprehensive sets of SASW measurements performed at the Vogtle Electric Generating Plant Project (2010) was selected. The project was selected because of the two, 90-ft thick sandy backfills were placed. This backfill represent excellent soil profiles. Four sets of SASW tests were performed at Vogtle Electric Generating Plant (VEGP) Project during construction of the backfill at different stages. The four sets of SASW tests were conducted when the backfill was about 25-, 45-, 73- and 90-ft thick. In each sets, the backfill represented a normally dispersive soil profile, where the stiffness of the silty sand layer increased with depth (Figure 1.3a). Below the depth of the backfill, the Blue Bluff Marl (a stiff material) was located which also represented a significant (times two) velocity contrast in the V_s profile (Figure 1.3b). SASW data from Stage 1 (25-ft thick fill) and Stage 2 (45-ft thick fill) are used to evaluate the near-field effects.

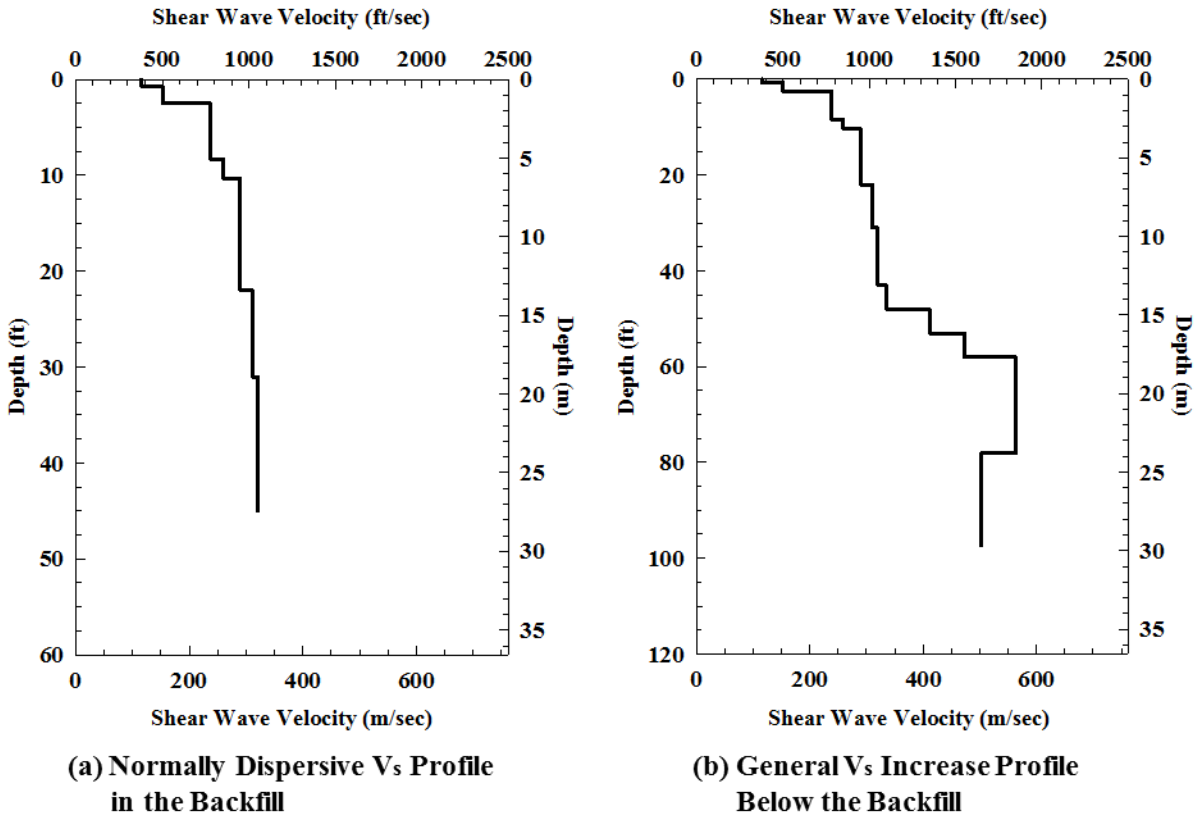

Figure 1.3 Representative V_s Profile for Vogtle Electric Generating Plant Project Site at Array 3A (Stage 2) : (a) in the Backfill only and (b) Including Material Below the Backfill

1.3 ORGANIZATION OF THE TEHSIS

Chapter 2 presents a general procedure of SASW testing method used in the field. Chapter 3 is a discussion of procedure to analyze the near-field effects on the field dispersion curve including the masking procedures used to create the cases of reference field dispersion curves and comparison between the reference average phase velocity and the phase velocity calculate with assumed near-field data. Chapter 4 presents the description of the VEGP site and analysis of Stage 1 (25-ft thick backfill) SASW data in

terms of the near-field effects. Chapter 5 presents the analysis of Stage 2 (45-ft thick backfill) SASW in terms of near-field effects. Chapter 6 contains the conclusions and recommendations. The Appendix A includes the all case dispersion curve of Stage 1 and Appendix B includes the all case dispersion curve of Stage 2.

CHAPTER 2 : DISCUSSION OF THE GENERAL SASW TESTING METHOD

2.1 INTRODUCTION

The Spectral-Analysis-of-Surface-Waves (SASW) method is a nondestructive and nonintrusive seismic testing method that is based on the dispersive characteristic of Rayleigh waves. Rayleigh waves are one type of surface waves that propagate along a solid-air interface. The dispersive characteristic is generally referred to simply as dispersion. This phenomenon arises when Rayleigh waves propagate through a multi-layered system with varying stiffnesses (Figure 2.1a). Different wavelengths (or frequencies) of Rayleigh waves stress (or load) different layers of varying stiffness. Shorter-wavelength (higher frequency) waves travel near-surface layers and sample the properties of shallow layers (Figure 2.1b). Longer-wavelength (lower-frequency) waves travel through near-surface and deeper layers so these waves sample a combination of shallower and deeper layers (Figure 2.1c). Therefore, by generating Rayleigh waves with a wide range in wavelengths, the shear wave velocity of the each layer can be evaluated using the proper modeling procedure.

The SASW method measures the vertical motion of Rayleigh waves by using vertical geophones. Rayleigh waves (R-waves) attenuate proportional to $1/\sqrt{r}$ (r stand for the radial distance from the wavefront to the surface source location) while body waves (compression and shear waves) attenuate proportional to $1/r^2$. Also, the vertical excitation at the ground surface generates a majority of the energy in Rayleigh waves. These two positive features (low attenuation and a majority of the energy) make Rayleigh waves

very useful in seismic testing. In other words, as the wave propagates further from the source, more energy for Rayleigh waves measurements will be sustained compared to body wave measurements. The general testing configuration in the SASW method is illustrated in Figure 2.2. In the figure, only two receivers that one receiver pair are shown. However in field testing, 3 or more receivers are used to create multiple pairs of receivers for efficiency. In each receiver pair, the distance from source to first receiver is kept equal to the distance between the two receivers in the pair. A wide range in receiver spacings is used in the field to measure a wide range in Rayleigh wavelengths.

The phase velocity at each frequency in the Rayleigh waveform is calculated by :

$$V_R = f \times \frac{360^\circ}{\emptyset} \times d \qquad (1)$$

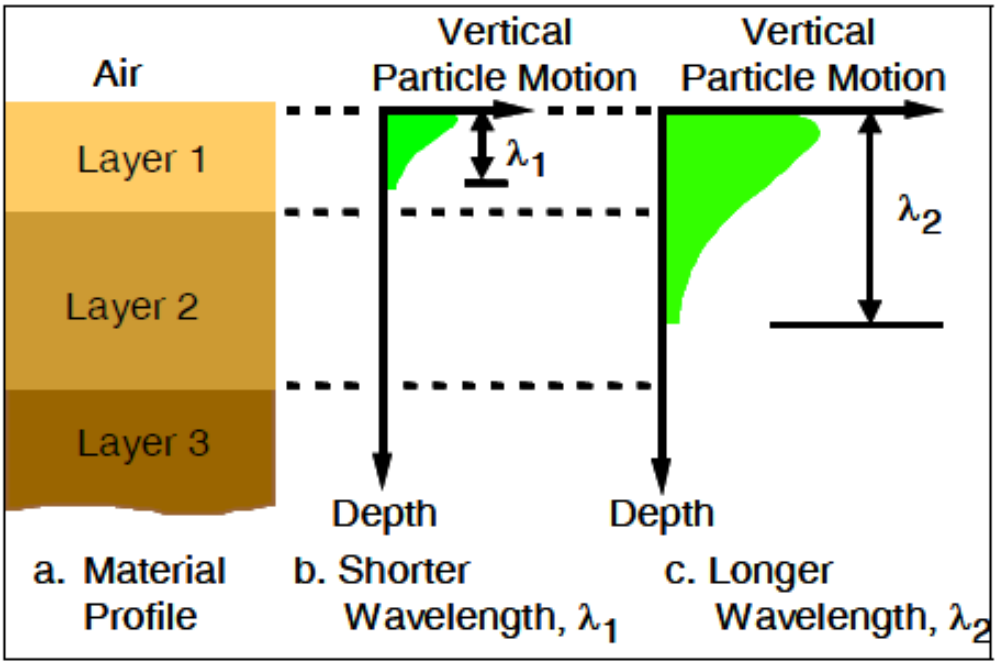

Figure 2.1 Illustration of Surface Waves with Different Wavelengths Sampling Different Materials in a Layer System (from Stokoe et al, 2005)

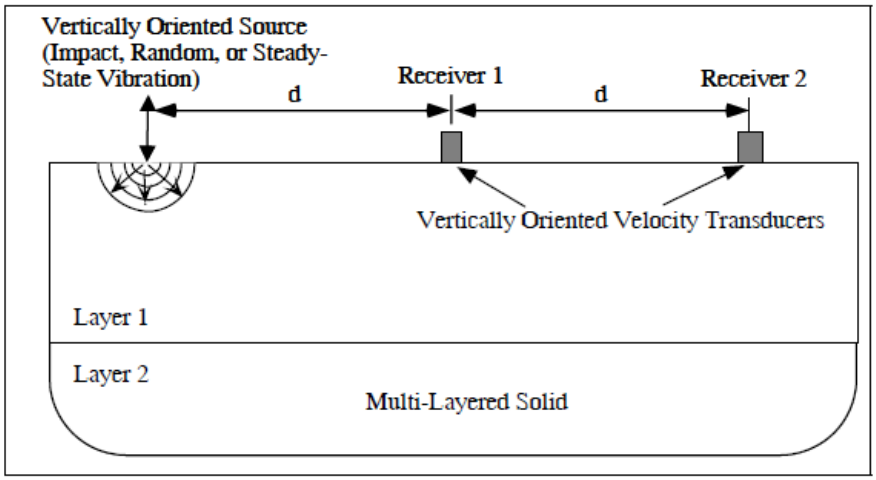

Figure 2.2 Schematic Diagram of the Generalized Equipment Arrangement Used in SASW Testing with One Receiver Pair (from Stokoe et al, 2005)

where V_R represents for Rayleigh phase velocity in ft/sec (or m/sec), f represents for frequency in Hertz, ∅ represents the phase difference in degrees (at frequency f), and d stands for distance (in ft or m) between receivers (Stokoe, et al 2005). Equation 1 is simply the frequency (f) times wavelength (λ) or it can be derived from dividing the distance by travel time. Phase differences between recorded waves at two locations make it possible to calculate the wavelength or the travel time of a wave with a single frequency. If the wave with a frequency of f_0 propagates from location A to B and the travel time is t_1, the wave motion at locations A (y1) and B (y2) can be expressed by the following (Joh, 1996):

$$y_1 = \sin(2\pi f_0 t) \quad (2a)$$

$$y_2 = \sin[2\pi f_0 (t - t_1)] \quad (2b)$$

$$y_2 = \sin[2\pi f_0 t - 2\pi f_0 t_1] \quad (2c)$$

$$y_2 = \sin[2\pi f_0 t - \emptyset] \tag{2d}$$

For Equation 2d, the relation between $\emptyset$ (phase difference between the two locations) and travel time can be express as

$$\emptyset = 2\pi f_0 t_1 \tag{3}$$

that is,

$$t_1 = \frac{\emptyset}{2\pi f_0} \tag{4}$$

Therefore, phase velocity associated with the frequency, f_0 can be expressed as the following:

$$V_R = \frac{d}{t_1} \tag{5a}$$

$$V_R = \frac{2\pi f_0}{\emptyset} \times d \tag{5b}$$

$$V_R = f \times \frac{360^\circ}{\emptyset} \times d \tag{5c}$$

$$V_R = f \times \lambda \tag{5d}$$

Figure 2.3 is an illustration of this concept.

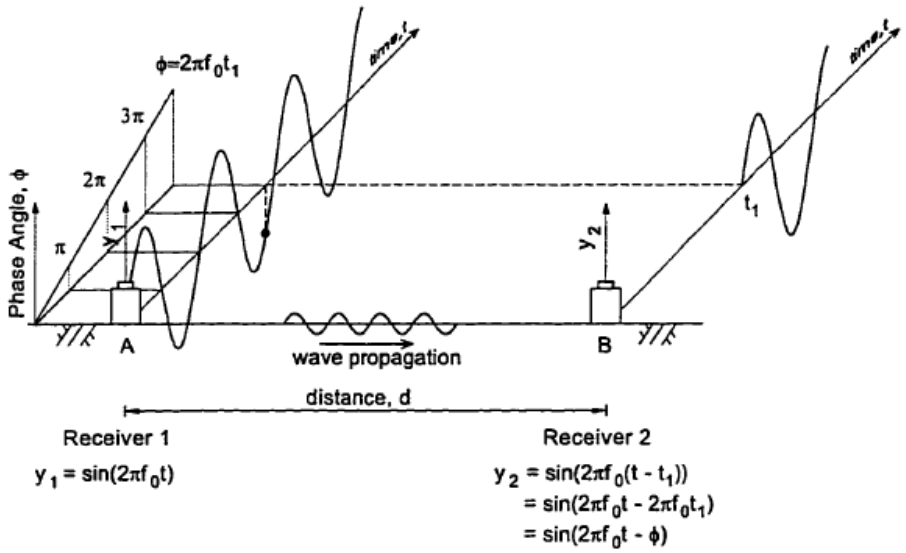

Figure 2.3 Phase Difference between Two Signals with the Same Frequency (Joh, 1996)

Phase velocity, V_R or V_{ph} is calculated from Equation 5c and plotted in terms of wavelength (λ) versus phase velocity (V_R or V_{ph}). This relationship is determined over a wide range in wavelengths and is called a dispersion curve. The dispersion curve is generated from every receiver spacing (d), and is called an individual compression curve discussed in Section 2.3 and 2.4. All individual dispersion curves from one site investigation are plotted together to form a composite dispersion as discussed in Section 2.4. The individual dispersion curves typically overlap for adjacent receiver spacings and combine into the composite dispersion curve called the experimental or field dispersion curve as discussed in Section 2.4. After generating the experimental dispersion curve, a theoretical dispersion curve which most closely matches the experimental dispersion curve is created through an iterative forward modeling procedure (Stokoe, et al 2005). The V_s profile of the theoretical dispersion curve which most closely matches the field dispersion curve is presented as the V_s profile of the site. More details about this procedure can be found in Section 2.4.

2.2 SASW PROCEDURE

In this research, the SASW procedure that is outlined above was used. To demonstrate the procedure, photographs and phase plots from one site of the Los Angeles Silver Lake Replacement Project are presented as an example, which had the most complete set of photographs. In this case, the SASW array used three receivers at each source location to reduce the testing time compared with only one receiver pair. This arrangement enables two receiver pairs to be measured, with source-to-near-receiver distance in each receiver pair equal to the receiver-to-receiver distance in the pair. The

basic array configuration is presented in Figure 2.4 (Geotechnical Engineering Report GR09-13).

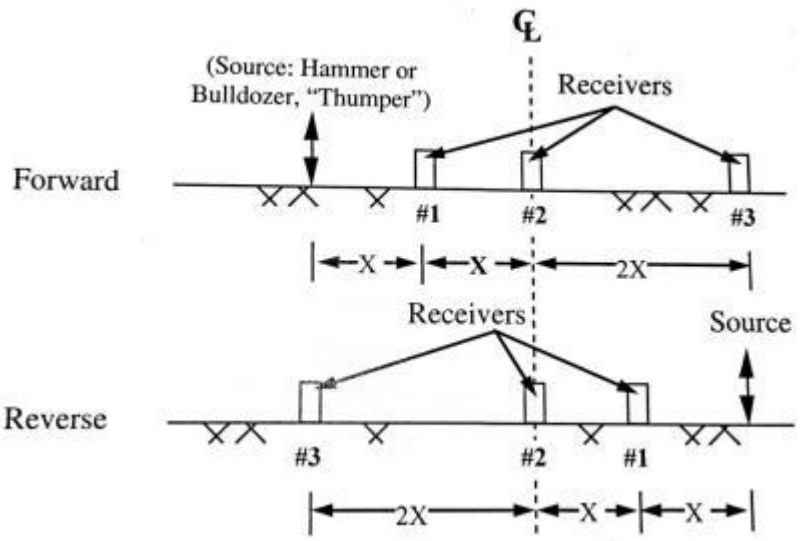

Figure 2.4 Typical Source and Receiver Spacings Used in SASW Testing and Used at the Silver Lake Project (from Stokoe et al, 2005)

Receiver spacings can vary between projects. The appropriate spacings depend on the clearness and completeness of the individual phase plots and the maximum profiling depth. The judgements on receiver spacings are often made in the field. For this project, the general spacings were: 3, 6, 12.5, 25, 50, 75, 100 and 150-ft. Using an appropriate frequency range for each spacing so that measurements two or more cycles of phase shift are made, reliable experimental dispersion curve can be constructed due to extensive overlapping. For the shorter wavelength measurements, spacings of 3- and 6-ft spacing were generally used in this project. A hand-held hammer was used for an impact source at theses short spacings as shown in Figure 2.5. For the longer wavelength measurements,

a Caterpillar D8R Bulldozer was used as an active source. Figure 2.6 shows the longest receiver array and the bulldozer location.

Figure 2.5 Photograph of Using Hammer Source at Silver Lake Project, Los Angeles, CA

Figure 2.6 Photograph of Longest Receiver Spacing (150-ft) at the Silver Lake Project and Location of Caterpillar D8R Bulldozer in SASW Testing

One-Hz vertical geophones, also called vertical velocity transducers (Mark Products L4, Serial Number (1085, 1079, 1091), were used as receivers. There are three important requirements for the seismic receiver. First, the receiver should have significant output over the frequency range required at the test site. Second, the phase difference between receivers should be within certain limits, often taken as less than 7.2 degrees, or 2% of one cycle (360 degrees). Mark Products L4 vertical geophones have outputs in excess of 10 volts/(in./sec) and phase differences between receivers over the useable frequency range are less than 6 degrees which fulfill these requirements. Third, temperatures of the geophone surface should be lower than about 95ºF so that the geophone performance is not adversely affected. In Figure 2.7, a 1-Hz geophone is being leveled on the ground surface. The phase difference between the three receivers used in this work is shown in Figure 2.8, using Geophone 1085 as the reference geophone (the middle geophone in the two pairs of geophone).

Figure 2.7 Photograph of 1-Hz Vertical Geophone being Plumbed

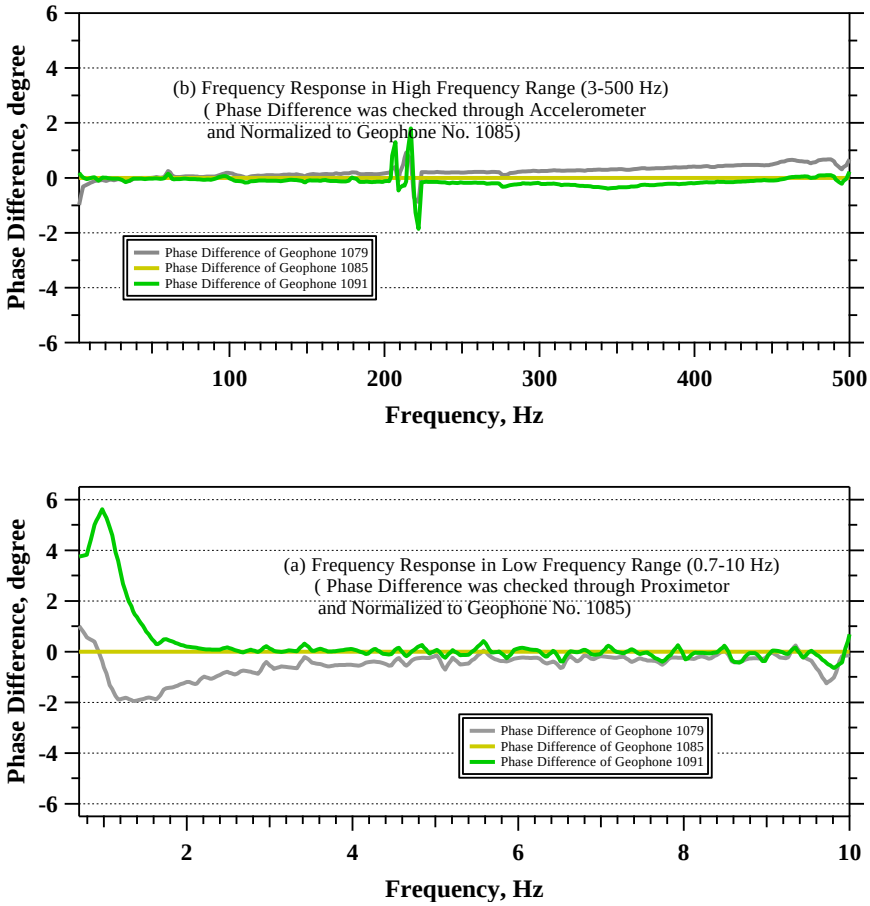

Figure 2.8 Phase Difference between Mark Products L4 Geophones 1079, 1085 and 1091 in the Low-Frequency Range (0.7-10Hz) and the High-Frequency Range (3-500Hz) ; Note : Geophone 1085 is used as the Reference Geophone

A 4-Channel Quattro Dynamic Signal Analyzer was used in this work to record the seismic signals and perform spectral analyses of each receiver pair. A photograph of the Quattro Analyzer is presented in Figure 2.9. Three channels were used to record the outputs from the three geophones. To measure the phase difference between geophone pairs, the transfer function was calculated and presented on the frequency versus phase plot to review the data during field collection. In the case of a random-noise source like the bulldozer and hammer, a wide range of frequencies is generated at the same time. On

the other hand, if a vibroseis is used as the source, frequencies are controlled by the Quattro Analyzer in a stepped-sine mode (from high to low frequencies).

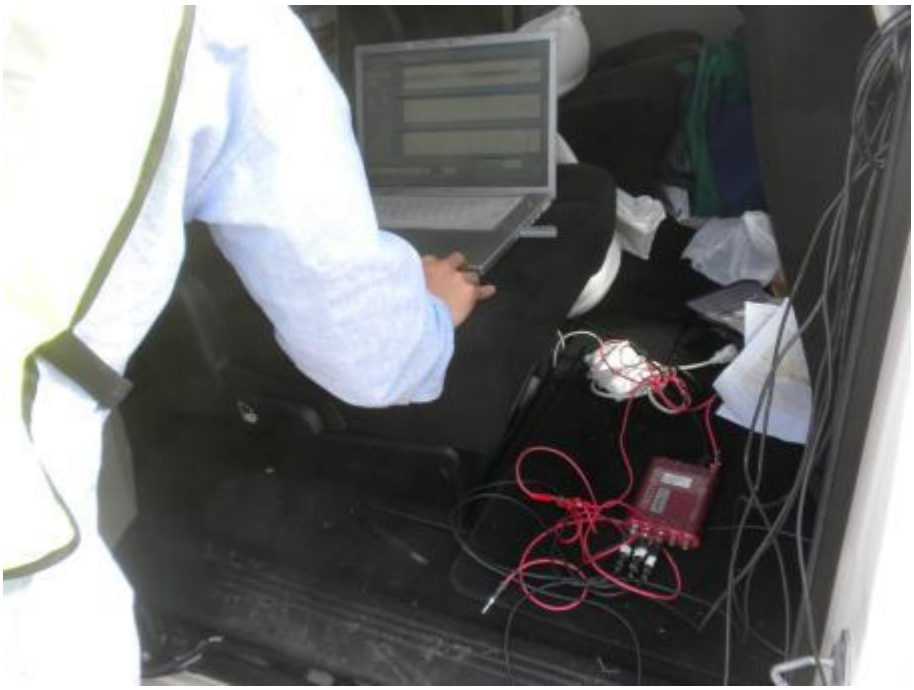

Figure 2.9 Photograph of Quattro and Lap-top Computer Data Recording System Used in the Silver Lake Project, LA.

2.3 SPECTRAL CALCULATIONS FOR EACH RECEIVER PAIR

The output voltage of the pair of receiver geophones are measured in the time-domain (x(t) and y(t)) and are then transformed into the Laplace form (X(s) and Y(s)) as illustrated in Equations 1 and 2. The Equation 3 is then used to calculate the transfer function H(s) as:

$$\mathrm{X(s)} = \mathcal{L}\{\mathrm{x(t)}\} \stackrel{\text{def}}{=} \int_{-\infty}^{\infty} x(t)e^{-st}dt \qquad (1)$$

$$\mathrm{Y(s)} = \mathcal{L}\{\mathrm{x(t)}\} \stackrel{\text{def}}{=} \int_{-\infty}^{\infty} y(t)e^{-st}dt \quad (2)$$

$$\mathrm{H(s)} = \frac{Y(s)}{X(s)} \quad (3)$$

In a linear time-invariant system, the input frequency ω has not changed, only the amplitude and phase angle of the sinusoid has been changed by the layered system. This change for every frequency ω is described by the frequency response, $H(j\omega)$. The phase difference between two receivers is $\emptyset(\omega)$ (Geotechnical Engineering Report GR09-13) and is expressed as:

$$\mathrm{G}(\omega) = \frac{|Y|}{|X|} = |H(j\omega)| \quad (4)$$

$$\emptyset(\omega) = \arg(Y) - \arg(X) = \arg(H(j\omega)) \quad (5)$$

The phase difference calculated from the transfer function is the key spectral quantity evaluated in the SASW testing. Phase velocity is then calculated from the phase difference versus frequency plot during the test or at a later tune. The unwrapped and wrapped phase spectra from the 100-ft spacing at Array 9 (Silver Lake Project) are presented in Figures 2.10a and 2.10b, respectively.

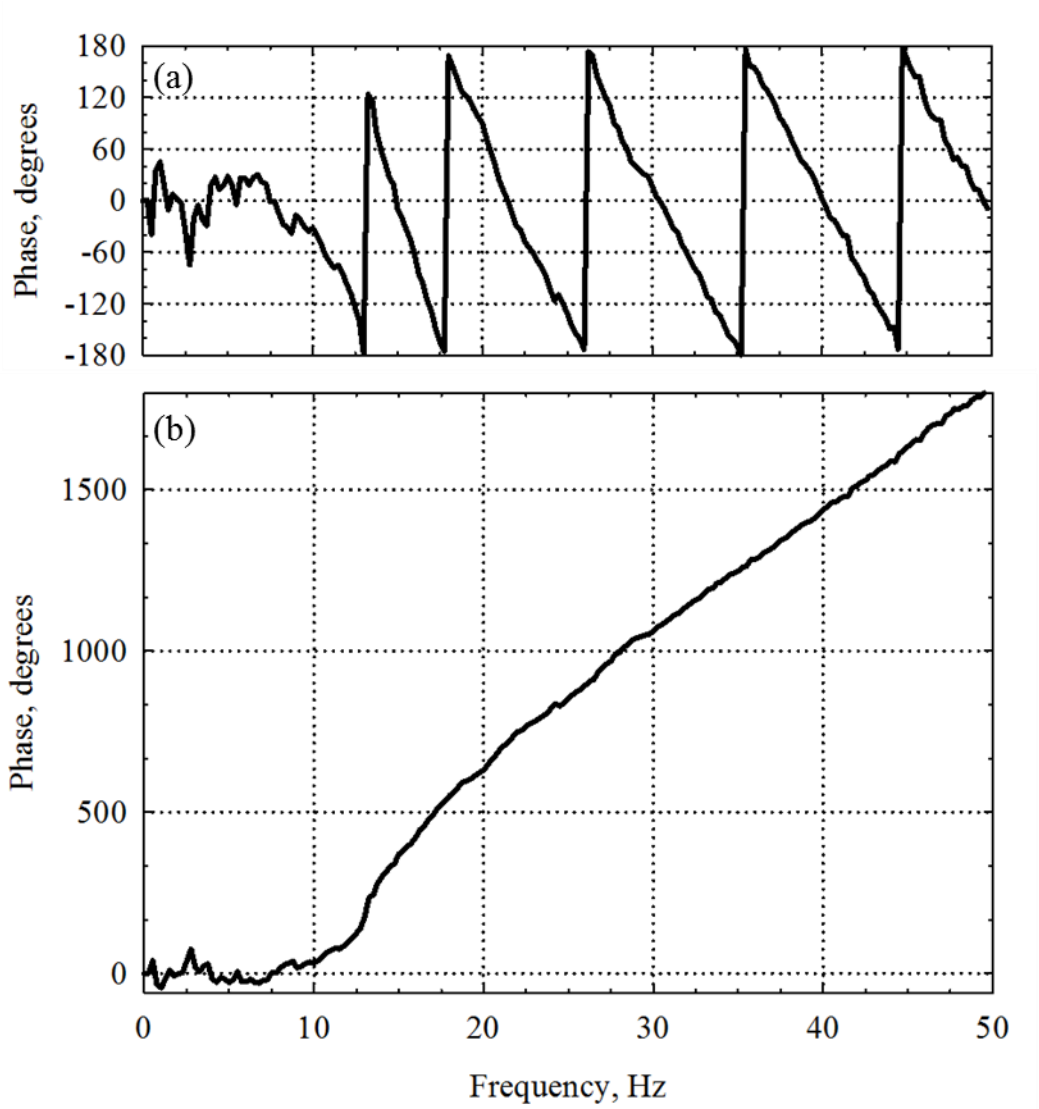

Figure 2.10 Wrapped (a) and Unwrapped (b) Phase Difference of the Transfer Function Measured at Array 9 (Silver Lake Project) with a 100-ft Spacing

2.4 DEVELOPMENT OF EXPERIMENAL DISPERSION CURVES

The collected field data for each receiver part is in the form of a phase difference versus frequency plot. These data for all receiver pairs are imported to the program

WinSASW, developed by Prof. Sung Ho Joh (1996). WinSASW enables the user to manually mask out the portion of the data with poor signal quality or the portion of the data that is suspected of being contaminated by the near-field effects. With the masking information, the WinSASW program unwraps the phase plot and the individual dispersion curve is calculated for each receiver pair. The masking procedure to eliminate the near-field effects at the Silver Lake Array 9 with 100-ft receiver spacing is shown in Figure 2.11. In this example, points #1 and #2 in Figure 2.12 represent one (360°) and half of (720°) wavelength between receivers, respectively. The frequency correspond with the points are 14.9Hz and 21.4 Hz. Therefore, by using Equation 1, the phase velocities associated with points #1 and #2 are 1490 and 1075 ft/sec, respectively. The complete individual dispersion curve calculated from the unmasked portion of the wrapped phase in Figure 2.11 is shown in Figure 2.12 with all five points in the wrapped phase identified in the dispersion curve.

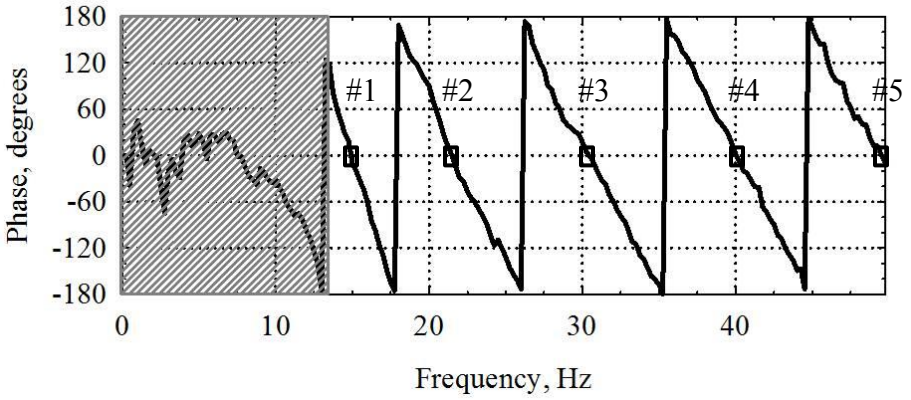

Figure 2.11 Masking Procedure Used to Eliminate the Near-field Effects; Unwrapped Phase Difference of the Transfer Function Determined at Array 9 (Silver Lake Project) with a 100-ft Receiver Spacing

This process is repeated through all pairs of receivers spacing creating the field dispersion curve for Array 9. All receiver pairs and the masking procedure are shown in Figures 2.13 and 2.14 and the resulting field dispersion is shown in Figure 2.15.

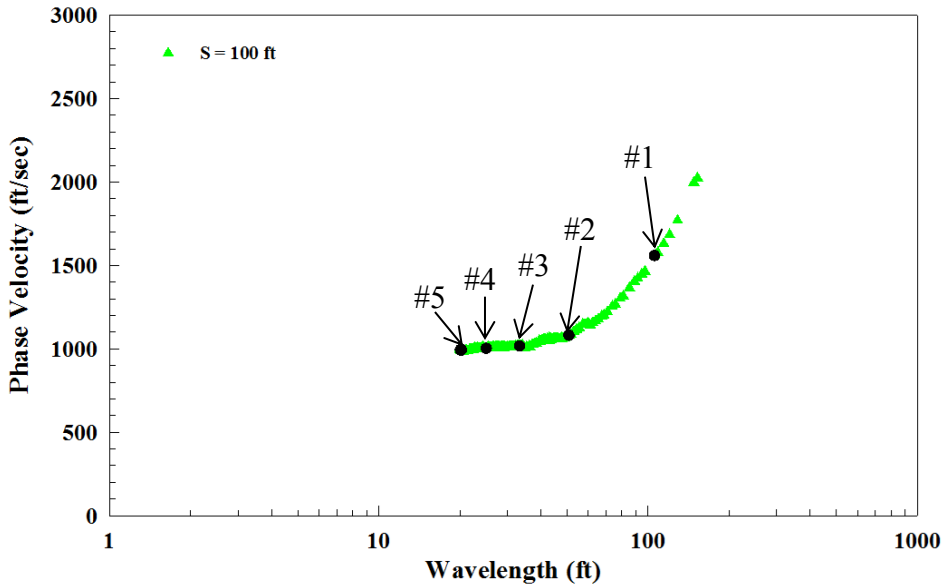

Figure 2.12 Individual Field Dispersion Curve from Unwrapped Phase Record Shown in Figure 2.11 Measured at Array 9 (Silver Lake Project) with a 100-ft Receiver Spacing

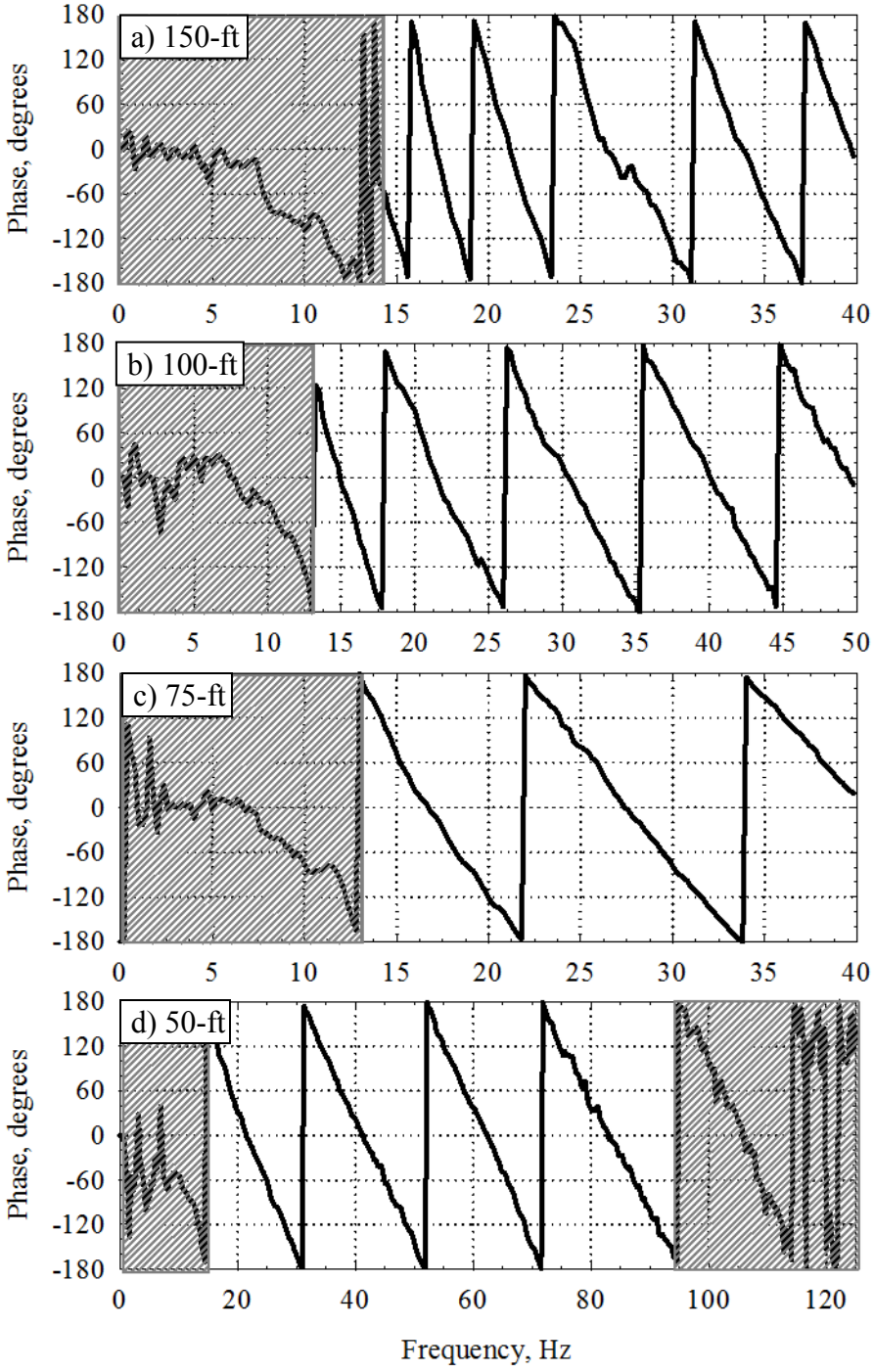

Figure 2.13 Masking Procedure to Eliminate the Near-field Effects; Unwrapped Phase Difference of the Transfer Function at Array 9 for Receiver Spacings of 150, 100, 75 and 50-ft (Silver Lake Project)

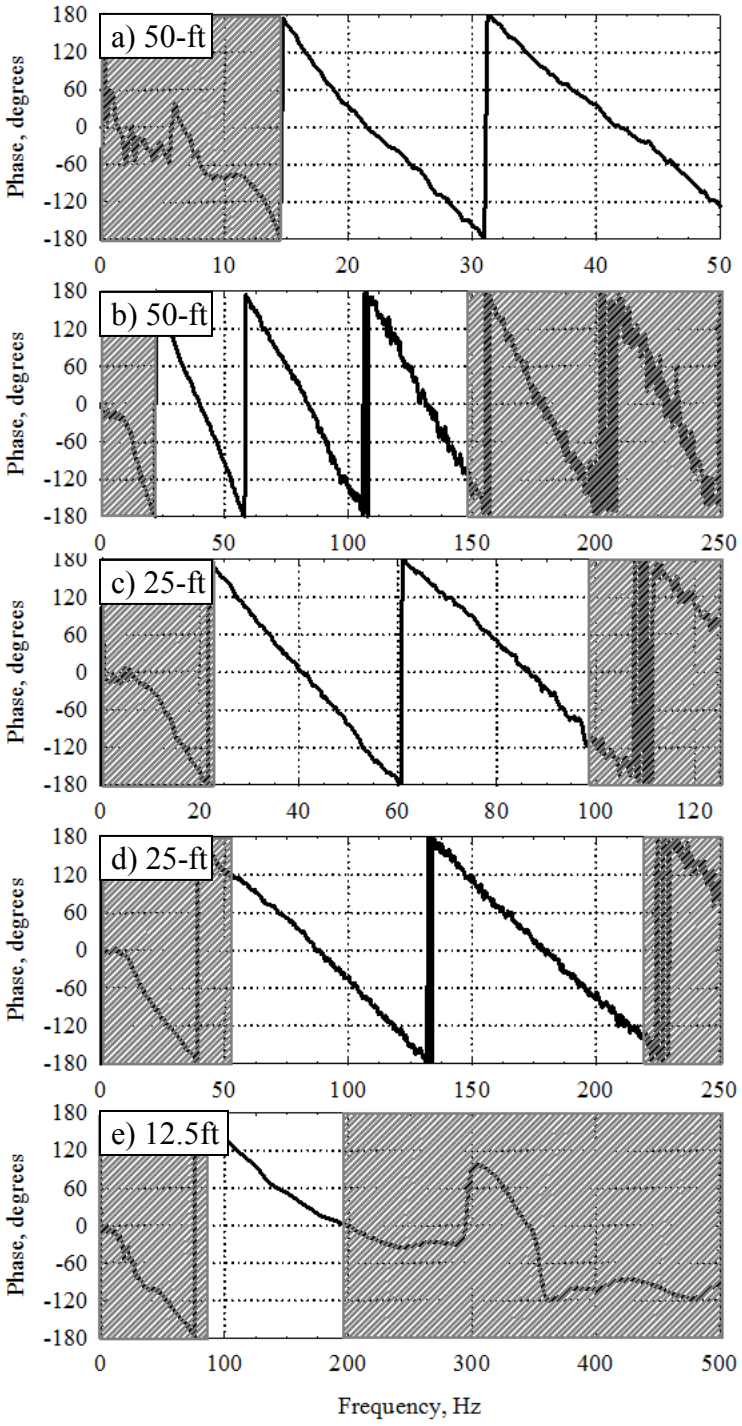

Figure 2.14 Masking Procedure to Eliminate the Near-field Effects; Unwrapped Phase Difference of the Transfer Function at Array 9 for Receiver Spacings of 50, 25, 12.5 and 6-ft (Silver Lake Project)

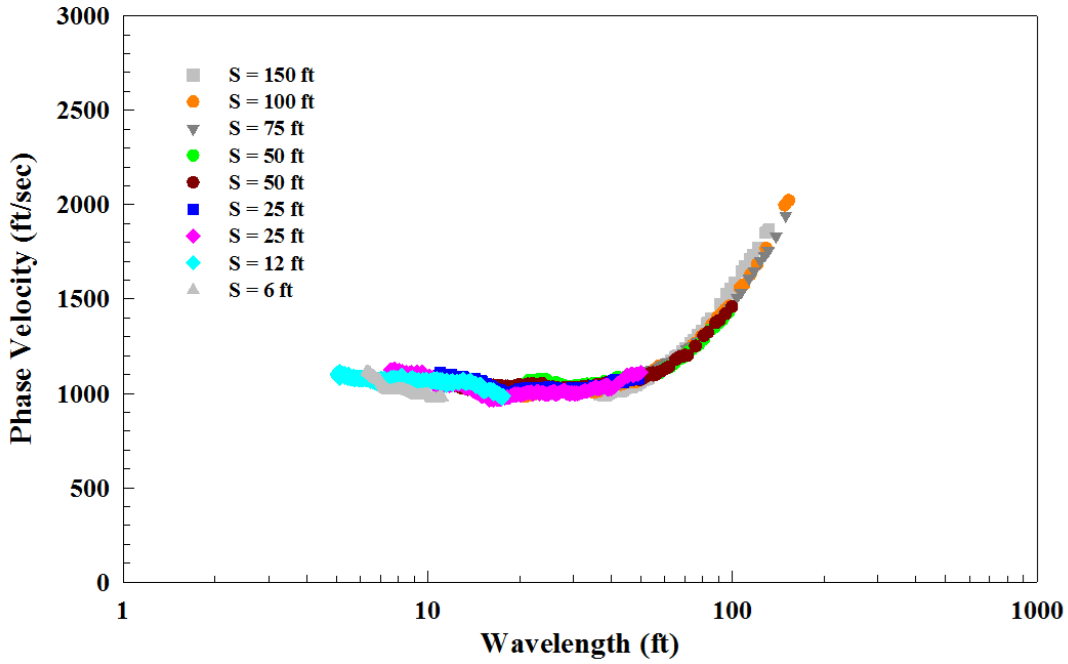

Figure 2.15 Field Dispersion Curve Generated from Wrapped Phase Data of All Receiver Spacings at Array 9(Silver Lake Project)

After creating the field (experimental) dispersion curve, a theoretical dispersion curve is generated using the WinSASW program in a forward modeling mode. The WinSASW program employs the dynamic stiffness method and formulation for the response of a horizontally layered system developed by Professor Jose Roesset to generate a theoretical dispersion curve for a given shear wave velocity profile (Kausel and Roesset, 1981). The theoretical dispersion curve is generated by assuming either the surface wave as a plane wave (2D solution) or as a superposition of muliple modes resulting from the combination of surface waves and body waves (3D solution) (Foinquinos, 1991, and Roesset et al, 1991). In the case of SASW testing, the 3D solution is always employed for a more accurate result. For this approach, several parameters

should be provided, including the assumed Poisson's ratio, assumed total unit weight, and initial shear wave velocity.

Poisson's ratio above the water table is assumed based on the initial shear wave velocity and the type of material (soil vs rock). In the range of shear wave velocity (V_s) between 200 and 2000 ft/sec, Poisson's ratio is usually taken to be between 0.30 and 0.33. Greater than 2000 ft/sec, Poisson's ratio is often taken to be between 0.25 and 0.30. These values are reasonable for the unsaturated soil above the water table. Below the water table, the Poisson's ration is calculated by the relationship between V_p and V_s, with the assumption that V_p is in the range of 5000 to 6000 ft/sec.

The unit weight of the soil is also assumed based on shear wave velocity. In the range of shear wave velocity between 200 and 2000 ft/sec, unit weight of soil is assumed to be 110 pcf above the water table and 130 pcf below the water table. For the Vs value greater than 2000 ft/sec and below the water table, the unit weight is assumed to be 135 pcf, however, according to the Stokoe et al, 2005, difference in unit weights of the soil with depth affect the dispersion curve, but it has small to insignificant effects on the final shear wave velocity profile.

The initial guess of the shear wave velocity profile is determined from the field dispersion curve. Based on the initial shear wave velocity, the theoretical dispersion curve is generated and compared with the experimental dispersion curve. The fitting is always acceptable based on the RMS value, and another theoretical dispersion curve is generated from the initial shear wave velocity. This trial and error procedure, called iterative forward modeling, is continued until an acceptable fit to the field dispersion curve is achieved. The parameters used in the forward modeling of the field dispersion curve shown in Figure 2.15 are listed in Table 2.1. The comparison between the final

theoretical dispersion curve and the field dispersion curve is shown in Figure 2.16. The final V_s profile for Site 9 is shown in Figure 2.17.

Thickness	P-Wave Vel	S-Wave Vel	Density	Poisson's Ratio	Damping
1.2	0	740	120	0.33	0.02
0.4	0	920	120	0.33	0.02
6.4	0	1250	120	0.33	0.02
5	0	1000	120	0.33	0.02
14	0	1100	120	0.33	0.02
4	0	1350	120	0.33	0.02
10	5000	1400	125	0	0.02
10	5000	2300	125	0	0.02
99999	0	5600	130	0.3	0.02

Table 2.1 Parameters Used to Develop the Theoretical Dispersion Curve at Array 9 (Silver Lake Project)

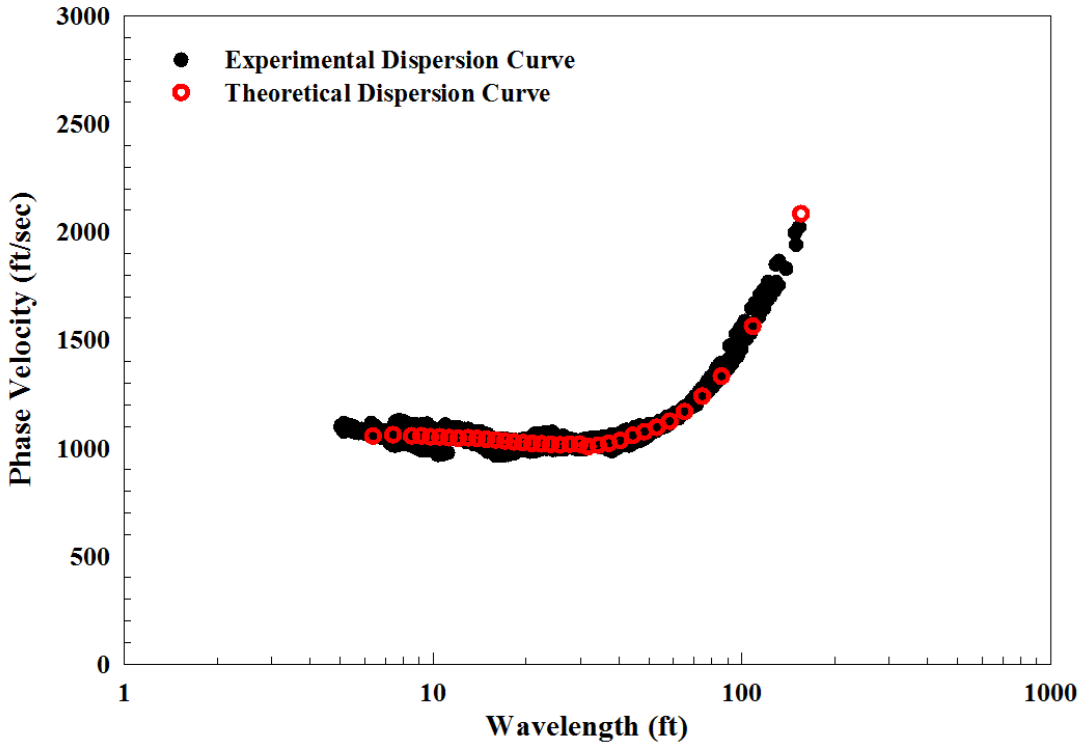

Figure 2.16 Comparison of the Fit of the Theoretical Dispersion curve to the Experimental Dispersion Curve at Array 9 (Silver Lake Project)

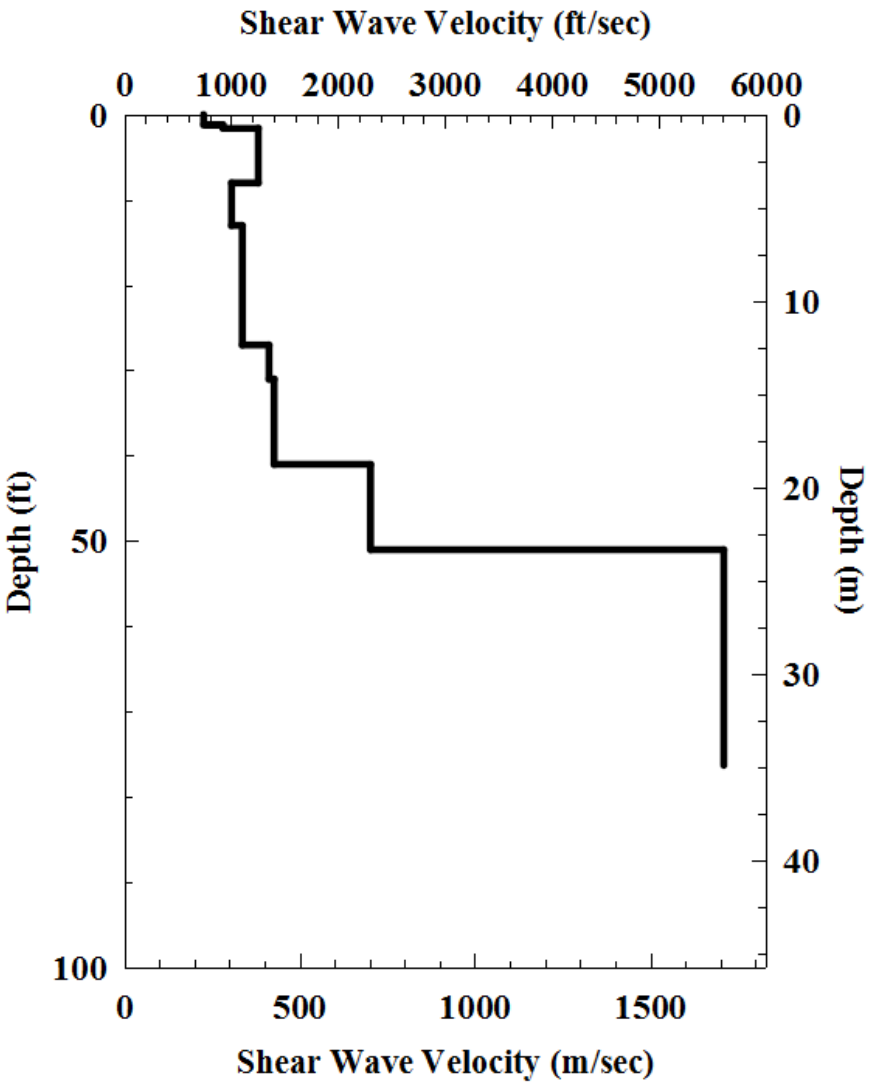

Figure 2.17 Final Shear Wave Velocity Profile Determined at Array 9 (Silver Lake Project)

2.5 SUMMARY

The SASW testing method is a nondestructive and nonintrusive seismic method. Rayleigh waves excited with vertically oriented surface source are measured by the vertical geophones located at various distances away from the source. Measurements of phase difference between receiver pairs are used to calculate the phase velocity and to generate individual dispersion curve. Individual dispersion curves from all receiver pairs are combined to create the field (experimental) dispersion curve of the site. The theoretical dispersion curves are generated by the forward modeling process to find a theoretical dispersion curve that matches the field dispersion curve. For shorter-wavelength measurements, hand-held hammers are used as the impact source. For the longer-wavelength measurements, a bulldozer (random-noise source) is used. The final V_s profile is determined based on the matched theoretical dispersion curve and plotted in terms of shear wave velocity versus depth profile.

CHAPTER 3 : PROCEDURE TO ANALYZE THE NEAR-FIELD EFFECTS ON THE FIELD DISPERSION CURVE

3.1 REFERENCE FIELD DISPERSION CURVE

When any type of surface wave testing is performed, there is always a concern that near-field data are included in the measurements. This concern arises because near-field data are not modeled in the forward modeling or inversion procedure that uses the field dispersion curve to determine the V_s profile of the site. Therefore, a field dispersion curve with near-field data could adversely distort the field V_s profile. This concern certainly arises in the SASW method as discussed in Section 2.4. The general masking procedure in the SASW method that is needed to generate the field dispersion curve involves selecting data with wavelengths no longer than twice the receiver spacing. This criteria is experimentally investigated in this thesis research by generating field dispersion curves at simple sites that are normally dispersive and comparing the curves with and without "suspected" near-field data.

In this section, a masking procedure to generate the reference field (experimental) dispersion curve is presented. With this procedure the reference field dispersion curve is assumed to include no near-field data and, hence, to be the profile that can be inverted. The reference averaged phase velocity versus wavelength curve is created using a moving average method over the reference field dispersion curve. The reference averaged phase velocity for each wavelength is taken from this curve. The procedure to create the reference field dispersion curve is presented using example SASW data determined at Array 3A (Stage 1) of the project at the Vogtle Electric Generating Power Plant Project near Augusta, Georgia.

For the quantitative analysis of near-field effects, a reference field dispersion curve that is free of near-field data must be generated. Most of the filtering criteria to minimize the near-field effects are determined by a goodness of fit of the dispersion curve after masking out that portion of the data contaminated by near-field effects. The goodness-of-fit is often determined by the judgment of the person analyzing the data. Unfortunately, the filtering criteria can differ from site to site due to different site conditions as expressed by the shear wave velocity.

As outlined in Table 1.1, researches generally have recommended using values of x_1 / λ for the near-field criteria, where x_1 is the source-to-first-receiver-distance and λ is the Rayleigh wavelength when the receiver-to-receiver-distance is the same as the source-to-first-receiver-distance. One of the recommendations is $x_1 / \lambda > 1$. In other words, near-field effects begins to occur when the wavelength is longer than the receiver spacing. Therefore, one of the reference field dispersion curves in this study is calculated from 360° (1 λ) to the Maximum phase difference (Minimum λ) as illustrated in the Figure 3.1. In this work, the dispersion curve generated with the 1 λ to Min-Useable λ phase difference is referred to as the C-R (reference case) dispersion curve.

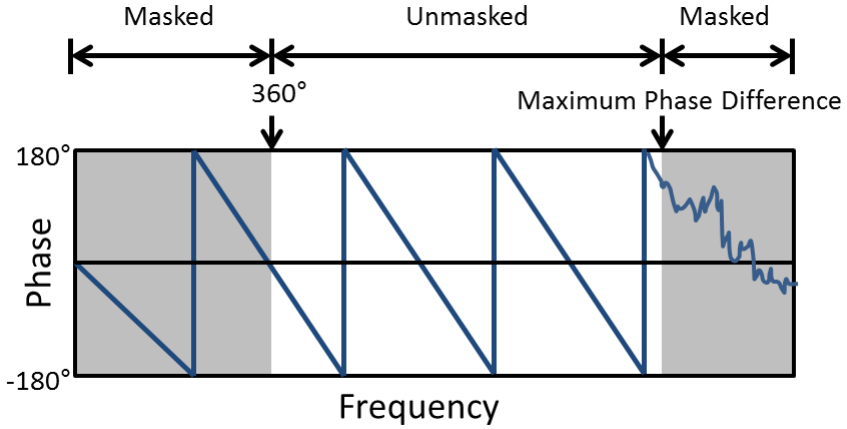

Figure 3.1 Idealized Wrapped Phase Data Showing the Unmasked, Useable Portion from 1 λ to Minimum λ (Maximum Useable Phase)

The maximum useable phase difference generally differs from receiver spacing to receiver spacing due to the clearness of the phase plot. As shown in the Figure 3.2, in case of the 100-ft receiver spacing, the reference dispersion curve is calculated from about 1 λ to 0.13 λ and in case of the 50-ft receiver spacing, the reference dispersion curve is calculated from 1 λ to slightly less than 0.3 λ.

This general procedure was repeated to create the C-R field dispersion curve for all receiver spacings from 2 to 100-ft as shown in Figures 3.2 and 3.3. The 2-ft receiver spacing data shown in Figure 3.3d only used in the reference dispersion curve in the range of 0.67 λ to 0.4 λ reference averaged phase velocity versus wavelength curve due to interference of a higher mode or the lack of high frequency energy. This masking procedure enables extensive overlapping at most wavelengths in the curve. By comparing the phase velocity at the same wavelength from other receivers, one can increase their confidence in the reliability of the reference phase velocity.

The C-R field dispersion curve is calculated from the unmasked portion of the data from all receiver spacings. Then reference averaged phase velocity versus wavelength curve is generated by using the moving average method over the C-R field dispersion curve. The WinSASW 3.2.6 program was employed to generate the reference field dispersion curve and the reference averaged phase velocity versus wavelength curve. The main concept of the averaging process is a moving average which is a linear operation calculating the series of arithmetic averages from consecutive V_{ph}-λ data points. The moving average process is often used in geophysical data processing, and it is effective in processing SASW data to extract the basic trends (Joh, 1996). Care and judgment must be exercised, however, not to combine data from different modes at different spacings, hence lose very important data. The reference field dispersion curve and averaged phase velocity versus wavelength curves are presented in Figure 3.4.

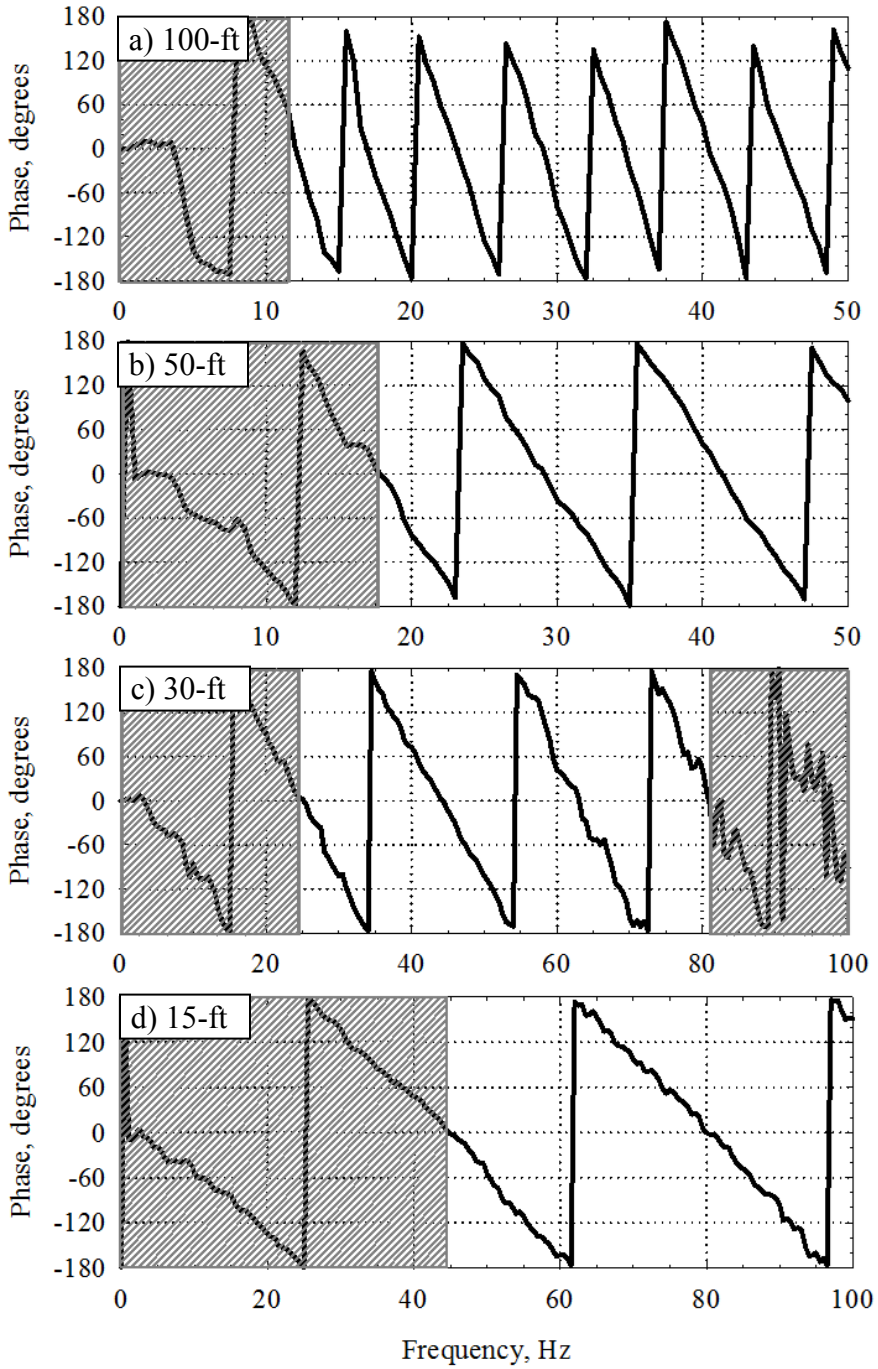

Figure 3.2 Masking Procedure Used to Create the C-R Field Dispersion Curve for 1 λ to Min-Useable λ; Wrapped Phase Difference of the Transfer Function Determined at Array 3A (Stage 1 at Vogtle Electric Generating Plant) with Receiver Spacings of 100, 50, 30 and 15 ft

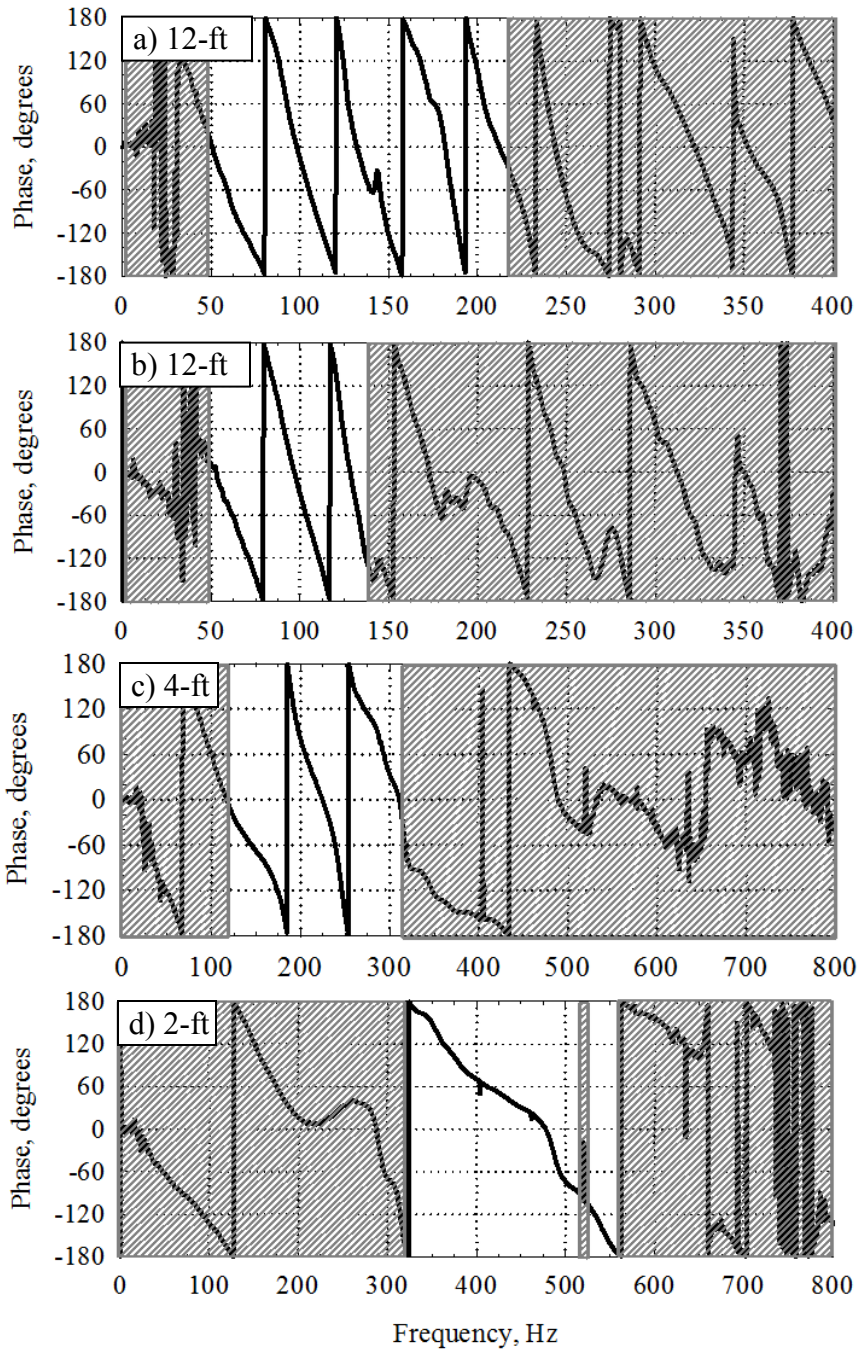

Figure 3.3 Masking Procedure Used to Create the C-R Field Dispersion Curve for 1 λ to Min-Useable λ; Wrapped Phase Difference of the Transfer Function Determined at Array 3A (Stage 1 at Vogtle Electric Generating Plant) with Receiver Spacings of 12, 4 and 2 ft (Note : 2-ft spacing had useable 0.67 λ to 0.4 λ)

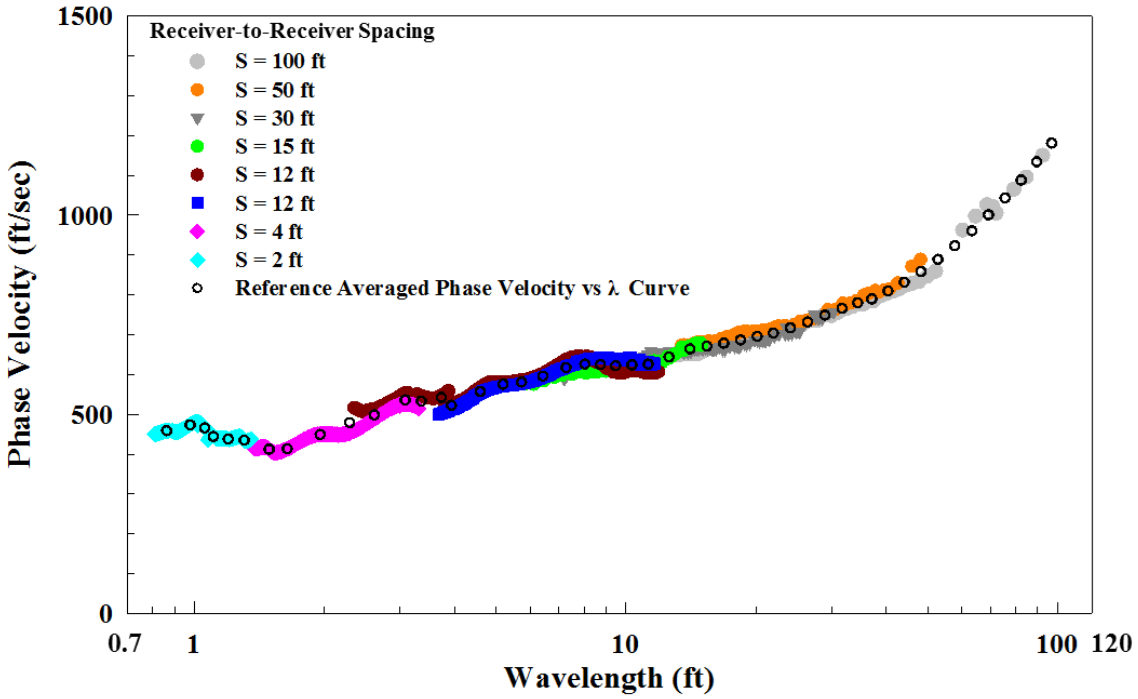

Figure 3.4 All Field Dispersion Data Used to Create the C-R Field Dispersion Curve and Reference Averaged Phase Velocity versus λ Curve for the 1 λ to Min-Useable λ Data at Array 3A Presented in Figures 3.2 and 3.3. (Stage 1 Testing at VEGP Site)

3.2 DETERMINATION OF REFERENCE FIELD DISPERSION CURVE

Reference dispersion curves can be generated as discussed in Section 3.1 and as presented in Figure 3.4 for the criteria of 1 λ to Min-Useable λ. However, other criteria can also be used to investigate the reference dispersion curve. These other dispersion curves are developed in this section and the results are used to determine which criteria are most appropriate, at least for the VEGP Site.

Reference field dispersion curves are generated with four phase-difference criteria as follows: (1) 360° to 720° (1 λ to 2 λ), (2) 720° to 1080° (2 λ to 3 λ), (3) 1080° to

1440° (3 λ to 4 λ), and (4) 1440° to maximum (4 λ to Min-Useable λ). The reference averaged phase velocity versus wavelength curve denoted as reference case or C-R is compared at each wavelength with the different reference field dispersion curves. In this work, dispersion curves generated as follows: (1) 1 λ to 0.5 λ phase difference is referred to as the C-1 dispersion curve, (2) 0.5 λ to 0.33 λ phase difference is referred to as the C-2 dispersion curve, (3) 0.33 λ to 0.25 λ phase difference is referred to as the C-3 dispersion curve and (4) 0.25 λ to Min-Useable λ phase difference is referred to as C-4 dispersion curve. All criteria are illustrated in Table 3.1. One additional dispersion curve , called C-5, is discussed in Section 3.3.

Table 3.1 Wavelength Ranges Used to Create Reference Field Dispersion Curve

No.	Wavelength (or Phase) Range for Each Receiver Spacing Used in SASW Testing	Case Name
1	1 λ to Min-Useable λ (360° to Max-Useable Phase)	C-R
2	1 λ to 0.5 λ	C-1
3	0.5 λ to 0.33 λ	C-2
4	0.33 λ to 0.25 λ	C-3
5	0.25 λ to Min-Useable λ	C-4
6	Min-Useable λ to Max-Useable λ (λ > Receiver Spacing)	C-5

3.2.1 C-1 REFERENCE FIELD DISPERSION CURVE

In Figure 3.5, the idealized wrapped phase plot for the C-1 dispersion curve is shown using 1 λ to 0.5 λ unmasked portion. Figures 3.6 and 3.7 show the actual wrapped phase plot for the C-1 dispersion curve from all receiver spacings at Array 3A for Stage 1 at the VEGP Site.

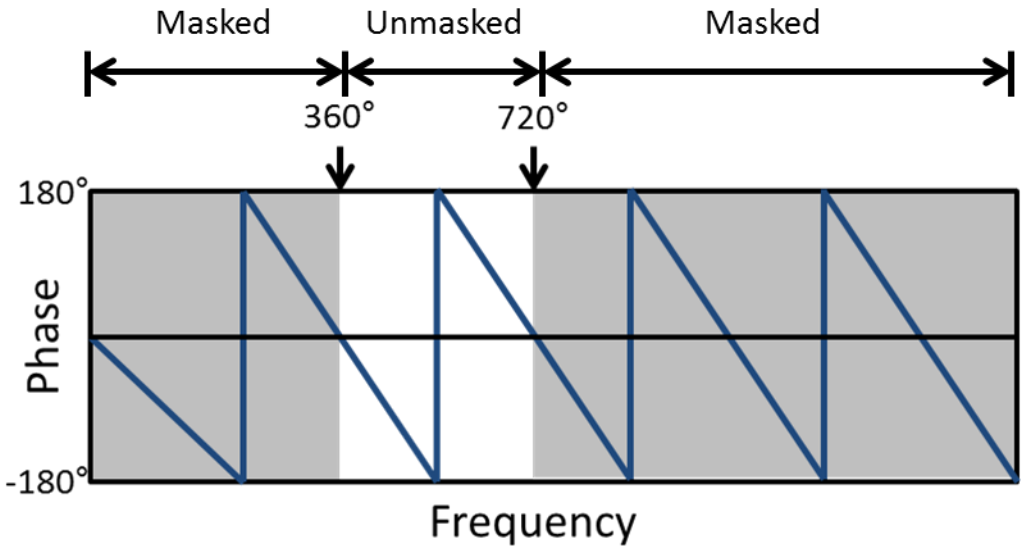

Figure 3.5 Idealized Wrapped Phase Data Showing the 1 λ to 0.5 λ Unmasked Portion; Case 1 (C-1)

The field C-1 dispersion curve was calculated from the unmasked portion of the phase plots shown in Figures 3.6 and 3.7. In this case, wavelengths in the range of 0.5 to 1.0 times the receiver spacing were used. Figure 3.7 shows the field C-1 dispersion plotted by the colored symbols. It is easy to see how well this curve fits within the reference averaged phase velocity versus wavelength curve and the ± 5% boundaries. Nearly all values are within the ±5% range, inside the black dotted line. Therefore, this criterion works quite well for this soil profile and data set (receiver spacings). As expected, this criterion permits the longest wavelength data to be included.

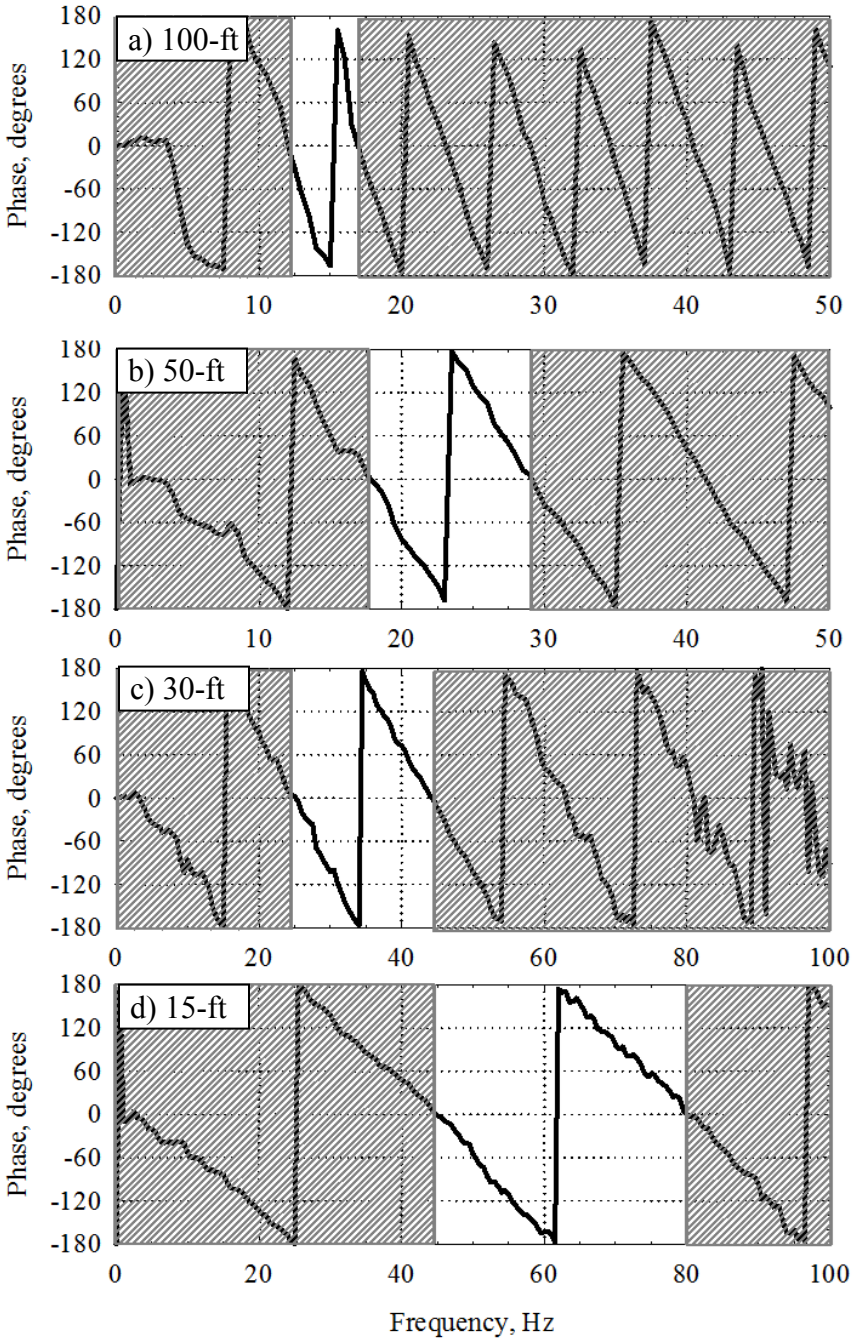

Figure 3.6 Masking Procedure Used to Create the Field C-1 Dispersion Curve for 1 λ to 0.5 λ; Wrapped Phase Difference of the Transfer Function Determined at Array 3A (Stage 1 at VEGP Site) with Receiver Spacings of 100, 50, 30 and 15 ft

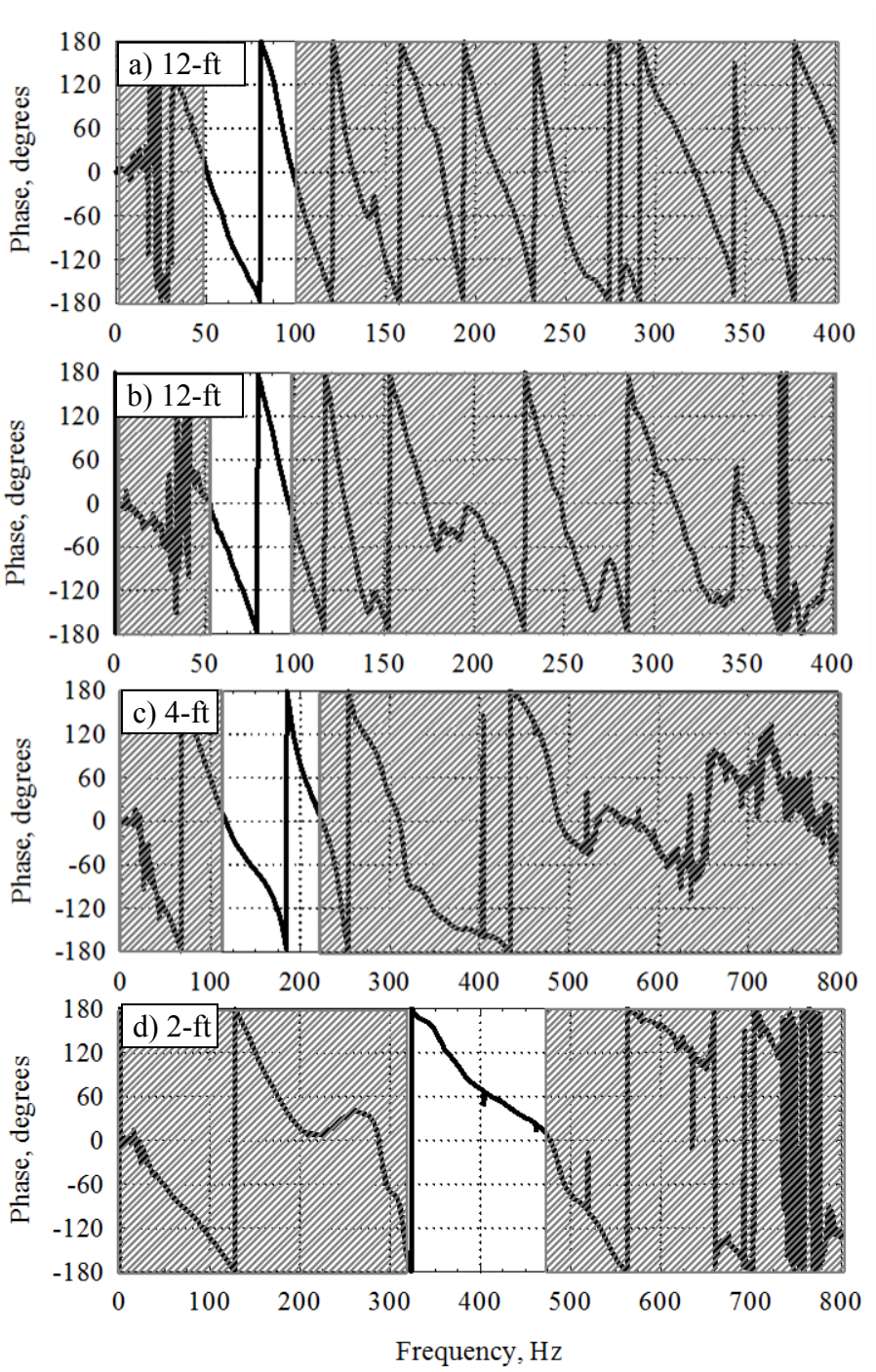

Figure 3.7 Masking Procedure Used to Create the Field C-1 Dispersion Curve for 1 λ to 0.5 λ; Wrapped Phase Difference of the Transfer Function Determined at Array 3A (Stage 1 at VEGP) with Receiver Spacings of 12, 4 and 2 ft

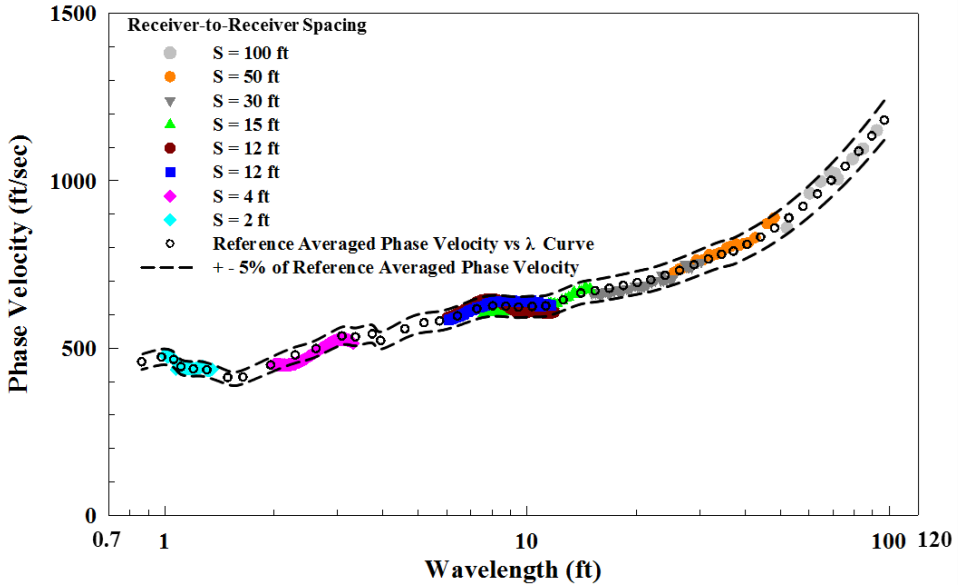

Figure 3.8 Comparison of the Reference Averaged Phase Velocity versus λ Curve (Case C-R) and Field C-1 Dispersion Curve at Array 3A; Stage 1 at VEGP Site

3.2.2 C-2 REFERENCE FIELD DISPERSION CURVE

In Figure 3.9 shows the idealized wrapped phase plot for the C-2 dispersion curve is shown using the 0.5 λ to 0.33 λ unmasked portion. Figures 3.10 and 3.11 show the actual wrapped phase plots for the C-2 dispersion curve from receiver spacings at Array 3A for Stage 1 at the VEGP Site.

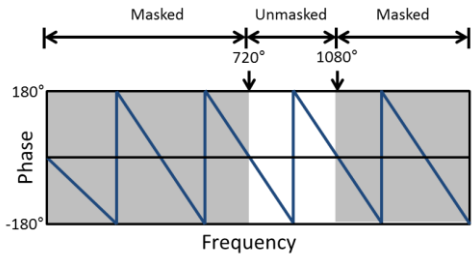

Figure 3.9 Idealized Wrapped Phase Data Showing the 0.5 λ to 0.33 λ Unmasked Portion; Case 2 (C-2)

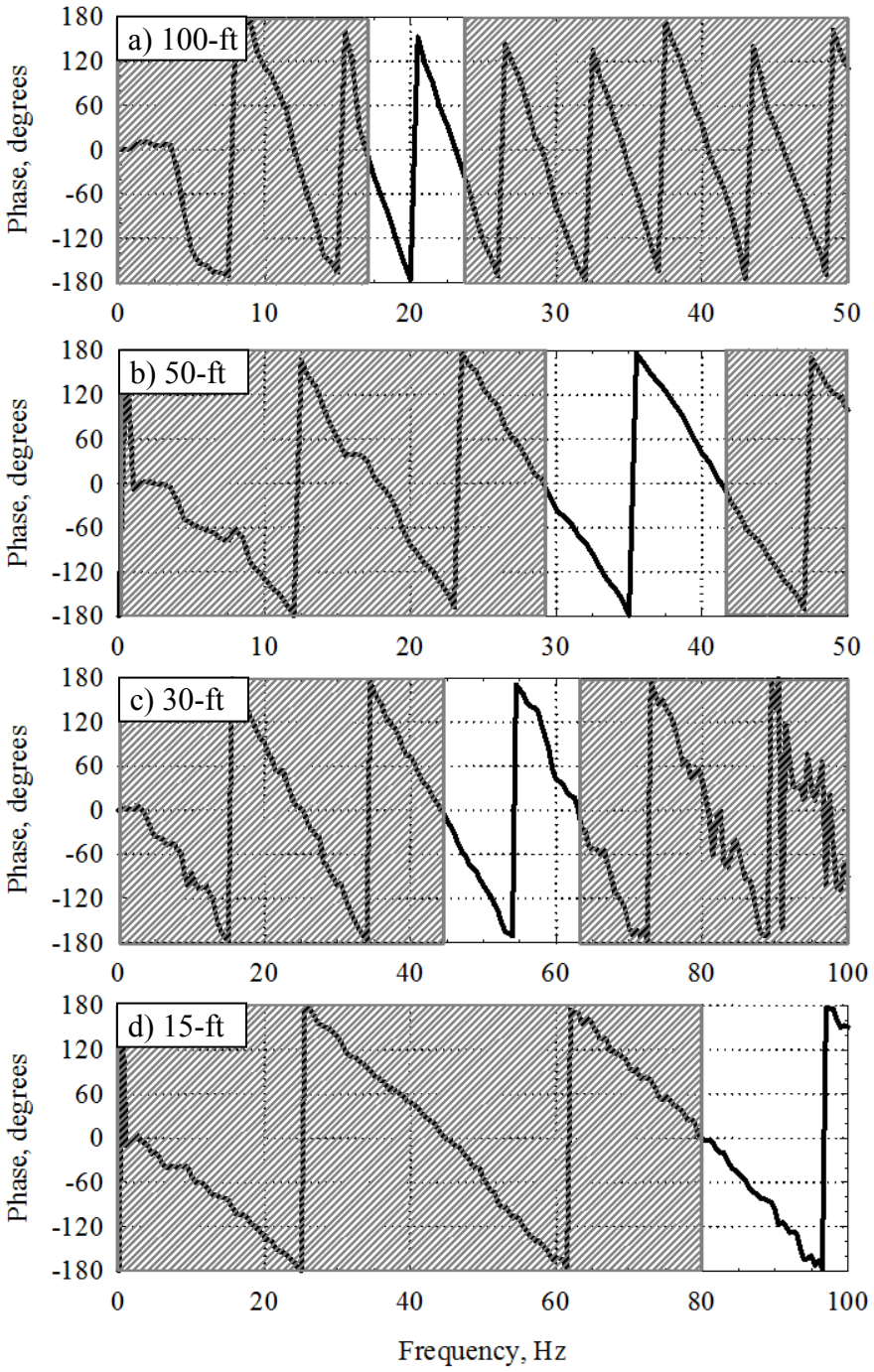

Figure 3.10 Masking Procedure Used to Create the Field C-2 Dispersion Curve for 0.5 λ to 0.33 λ; Wrapped Phase Difference of the Transfer Function Determined at Array 3A (Stage 1 at VEGP Site) with Receiver Spacings of 100, 50, 30 and 15 ft

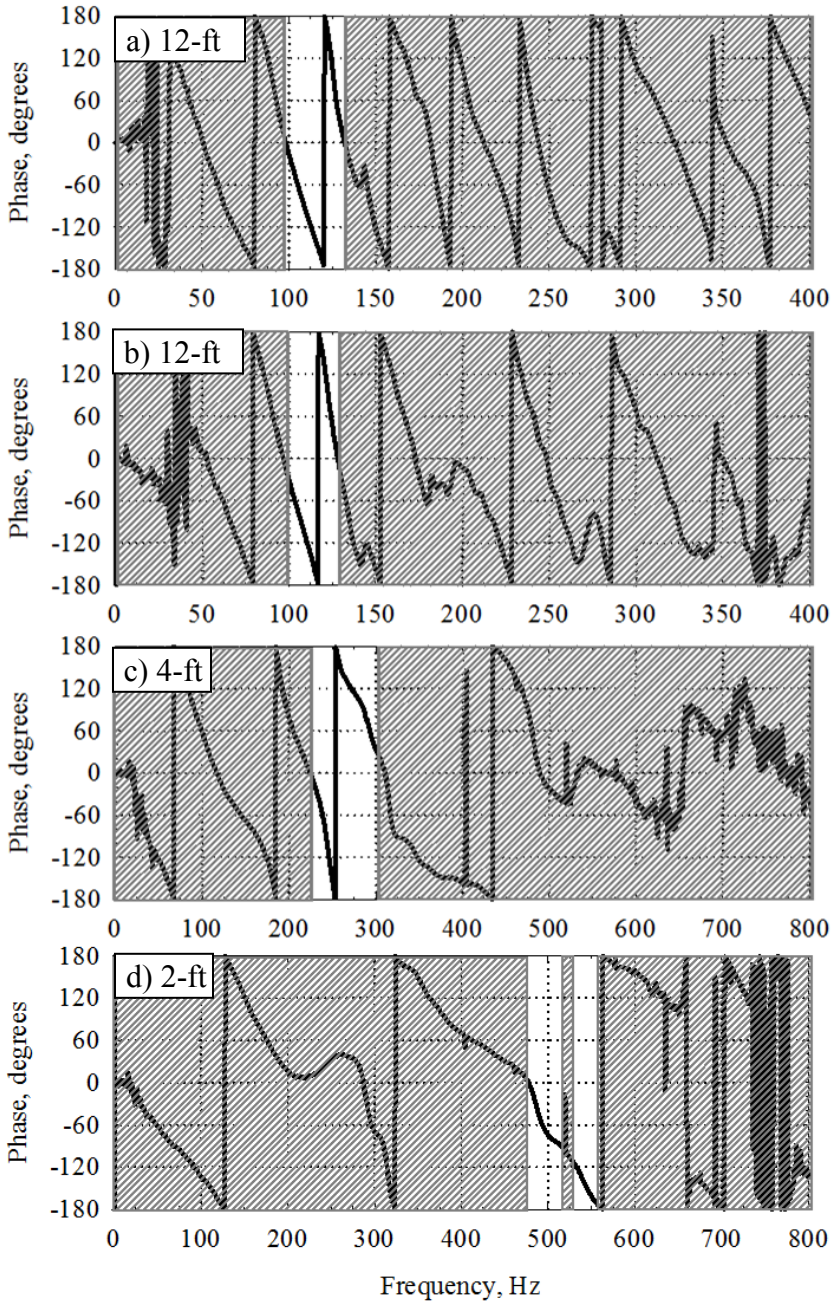

Figure 3.11 Masking Procedure Used to Create the Field C-2 Dispersion Curve for 0.5 λ to 0.33 λ; Wrapped Phase Difference of the Transfer Function Determined at Array 3A (Stage 1 at VEGP Site) with Receiver Spacings of 12, 4 and 2 ft

The field C-2 dispersion curve was calculated from the unmasked portion of the phase plots in Figures 3.10 and 3.11. In this case, wavelengths in the range of 0.33 to 0.5 times the receiver spacing were used. Figure 3.12 shows the field C-2 dispersion plotted by the colored symbols. As with the C-1 case, the C-2 dispersion curve fits well the reference averaged phase velocity versus wavelength curve and the ± 5% boundaries. Nearly all values are within the ±5% range, inside the black dotted line. Therefore, this criterion works well for this soil profile and data set. The benefit of this data is that there are shorter wavelength data compared with the C-1 dispersion curve.

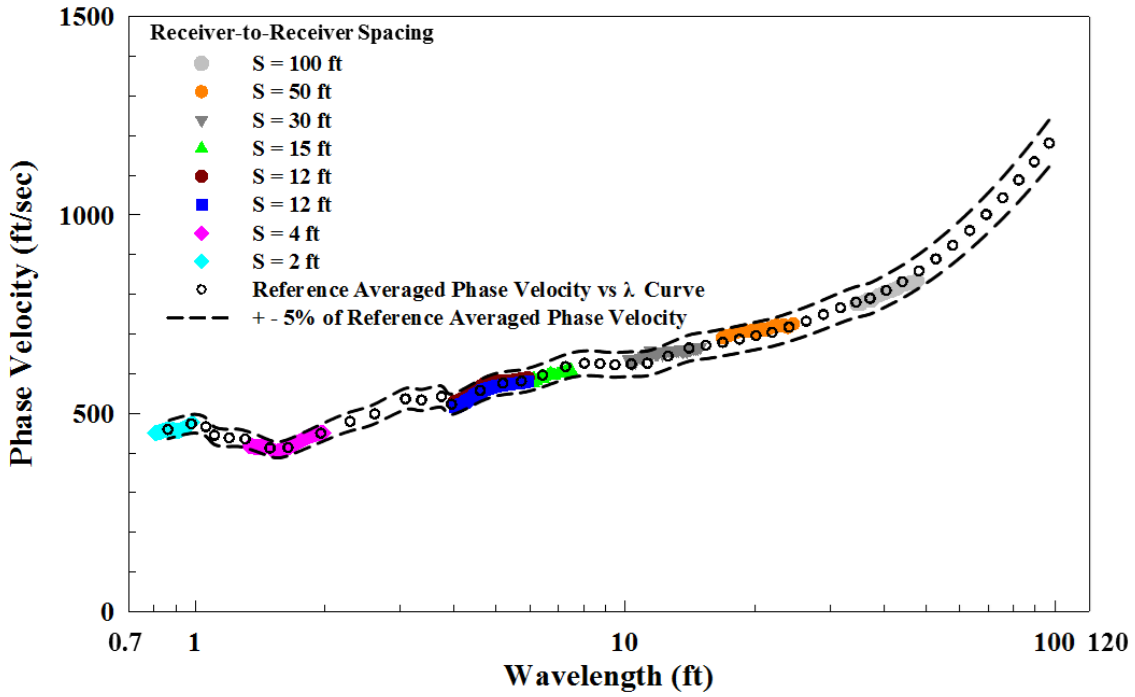

Figure 3.12 Comparison of the Reference Averaged Phase Velocity versus λ Curve (Case C-R) and Field C-2 Dispersion Curve at Array 3A; Stage 1 at VEGP Site

3.2.3 C-3 REFERENCE FIELD DISPERSION CURVE

In Figure 3.13, shows the idealized wrapped phase plot for the C-3 dispersion curve is shown using 0.33 λ-to-0.25 λ unmasked portion. For the C-3 dispersion curve, only 100-, 50-, 30- and 12-ft receiver spacing cover the frequency range of 0.33 λ t - 0.25 λ. Figure 3.14 shows the actual wrapped phase plot for the C-3 dispersion curve from all receiver spacings at Array 3A for Stage 1 at the VEGP Site.

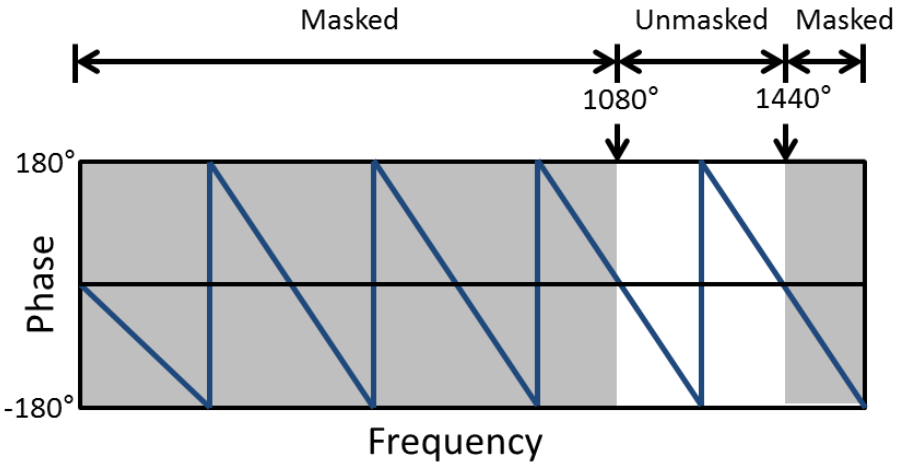

Figure 3.13 Idealized Wrapped Phase Data Showing the 0.33 λ to 0.25 λ Unmasked Portion; Case 3 (C-3)

The field C-3 dispersion curve was calculated from the unmasked portion of the phase plots in Figures 3.14. In this case, wavelengths in the range of 0.25 to 0.33 times the receiver spacing were used. Figure 3.15 shows the field C-3 dispersion curve plotted by the colored symbols and how this curve fits within the reference averaged phase velocity versus wavelength curve and the ± 5% boundaries. Nearly all values are within the ±5% range, inside the black dotted line. However, even though criterion works well, the data are too sparse to be used alone.

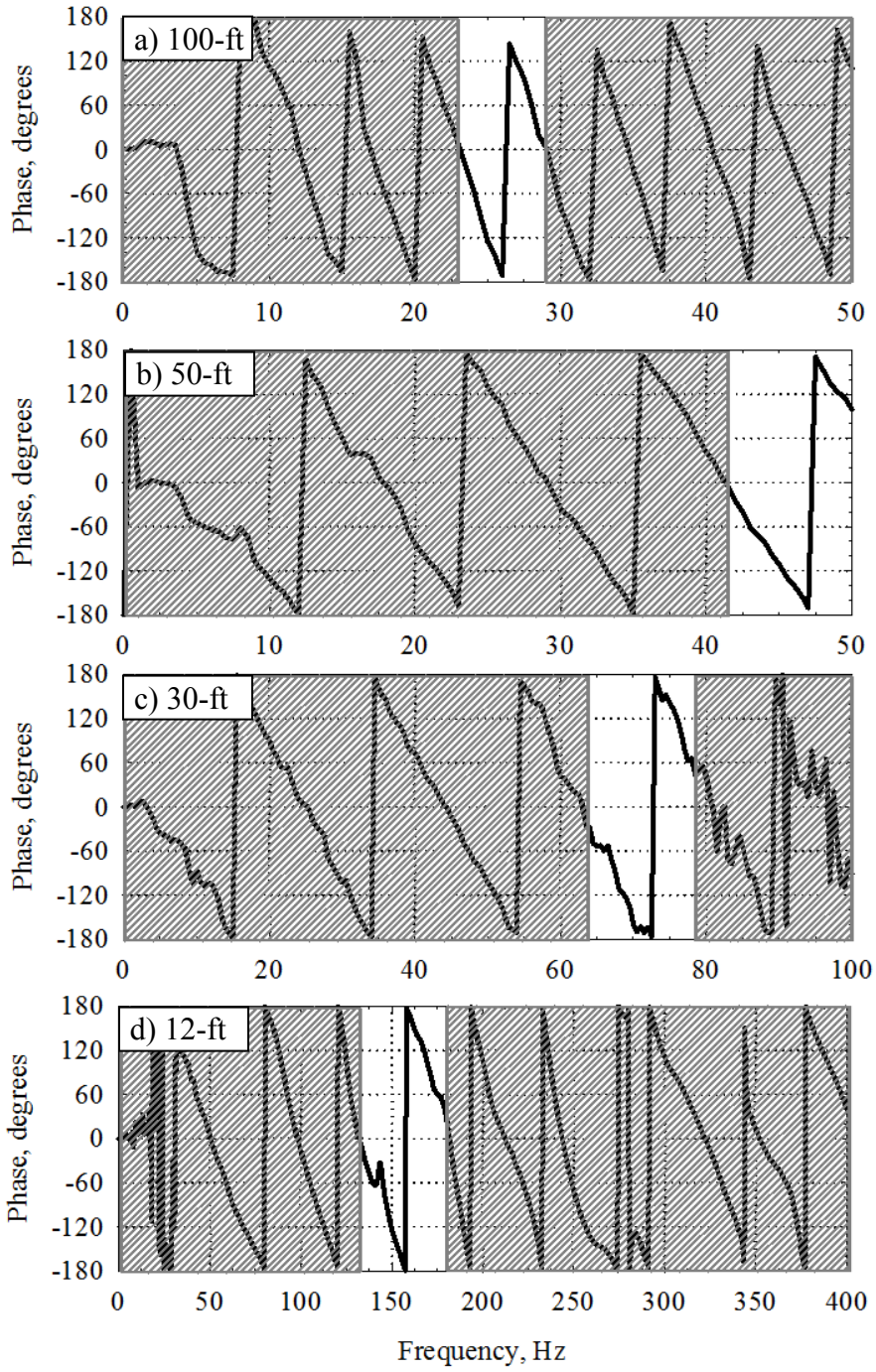

Figure 3.14 Masking Procedure Used to Create the Field C-3 Dispersion Curve for 0.33 λ to 0.25 λ; Wrapped Phase Difference of the Transfer Function Determined at Array 3A (Stage 1 at VEGP Site) with Receiver Spacings of 10, 50, 30 and 12 ft

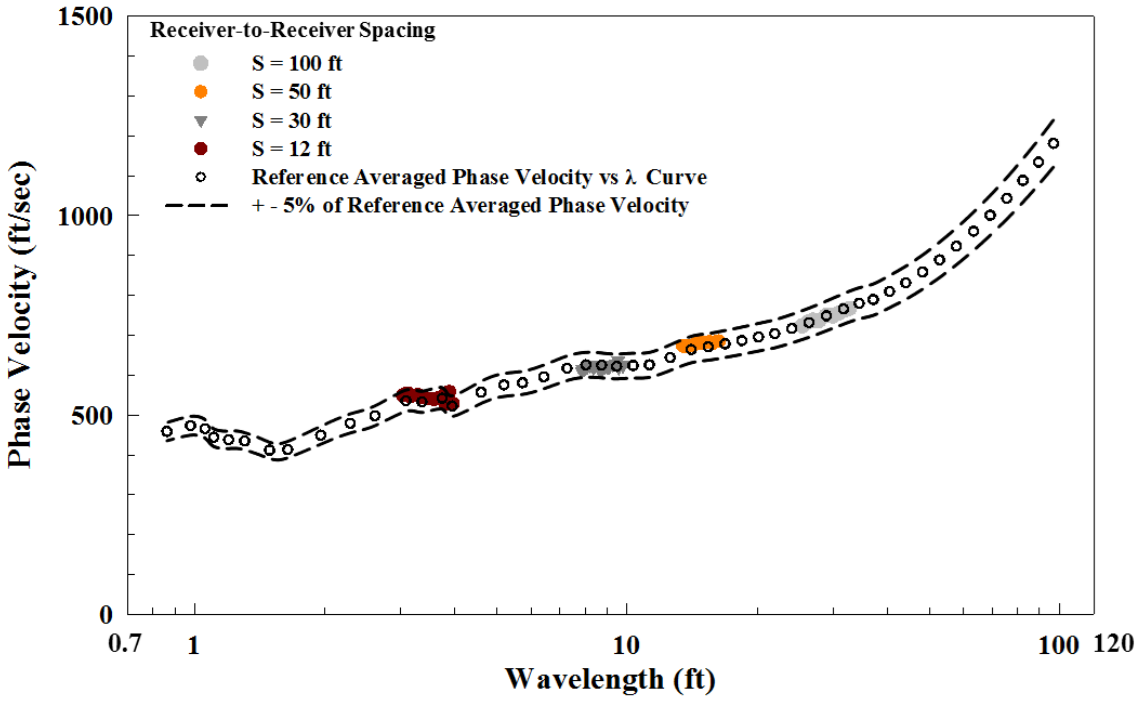

Figure 3.15 Comparison of the Reference Averaged Phase Velocity versus λ Curve (Case C-R) and Field C-3 Dispersion Curve at Array 3A; Stage 1 at VEGP Site

3.2.4 C-4 REFERENCE FIELD DISPERSION CURVE

For the C-4 dispersion curve, only the 100- and 12-ft receiver spacings included the frequency range of 0.25 λ to Min-Useable λ. Figure 3.16 shows the idealized wrapped phase plot for the C-4 dispersion curve using 0.25 λ to Min-Useable λ unmasked portion. Figure 3.17 shows the actual wrapped phase plot for the C-4 dispersion curve from receiver spacing at Array 3A for Stage 1 at the VEGP Site.

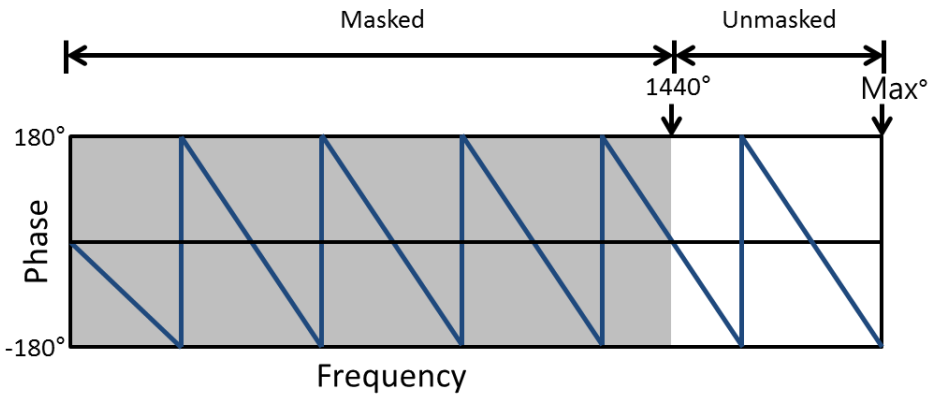

Figure 3.16 Idealized Wrapped Phase Data Showing the 0.25 λ to Min-Useable λ (Max-Useable Phase) Unmasked Portion; Case 4 (C-4)

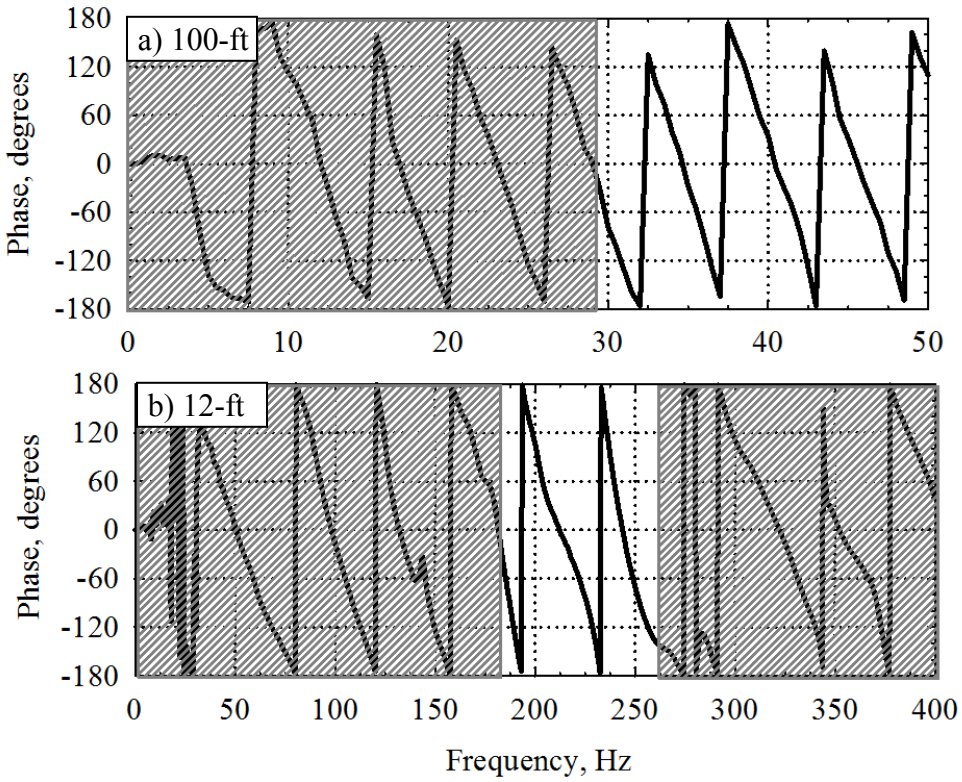

Figure 3.17 Masking Procedure Used to Create the Field C-4 Dispersion Curve for 0.25 λ to Min-Useable λ; Wrapped Phase Difference of the Transfer Function Determined at Array 3A (Stage 1 at VEGP Site) with Receiver Spacings of 100 and 12 ft

The field C-4 dispersion curve was calculated from the unmasked portion of the phase plots shown in Figure 3.17. Figure 3.18 shows the field C-4 dispersion curve plotted by the colored symbols and how this curve fits within the reference averaged phase velocity versus wavelength curve and the ± 5% boundaries. Nearly all values are within the ±5% range except below the 2.5-ft wavelength. This difference indicates that the reference velocity below 2.5-ft wavelength is slightly underestimated, likely due to the variability in the shallow layer. However, there will be no analysis in this research using wavelength less than 2.5-ft. Therefore, the phase velocity taken from the reference averaged phase velocity versus wavelength curve is used as a reference curve at the VEGP Site.

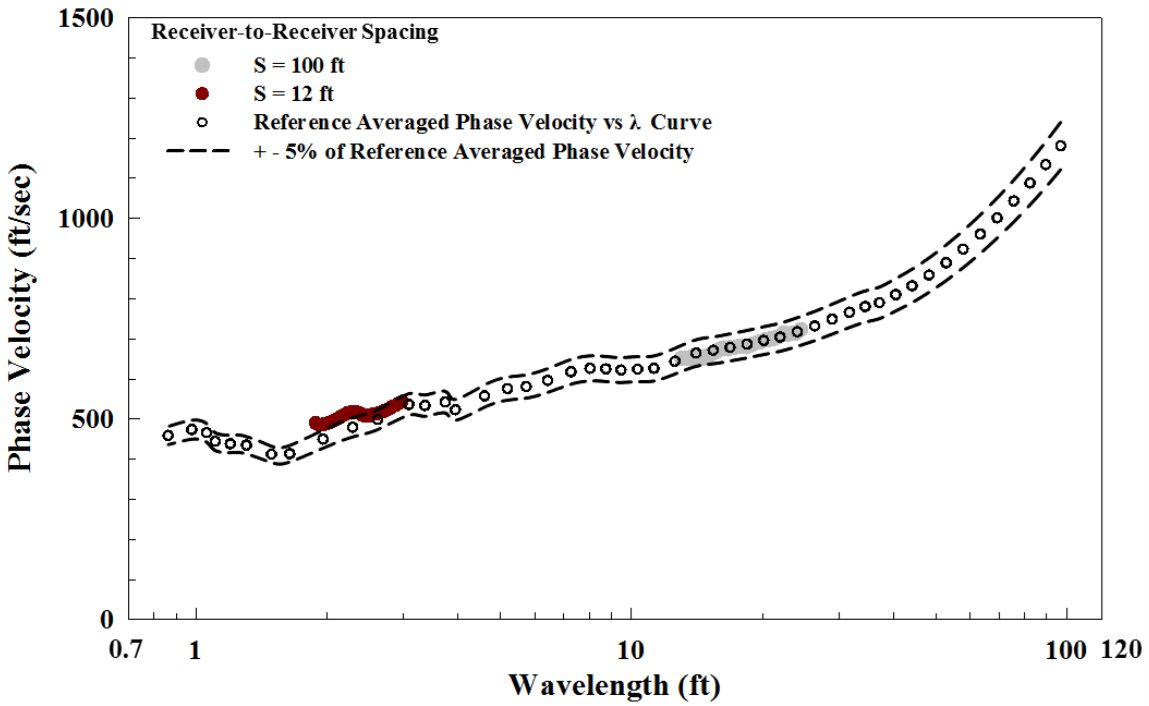

Figure 3.18 Comparison of the Reference Averaged Phase Velocity versus λ Curve (Case C-R) and Field C-4 Dispersion Curve at Array 3A; Stage 1 at VEGP Site

3.3 DISPERSION CURVE INCLUDING NEAR-FIELD EFFECTS

The basic concept of the analysis of near-field effects is comparing phase velocities for the same wavelength but from the different receiver spacings. For example, a phase velocity from a 90°-phase difference (a wavelength which is four times the receiver spacing, that may include near-field data) that was collected with 25-ft receiver spacing, can be compared with the phase velocity of a 100-ft wavelength that was collected with a 100-ft receiver spacing. The phase velocity from the 360°-phase difference (a wavelength equal to 100-ft receiver spacing) is used as the reference. Comparison of the two 100-ft wavelength phase velocities calculated from the different spacings reveal the quantitative error associate with any near-field effects in the 90°-phase difference calculation.

For this comparison, dispersion curves which include the near-field effects data are necessary. Dispersion curves including near-field effects data area those in the C-5 dispersion curve listed in Table 3.1, min-useable λ to max-useable λ. Figures 3.19, 3.20 and 3.21 show the making performed for C-5 dispersion curve at Stage 1 VEGP site.

For all receiver spacings, the masking procedure is performed to generate field C-5 dispersion curve. In case of 100-ft receiver spacing, near-field data was not necessary since there is no reference averaged phase velocity longer than 100-ft wavelength to compare with in this part of the analysis. Figure 3.22 shows the field C-5 dispersion plotted with the colored symbols. Clearly, various portions of these data do not fit within the reference averaged phase velocity versus wavelength curve and the ± 5% boundaries. This miss-fit is attributed to near-field effects as discussed below.

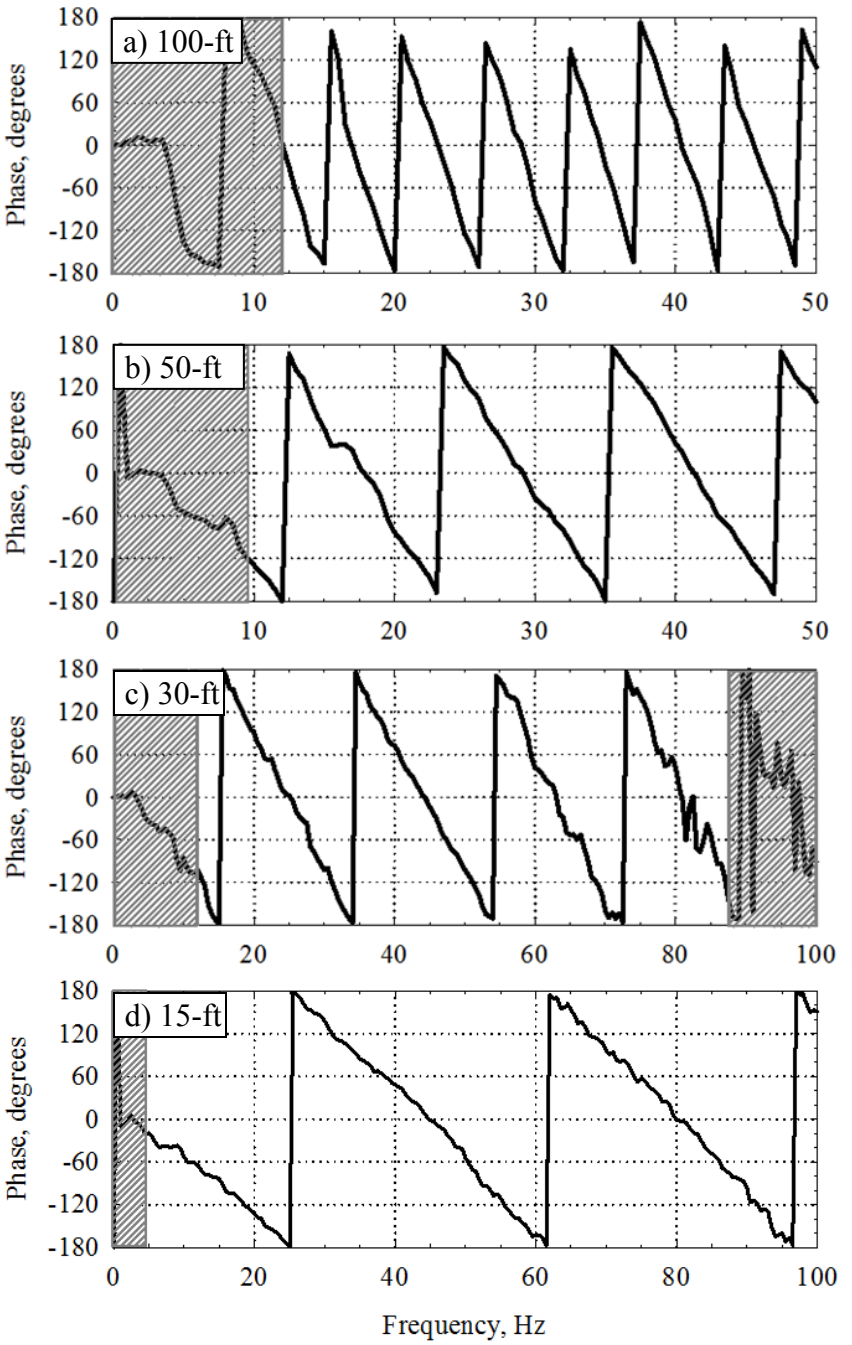

Figure 3.19 Masking Procedure Used to Create the Field C-5 Dispersion Curve for Min-Useable λ to Max-Useable λ; Wrapped Phase Difference of the Transfer Function Determined at Array 3A (Stage 1 at VEGP Site) with Receiver Spacings of 100, 50, 30 and 15 ft (Note : In this analysis, no wavelength > 100 ft were used)

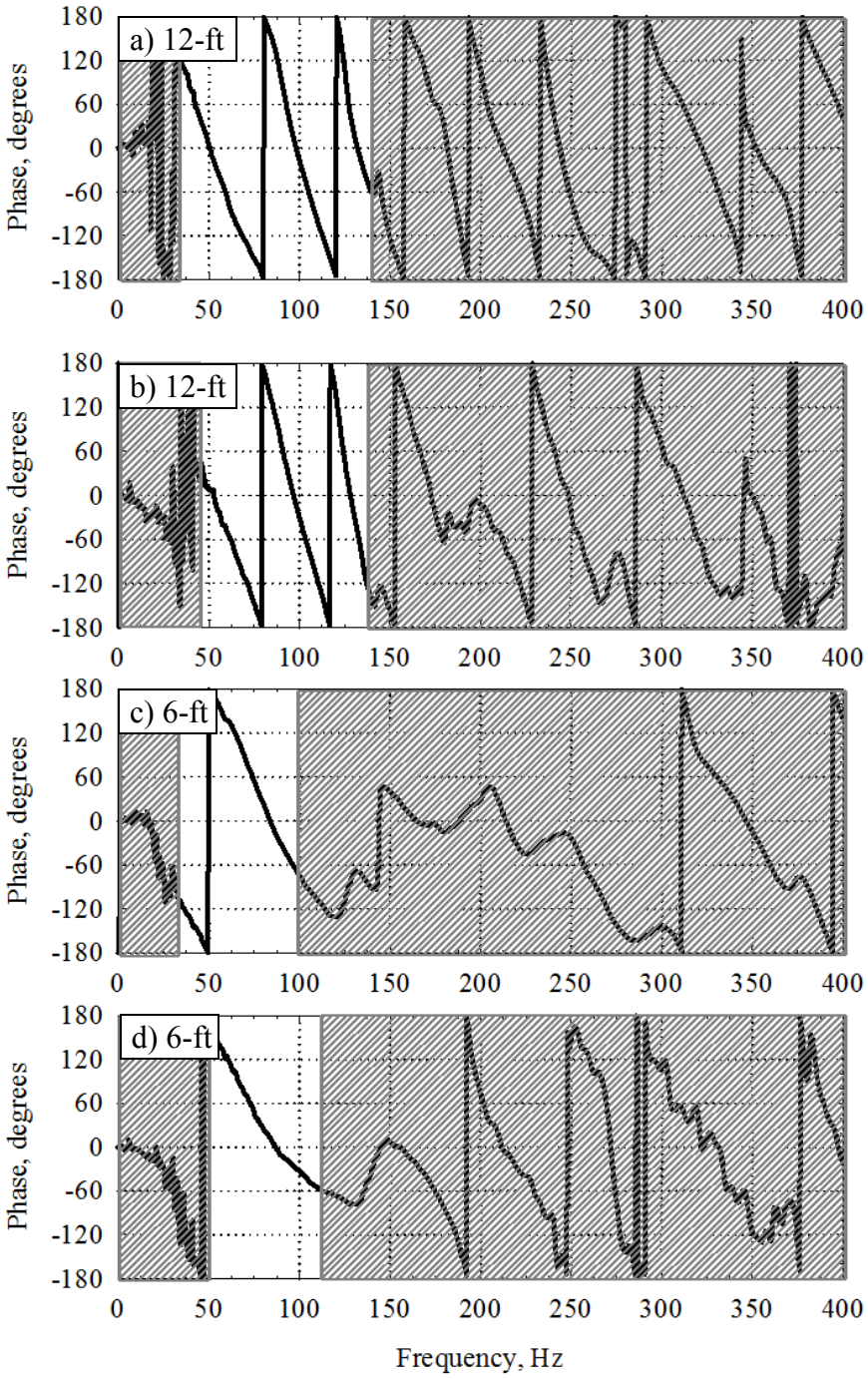

Figure 3.20 Masking Procedure Used to Create the Field C-5 Dispersion Curve for Min-Useable λ to Max-Useable λ; Wrapped Phase Difference of the Transfer Function Determined at Array 3A (Stage 1 at VEGP Site) with Receiver Spacings of 12 and 6 ft

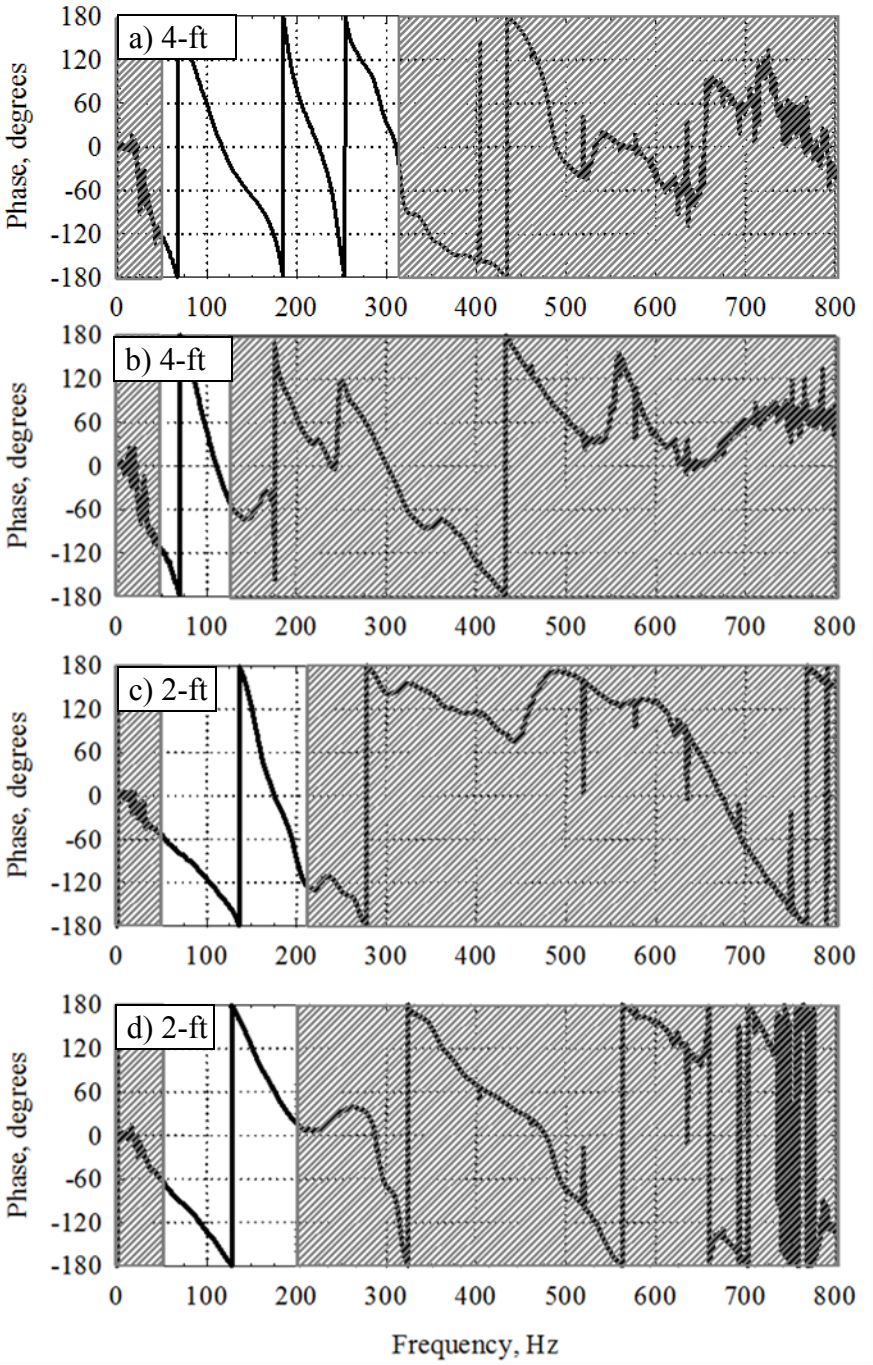

Figure 3.21 Masking Procedure Used to Create the Field C-5 Dispersion Curve for Min-Useable λ to Max-Useable λ; Wrapped Phase Difference of the Transfer Function Determined at Array 3A (Stage 1 at VEGP Site) with Receiver Spacings of 4 and 2 ft

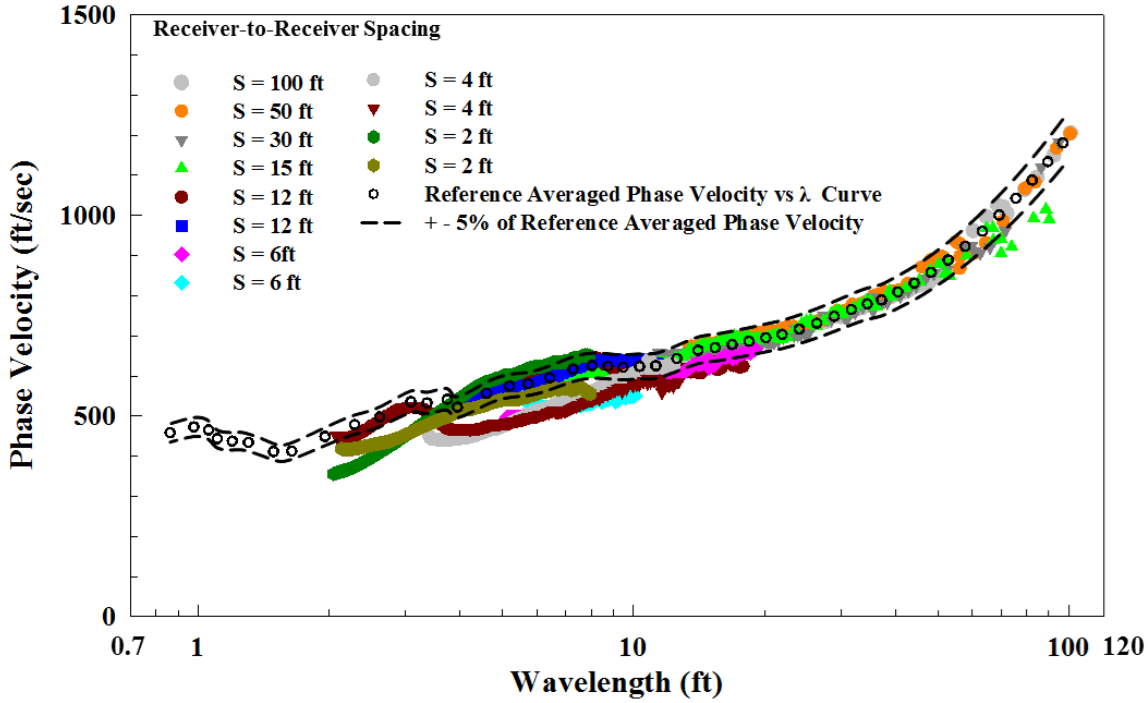

Figure 3.22 Comparison of the Reference Averaged Phase Velocity versus λ Curve (Case C-R) and Field C-5 Dispersion Curve at Array 3A; Stage 1 at the VEGP Site (Note : miss-fit attributed to near-field effects)

3.4 COMPARISON WITH REFERENCE VELOCITY

To evaluate the magnitude of error created by near-field effects, the comparison of the reference averaged phase velocity curve and the field dispersion curve that is assumed to be included near-field effects (field C-5 dispersion curve) is conducted. To conduct this comparison, the comparison two types of graph have been created. In both graphs, the phase velocities from each receiver spacing normalized by the reference averaged phase velocities at the site (the SASW array containing all receiver spacings) are plotted on the Y-axis. In the first graph, the wavelengths are plotted on the X-axis. The first graphs are shown in Figures 3.23 and 3.24. The general trend of the measurements at

Array 3A in terms of near-field effects is shown in Figure 3.23. Figure 3.24 presented simply to focus on the near-field effects at short receiver spacings. Both plots are discussed in more detail in Chapter 4 and 5. Any data that deviates in a consistent trend by more than ± 5% is considered to exhibit near-field effects. The adverse effects are shown in Figure 3.23 at wavelengths less than 20 ft and, for 15-ft receiver spacing, wavelength greater than about 60 ft.

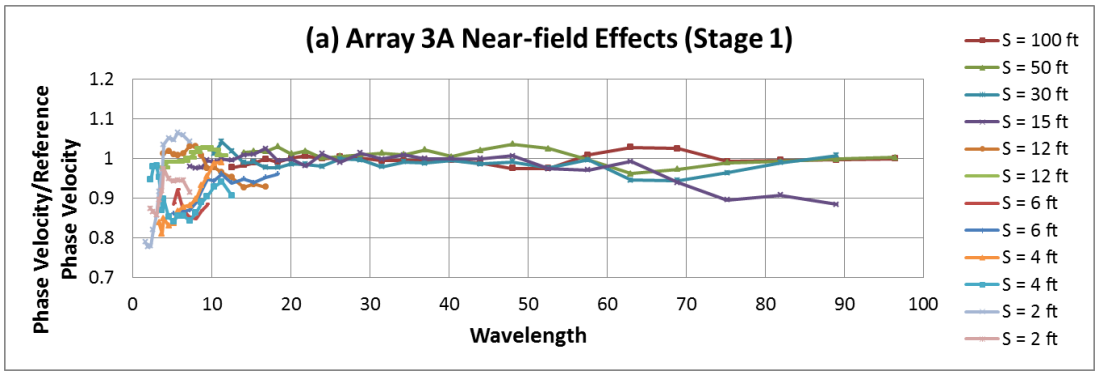

Figure 3.23 Comparison of the Reference Averaged Phase Velocities and the Phase Velocities from the C-5 Dispersion Curve at Array 3A with All Receiver Spacings (Phase Velocity Normalized by Reference Averaged Phase Velocity versus Wavelength)

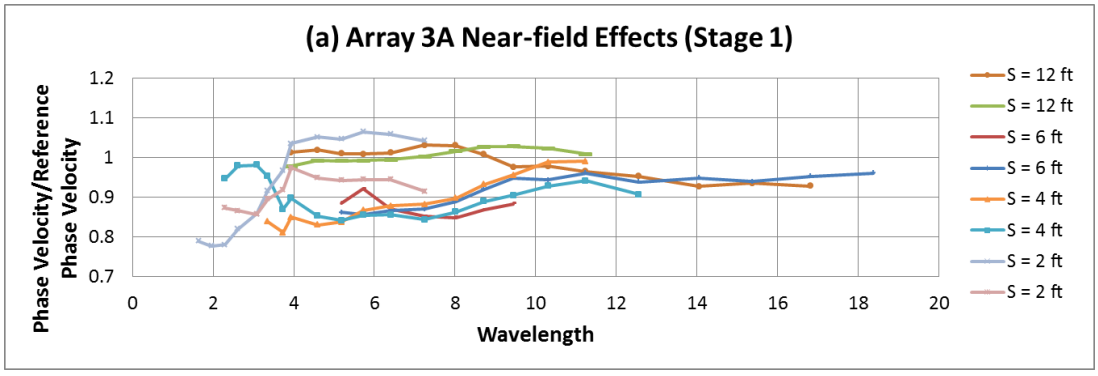

Figure 3.24 Comparison of the Reference Averaged Phase Velocities and the Phase Velocities from the C-5 Dispersion Curve at Array 3A with Short Reciever Spacings (Phase Velocity Normalized by Reference Averaged Phase Velocity versus Wavelength)

Figures 3.25 and 3.26 illustrate the second graphical format that is used to investigate near-field effects. The Y-axis is the same normalized phase velocity as used in the first formant. However, near-field effects are more clearly seen that the receiver spacing is divided by the wavelength and plotted on the X-axis. The X-axis is also called a spacing-to-wavelength ratio (SWR) or normalized spacing. When the receiver spacing normalized by wavelength has a value less than 1.0, the wavelength is longer than the receiver spacing and the near-field effects begin to be exhibited. Figure 3.25 shows this plot for the longer receiver spacings. Figure 3.26 shows this plot for the shorter receiver spacings. Clearly, near-field effects are shown at the SWR < 0.5 in Figure 3.25 and < 1.5 in Figure 3.26. These data are discussed in detail in Chapters 4 and 5.

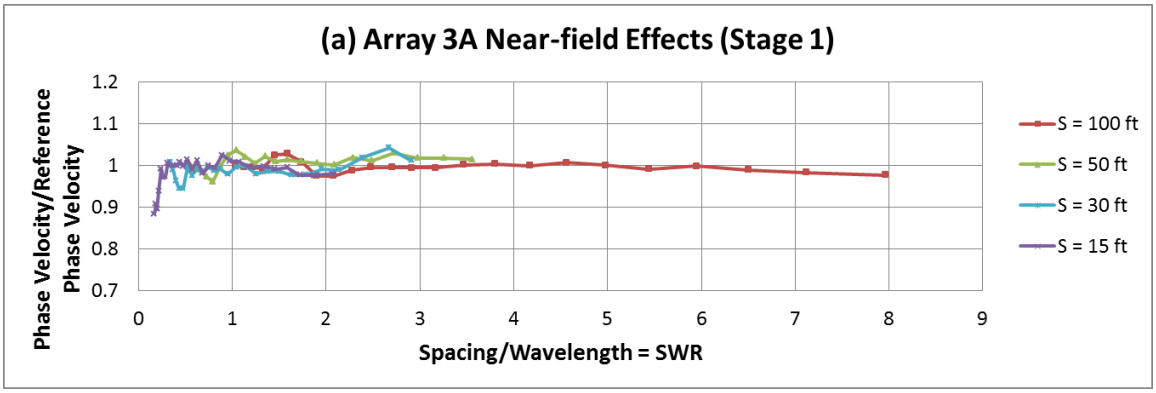

Figure 3.25 Comparison of the Reference Averaged Phase Velocities and the Phase Velocities from the C-5 Dispersion Curve at Array 3A with Long Receiver Spacings (Phase Velocity Normalized by Reference Velocity versus Receiver Spacing Normalized by Wavelength = SWR)

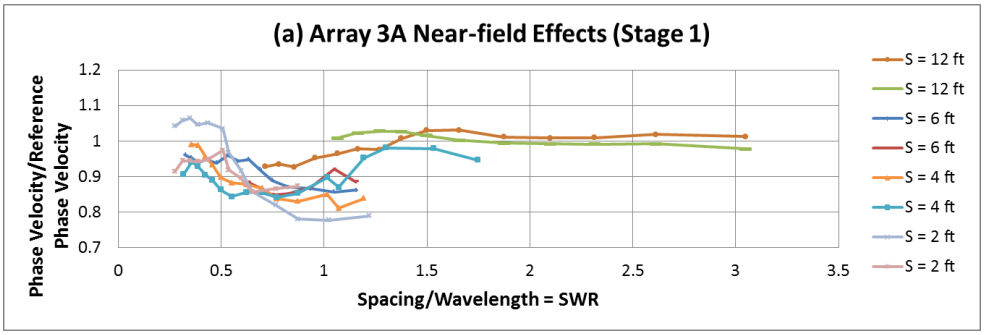

Figure 3.26 Comparison of the Reference Averaged Phase Velocities and the Phase Velocities from the C-5 Dispersion Curve at Array 3A with Short Receiver Spacings (Phase Velocity Normalized by Reference Velocity versus Receiver Spacing Normalized by Wavelength = SWR)

3.5 SUMMARY

To evaluate potential errors associated with near-field effects, reference averaged phase velocities that can be shown without including near-field effects are required for the comparison. Reference averaged phase velocities were determined by averaging the C-R field dispersion curve which was calculated with field data measured at phase greater than 360° to the maximum (1 λ-to-Min-Useable λ) phase difference from each spacing. For determination of the reference averaged phase velocity curve, field C-1, -2, -3 and -4 dispersion curves were plotted on the same graph and checked the goodness-of-fit to validate the reference values. The field C-5 dispersion curve was analyzed using an extended masking procedure that included data with $\emptyset < 360°$ even $\emptyset < 180°$ which was believed to contain near-field data. Phase velocities taken from reference averaged phase velocity versus wavelength curve and the field Case 5 dispersion curve at same wavelength were compared and plotted in terms of wavelength and also in terms of wavelength normalized by the receiver spacing. These two type graphical presentation were created for each SASW array at the VEGP sites. Clearly near-field effects are captured in these figures which are discussed in Chapter 4 and 5.

CHAPTER 4 : STAGE 1 IN UNIT 3 AT VOGTLE ELECTRIC GENERATING PLANT (VEGP) SITE

4.1 SITE DESCRIPTION

SASW testing was performed during construction of a 90-ft thick fill at the Vogtle Electric Generating Plant (VEGP) at different stages during the backfilling operation. Sets of SASW tests were conducted at each of four backfilling stages when the fill was about 25-, 45-, 73- and 90-ft thick. Figure 4.1 show a cross-section of the backfill at each of the four SASW testing stages.

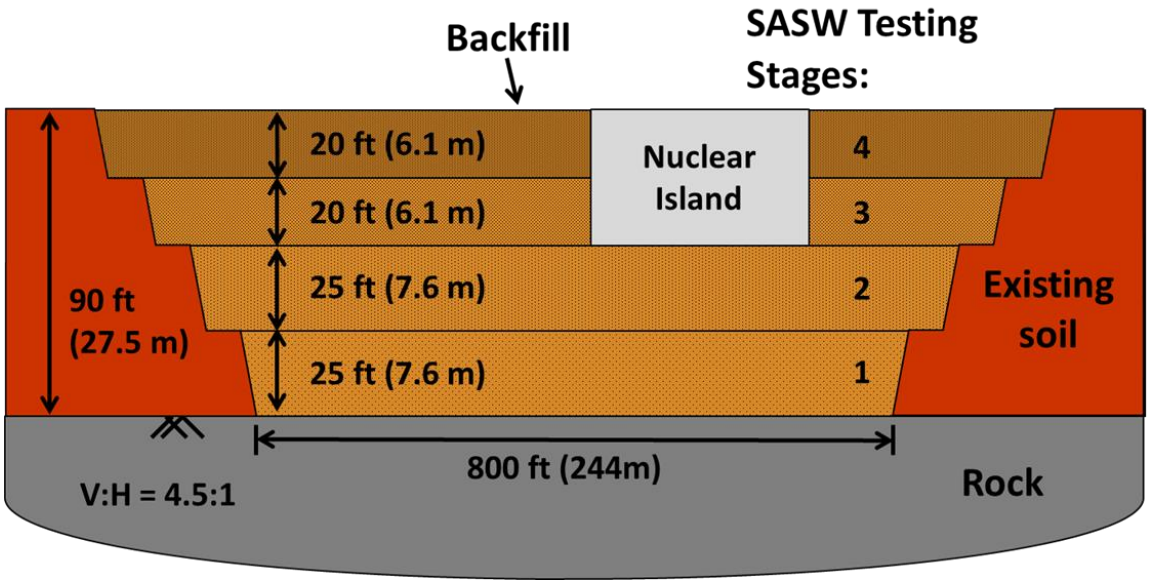

Figure 4.1 Cross-Section of Backfill at the Vogtle Electric Generating Plant (VEGP) Site (from Stokoe et al, 2013) Showing the Four SASW Testing Stages

Two new nuclear power plants, Units 3 and 4, were being constructed at the VEGP site. Hence, two identical fills were being placed. The fill material was a select silty sand that was available on site. Equal numbers of SASW tests were performed in each fill at each SASW test depth. Each site at Unit 3 and Unit 4 was excavated to the Blue Bluff Marl, located at a depth of approximately 90 ft below existing grade. After initial excavation was completed, the site was backfilled in 12-in. loose-thickness layers that were compacted to about 98% modified Proctor. SASW testing was performed at four stages (four fill thickness) after the fill reached prescribed thickness. The primary purpose of the SASW testing was to demonstrate that the backfill was achieving a shear wave velocity of at least 1,000 ft/sec at the base of the nuclear island when the backfill was completed at Stage 4 (90-ft thick fill). An aerial photograph is presented in Figure 4.2 of the Unit 3 and 4 at the construction site at a time between Stages 3 and 4.

Figure 4.2 Aerial Photograph Taken by Southern Company of Units 3 and 4 at the Vogtle Electric Generating Plant Site (from Stokoe et al, 2013)

The VEGP site was selected for this study of near-field effects for several reasons. First, due to the importance of the facility, this site was thoroughly investigated in terms of geotechnical properties. Second, the sites of Units 3 and 4 were initially excavated to the Blue Bluff Marl (BBM), and then carefully backfilled. As a result, the exact depth of the BBM is known. Third, dynamic laboratory tests using the resonant column method were also performed as part of the overall characterization of the backfill material. Finally, the sites are particularly well suited for this study because two types of soil profiles can be studied in terms of near-field effects as follows: (1) the normally dispersive soil profile above the BBM and (2) the "soft backfill" layer on the top of the stiffer BBM layer. The importance of each change in the V_s profile on near-field effects is considered herein.

Two sets of data at fill thickness of 25 and 45 ft were evaluated in this thesis research to study near-field effects. In this chapter, SASW testing data from Stage 1 (25-ft thick fill) at Unit 3 is evaluated in terms of near-field effects. In the next chapter, Chapter 5, the SASW test data from Stage 2 (45-ft thick fill) are presented.

4.2 SASW TESTING AT STAGE 1

Ten SASW test arrays were performed in Stage 1 (25-ft thick backfill) at Unit 3. As in Stage 1, the clearness of the data was excellent so six SASW arrays (3A, 3B, 3C, 3F, 3G, 3I) from Stage 1 were selected for this study of near-field effects simply to save time. Also, in the case of Arrays 3D, 3E and 3J, each array was located near the edge of the fill. Therefore, any influence of the near-by material was removed from this study by simply not considering these arrays. The locations of the arrays in Stage 1 at Unit 3 are shown in Figure 4.3.

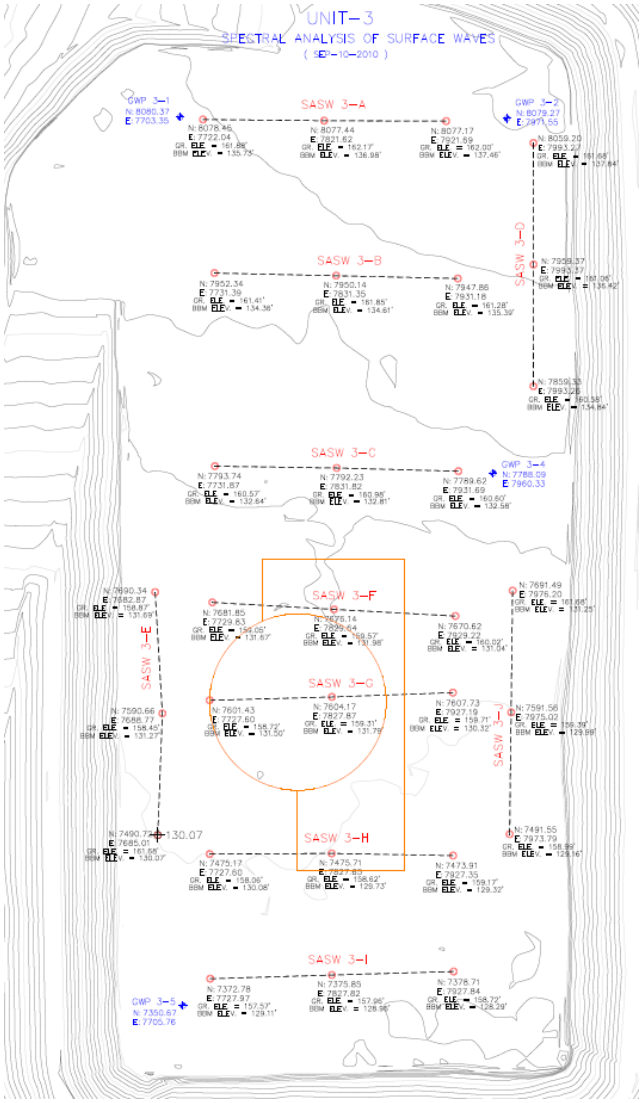

Figure 4.3 SASW Test Arrays in the Unit 3 Backfill at the Vogtle Electric Generating Plant Site in Stage 1 (Fill Thickness ≅ 25ft)

General receiver spacings in this project were 2, 4, 6, 12, 15, 30, 50 and 100 ft. These spacings allowed a reliable field dispersion curves to be developed due to extensive overlapping individual dispersion curves. (An individual dispersion curve is defined as one developed from a single receiver pair.) For the shorter-wavelength

measurements, shorter than the 15-ft receiver spacing, a hand-held hammer was used for the impact source. For the longer-wavelength measurements equal to or, longer than the 15-ft spacing, a Caterpillar D9 Bulldozer was used as the active source.

Due to the shear wave velocity profile in the compacted backfill, this site exhibits a normally dispersive velocity profile above the depth of the BBM. In this zone, the stiffnesses of all layers increase with depth and there are no significant jumps in V_s from one later to the next. At the top of the BBM, there is a significant increase in the velocities in the profile as shown in Figure 4.4. However, in this figure, it is hard to identify the top of the BBM which does have a smooth transition zone over for about 15 ft. Therefore, the comparison in velocities is helped with the V_s profiles determined by resonant column (RC) testing reconstituted specimens of the backfill.

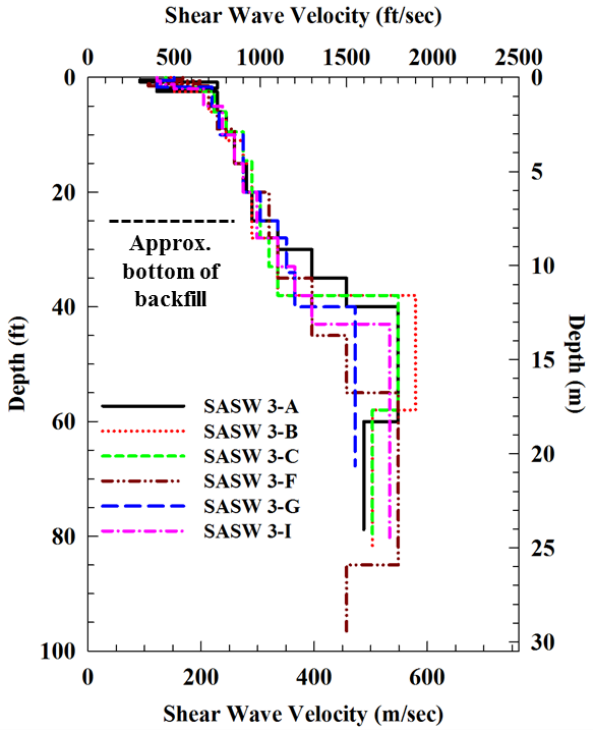

Figure 4.4 Six V_s Profiles from SASW Testing in Stage 1; Unit 3 at Vogtle Electric Generating Plant Site

As shown in Figure 4.5, shear wave velocities from the SASW tests begin to deviate from the laboratory determined V_s curve supporting the depth of the BBM that is known to be approximately at 25 ft below the testing surface at this time.

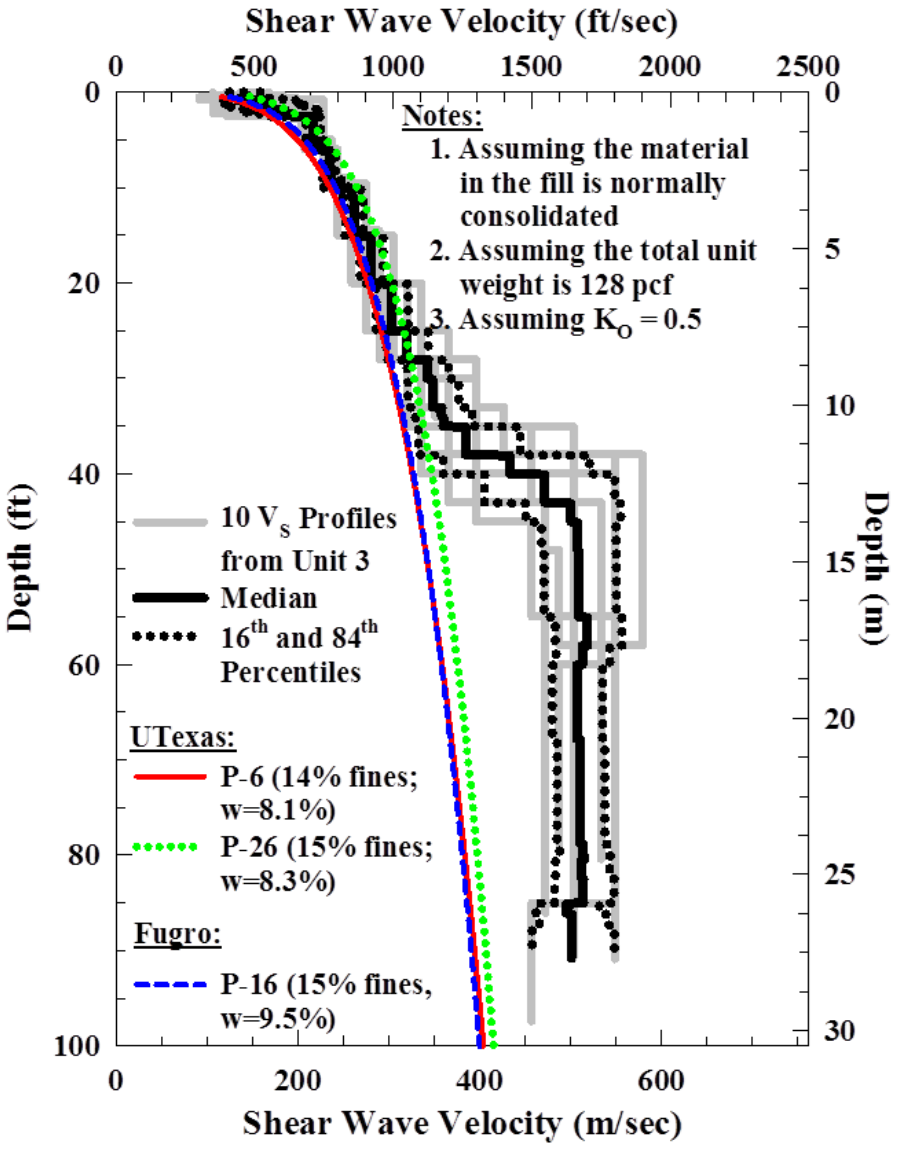

Figure 4.5 Comparison of V_s Values Determined by Laboratory Resonant Column Tests with Backfill Material and V_s Profiles Determined from SASW Tests at Stage 1 (from Stokoe et al, 2013)

4.3 ANALYSIS OF SASW DISPERSION DATA COLLECTED IN STAGE 1

Reference averaged phase velocity versus wavelength curves (V_R vs λ) were generated using a moving average over the field reference case (C-R) dispersion curve as discussed in Chapter 3. The goodness-of-fit of the C-R dispersion curve determined at Array 3A in Stage 1 is shown in Figure 3.6. This curve is compared with the field cases C-1 through C-5 dispersion curves in Section 3.2. All values are approximately in the ±5% range, so that the reference averaged velocity versus wavelength curve at this stage is considered to be validated as a reference value. The reference averaged phase velocity versus λ curve and comparisons with field cases C-1 through C-5 dispersion curves at each Array in Stage 1 are attached in the Appendix A.

In Stage 1, the depth of the BBM was approximately at 25 ft. This depth to the top of the BBM was also confirmed by the comparison between the laboratory Vs depth relationships and the field V_s profiles. Before any analysis of the near-field effects, it is important to understand how the dispersion curve is influenced by the stiff material (BBM) below the normally dispersive V_s profile in the soil layer. To understand the influence of the BBM, the field C-R dispersion curves at Stage 1 and theoretical dispersion curve generated with shear wave velocities from Resonant Column test (P-26) are compared in the Figure 4.6. As seen in the figure, the depth of about 25 ft to the BBM at Stage 1 was captured in the zone where field wavelengths around 50 ft have phase velocities that begin to exceed the predicted dispersion curve using the resonant-column predicted V_s profiles. (The RC V_s profile was used in WinSASW to generate a dispersion curve.) The need for a considerably longer wavelength than the 25-ft fill thickness is due to the way surface waves stress the subsurface as discussed below.

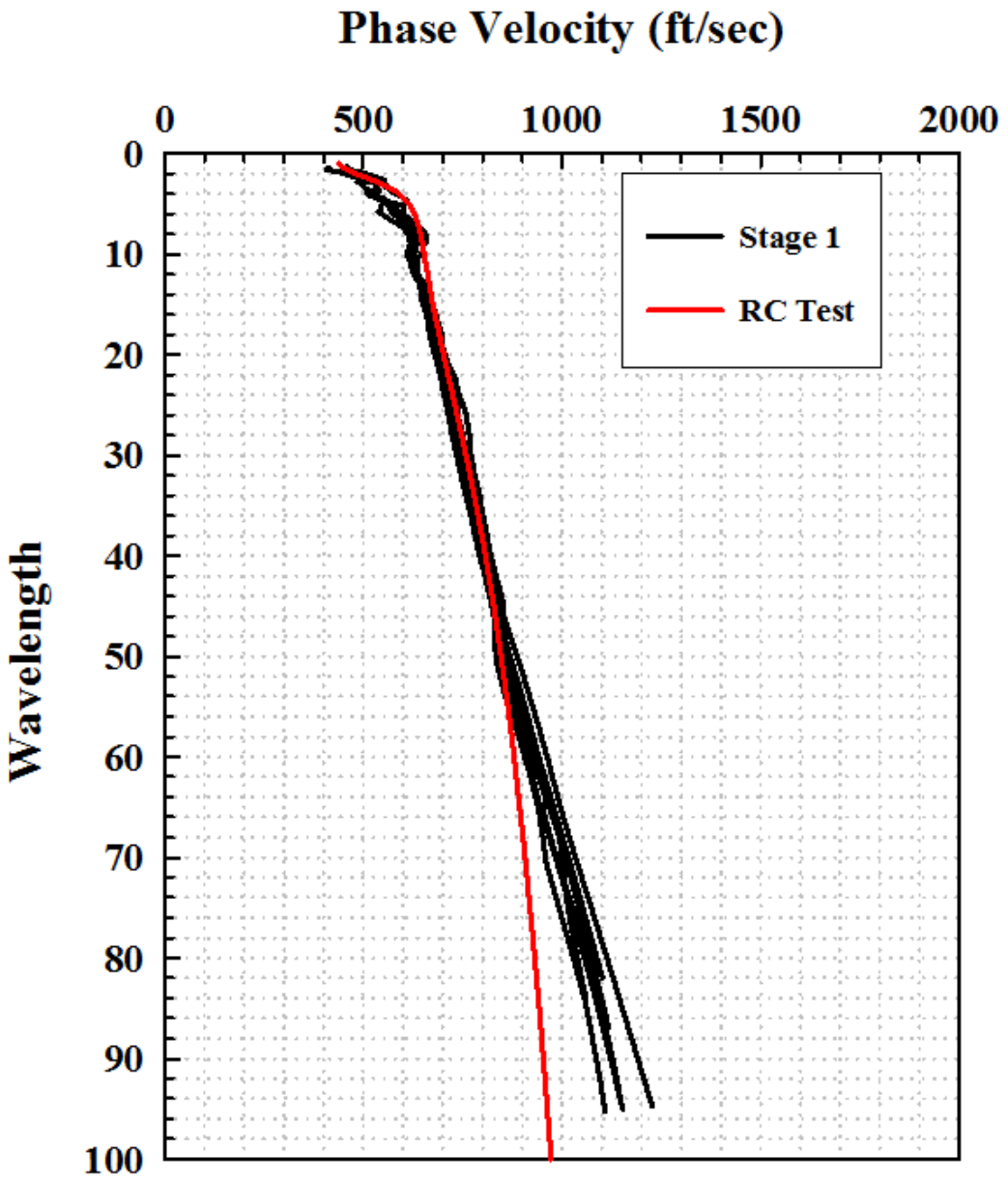

Figure 4.6 Comparison of the the Stage 1 Field C-R Dispersion Curves and the Theoretical Dispersion Curve Generated Using WinSASW with the Shear Wave Velocity Profile from Resonant Column Test on Reconstituted Backfill Material

Rayleigh waves stress a zone in the soil profile as illustrated in Figure 4.7. Although the 50-ft long wavelength samples (stresses) the BBM, the bulk of the stressing occurs in the upper half (say 25 ft in this case) of the stressed zone so that this section often controls the V_s values. The upper 25-ft in this case is completely in the softer backfill layer. Therefore, it is hard to distinguish the influence of the BBM. When the wavelength is about twice the depth to the BBM, the dispersion curve began to sense the difference in the stiffness of the material. Therefore, in terms of near-field effect, the focus in this part of the research study needs to be on phase velocity of wavelengths at about 50 ft and longer to investigate how near-field effects arise due to the existence of the BBM.

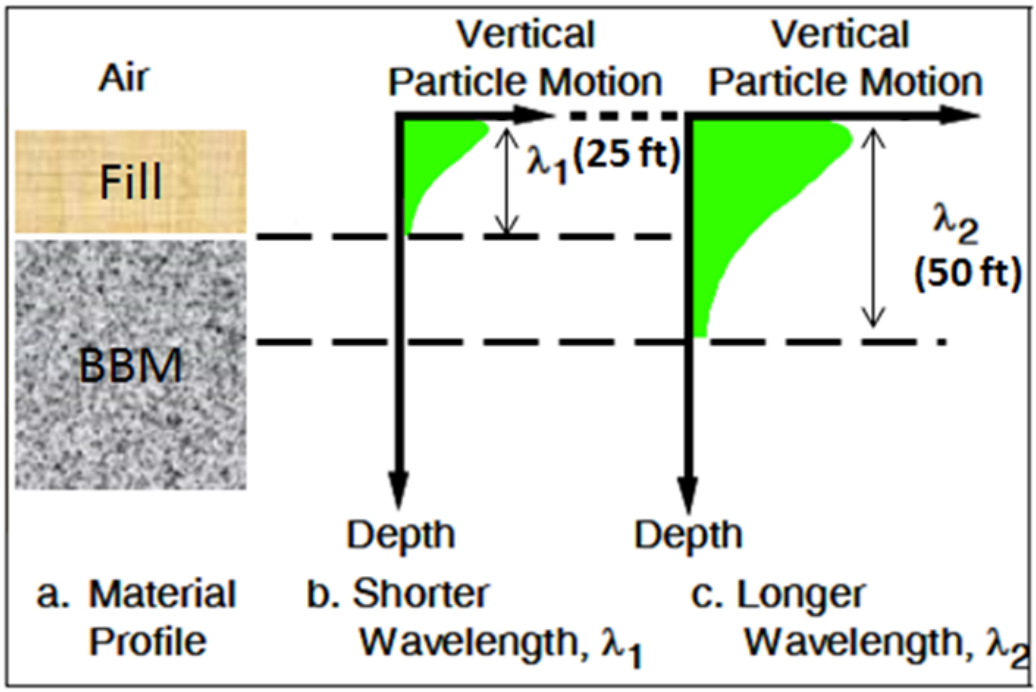

Figure 4.7 Illustration of Surface Waves with Different Wavelengths Sampling Different Materials in a Layer System (from Stokoe et al, 2005)

4.3.1 ANALYSIS OF SASW DISPERSION DATA COLLECTED IN THE BACKFILL LAYER IN STAGE 1

As shown in Figure 4.6, wavelengths in SASW dispersion curve that are less than about 50 ft show no effect of the BBM. Therefore, to study near-field effects in the normally dispersive Vs profile of the backfill, only wavelength data with $\lambda \leq 50$ ft were used. These figures, in terms of normalized phase velocity versus wavelength, are presented in Figures 4.8 and 4.9.

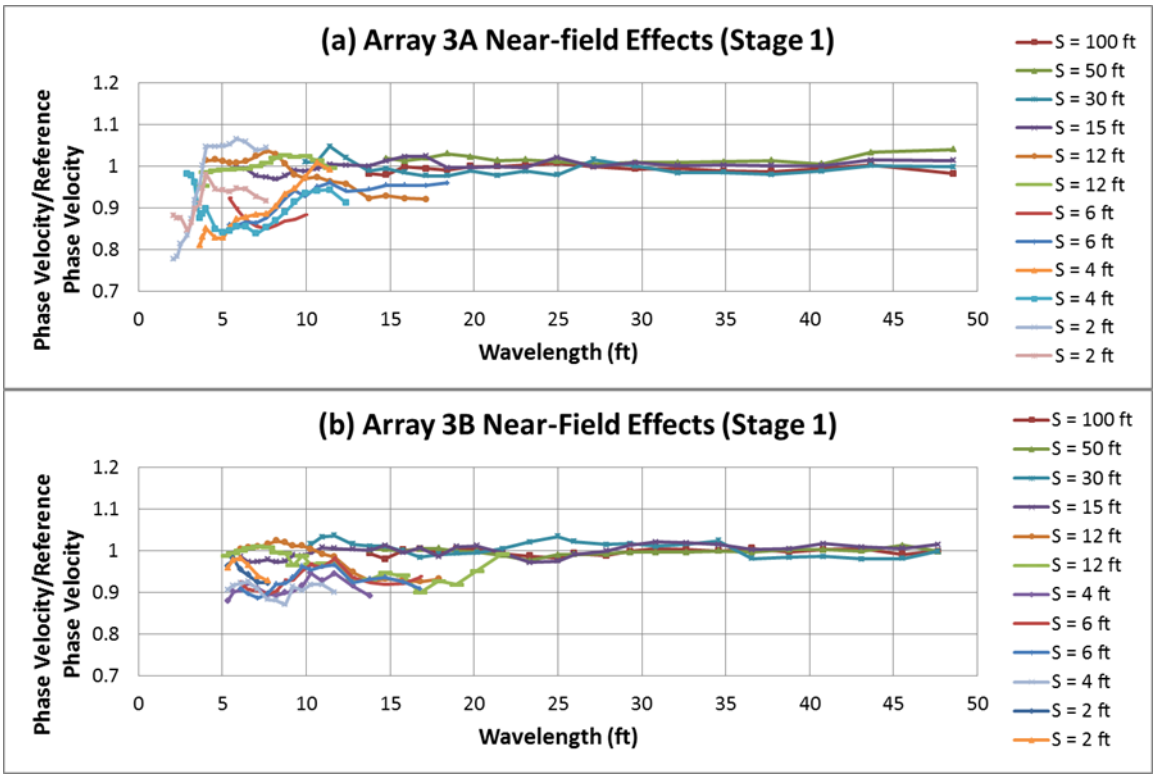

Figure 4.8 Near-Field Effects in the Stage 1 Fill Captured in Normalized Phase Velocity vs Wavelength Data at Array 3A and 3B

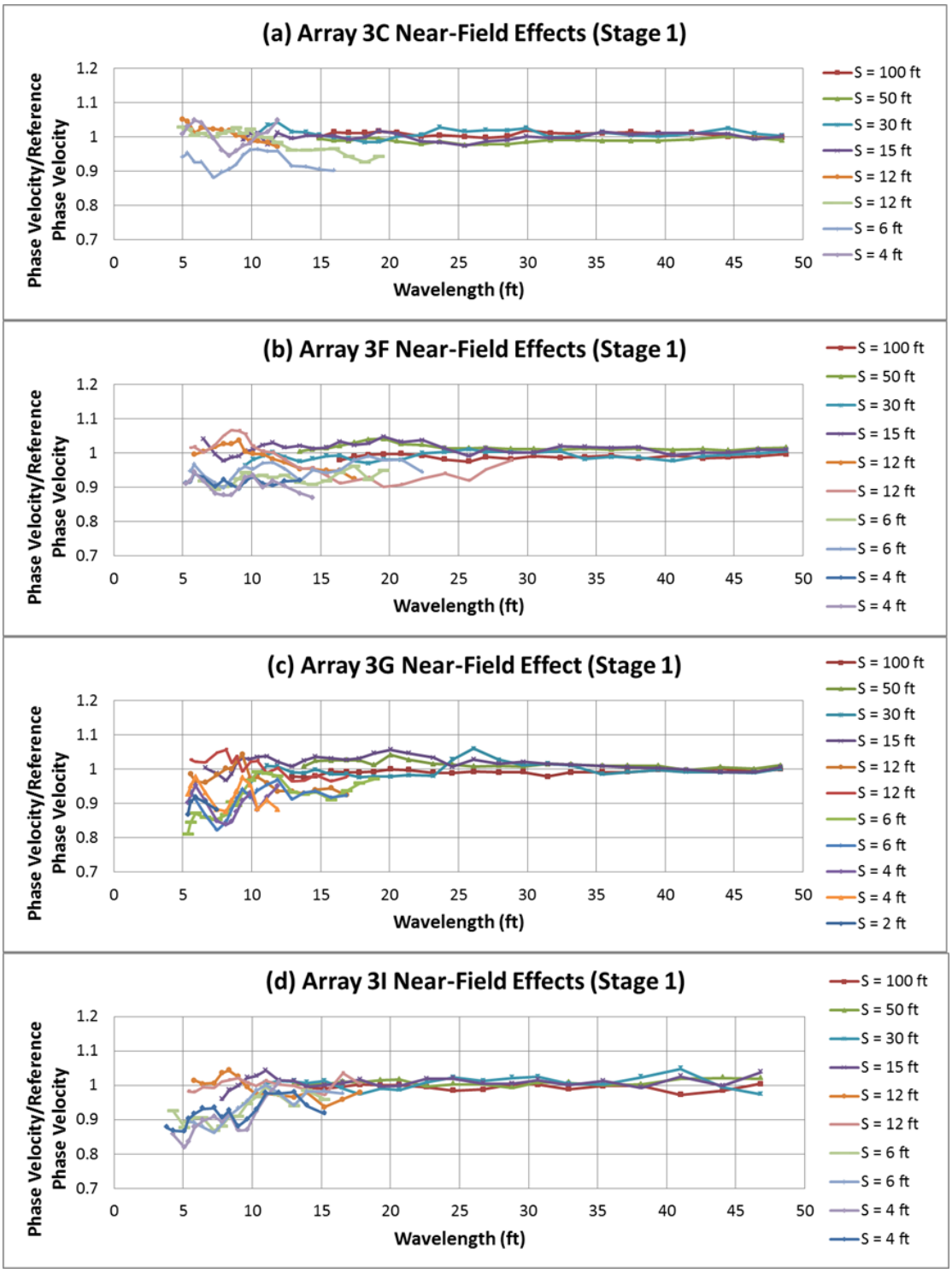

Figure 4.9 Near-Field Effects in the Stage 1 Fill Captured in Normalized Phase Velocity vs Wavelength Data at Array 3C, 3F, 3G and 3I

All results in the two figures for S = 15 to 100-ft receiver spacings show the same tendency. There are no influences of near-field effects at the S = 15- to 100-ft receiver spacing. Shorter than 50-ft wavelength phase velocity which mainly stresses the 25-ft thick backfill, magnitude of error associate with near-field effect is less than 5% at 15-, 30-, 50- and 100-ft receiver spacings. This indicates there is no significant influence of near-field effects where the stiffness of layer gradually increased with depth. (normally dispersive soil.)

It is easier to evaluate the magnitude of error associated with near-field effect at receiver spacing 15, 30, 50 and 100-ft by looking at Figures 4.10 and 4.11. For the spacing to wavelength ratio (SWR) < 1, indicates the interference of the near-field effects, wavelength is longer than the receiver spacing.

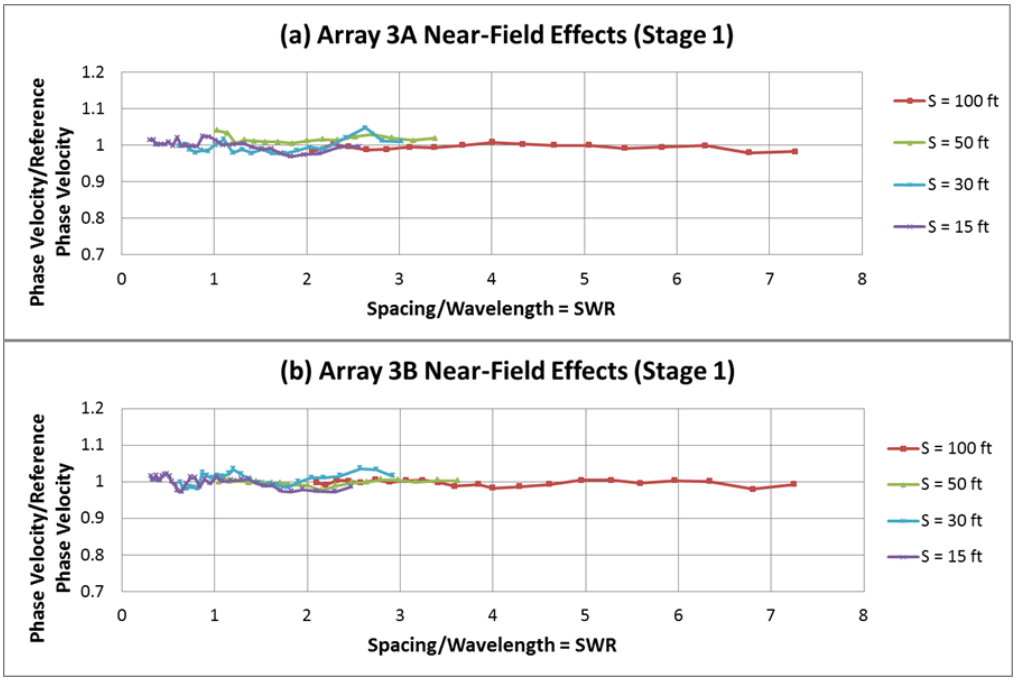

Figure 4.10 Near-Field Effects in the Stage 1 Fill Captured in Normalized Phase Velocity vs SWR at Array 3A and 3B with 100, 50, 30 and 15-ft Receiver Spacing

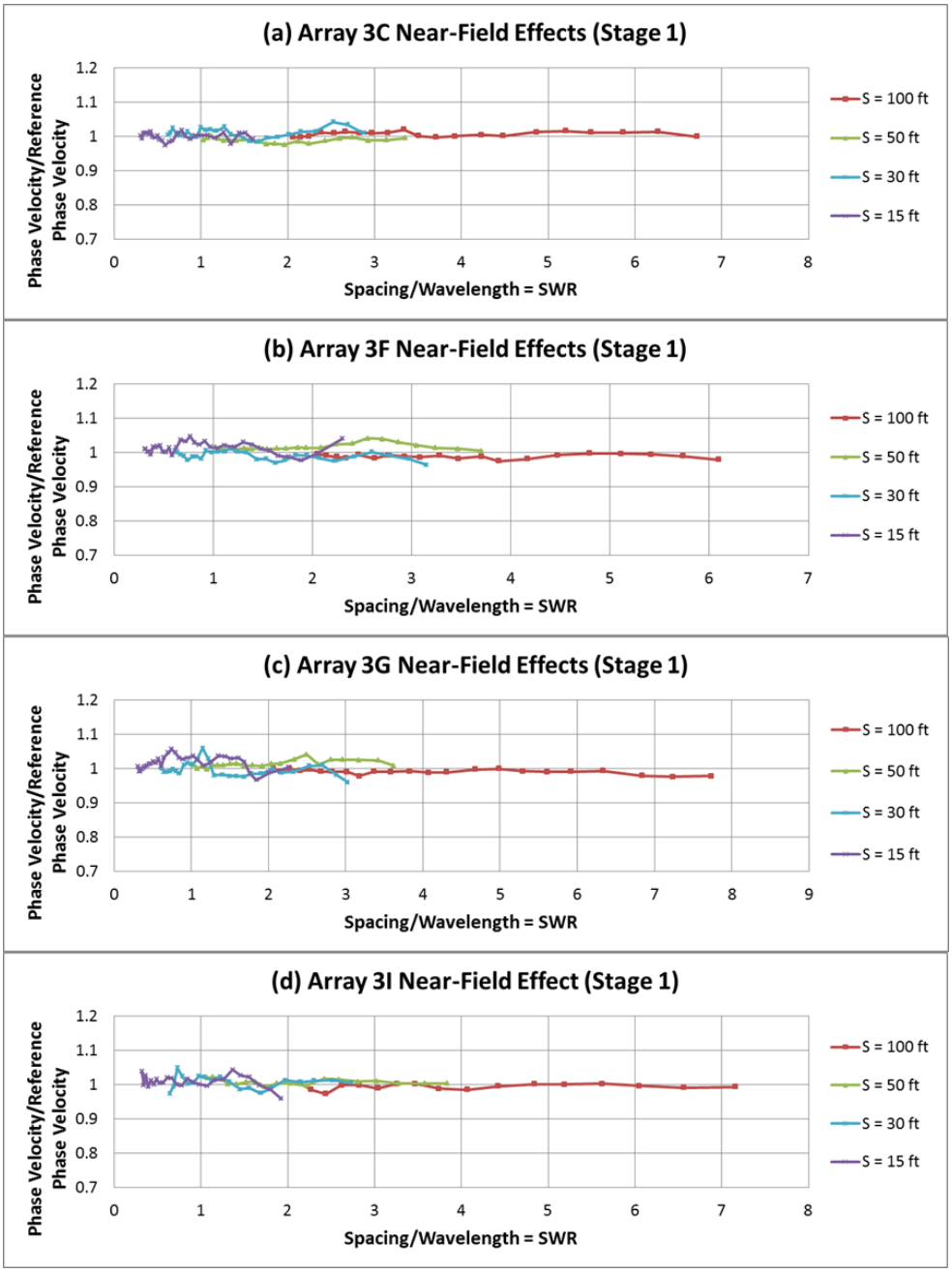

Figure 4.11 Near-Field Effects in the Stage 1 Fill Captured in Normalized Phase Velocity vs SWR at Array 3C, 3F, 3G and 3I with 100, 50, 30 and 15-ft Receiver Spacing

All receiver spacings exhibit the magnitude of error associated with near-field effect less than 5%, as shown in Figures 4.10 and 4.11.

To study the near-field effect at short spacing, Figures 4.12 and 4.13 are created. As shown in Figures 4.12 and 4.13, phase velocity calculated with 360º phase difference (1 λ) from each receiver spacing already underestimate the phase velocity, indicating case C-1 filtering criteria cannot be used in short receiver spacing where the largest contrast of V_s layers exist.

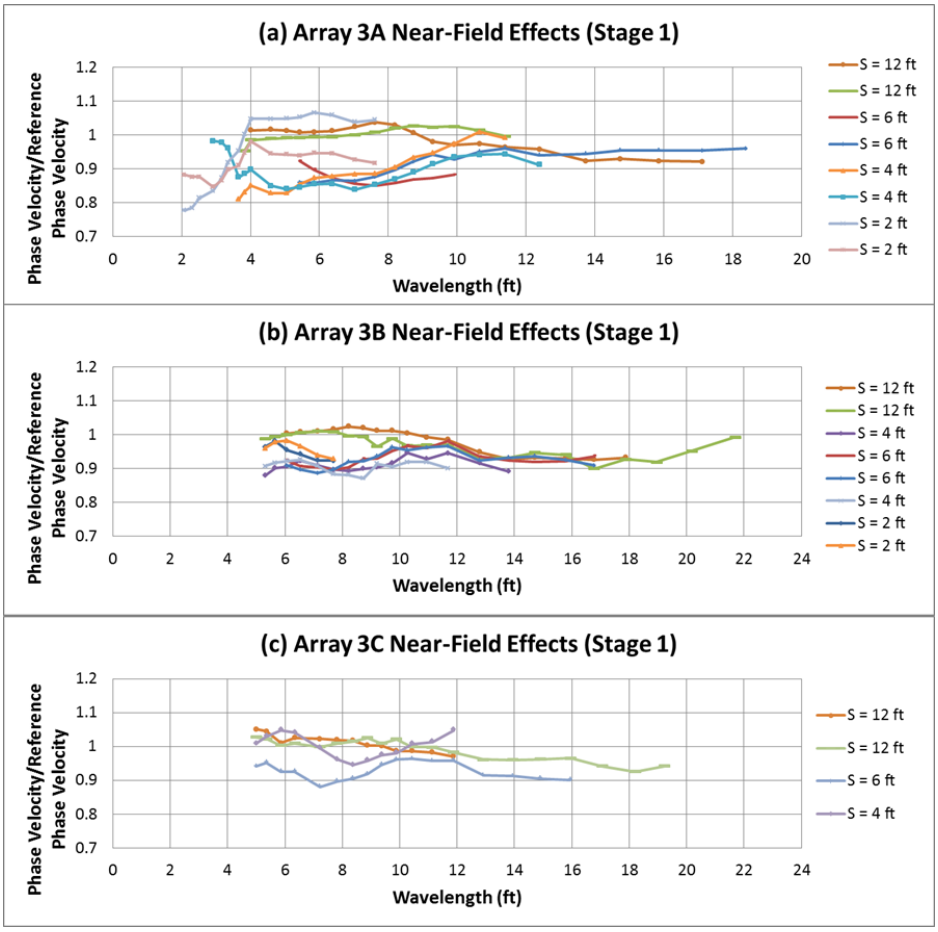

Figure 4.12 Near-Field Effects in the Stage 1 Fill Captured in Normalized Phase Velocity vs Wavelength Data at Array 3A, 3B and 3C with Short Receiver Spacing

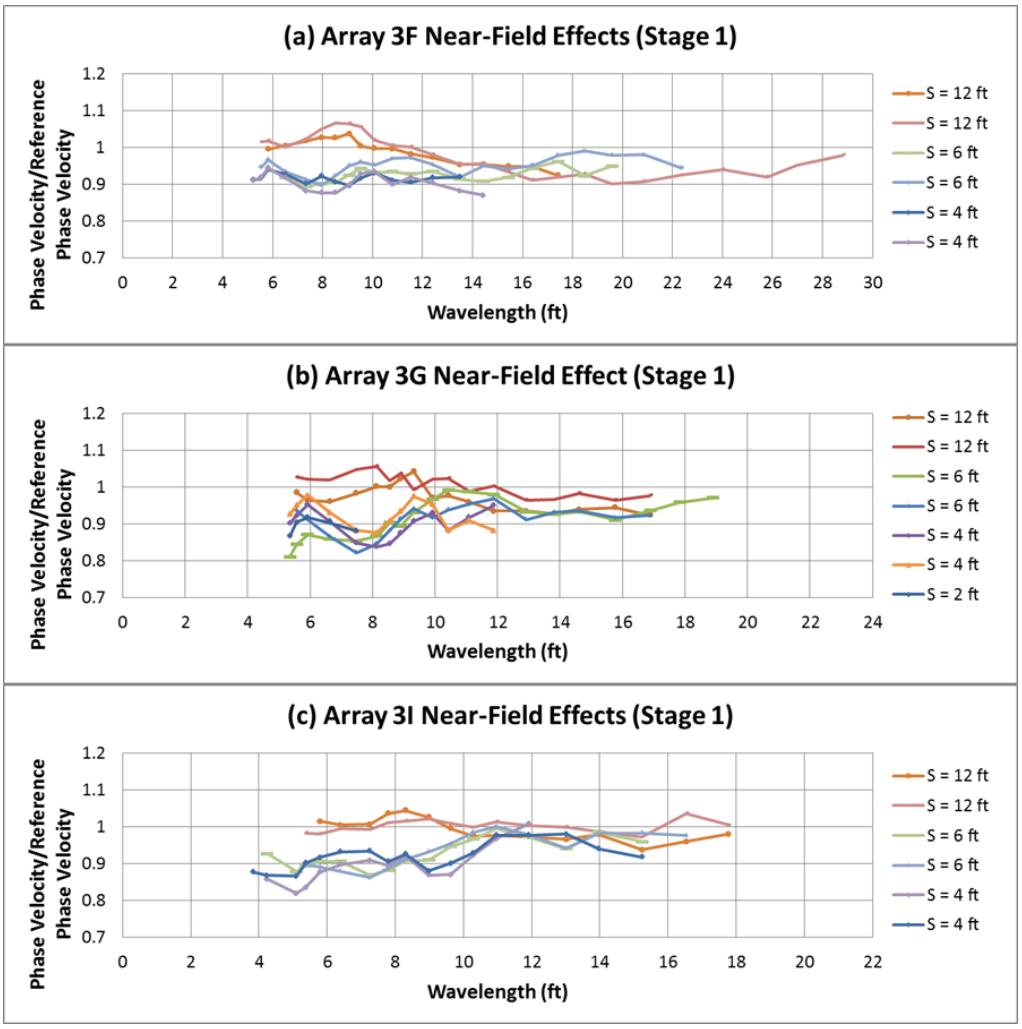

Figure 4.13 Near-Field Effects in the Stage 1 Fill Captured in Normalized Phase Velocity vs Wavelength Data at Array 3F, 3G and 3I with Short Receiver Spacing

As shown in Figures 4.12 and 4.13, the magnitude of error is more than 10%, even by as much as 20%. Also the magnitude of error associated with near-field effects increase as the receiver spacing decrease. This is because, the contrast of the shear wave velocity profile is larger at the shallow layer. Shear wave velocity ratio from surface to the depth of 10 ft is approximately 1.84 and from the depth of 10 to 25 ft is 1.17, respectively.

It is easier to evaluate the magnitude of error associated with near-field effect at receiver short spacing by looking at Figures 4.14 and 4.15 where less than SWR value 1 indicates the interference of the near-field effects.

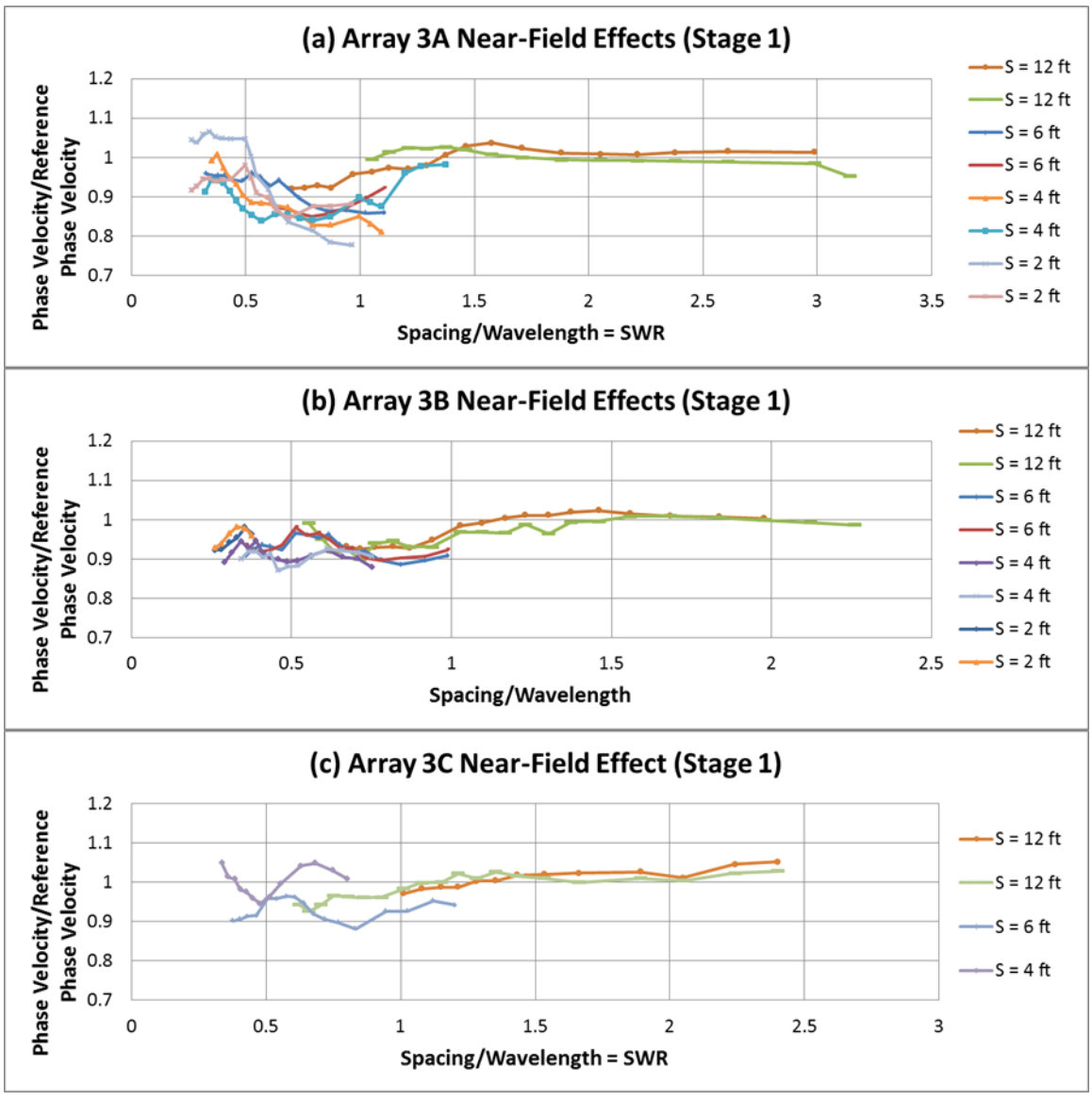

Figure 4.14 Near-Field Effects in the Stage 1 Fill Captured in Normalized Phase Velocity vs SWR at Array 3A, 3B and 3C with Short Receiver Spacing

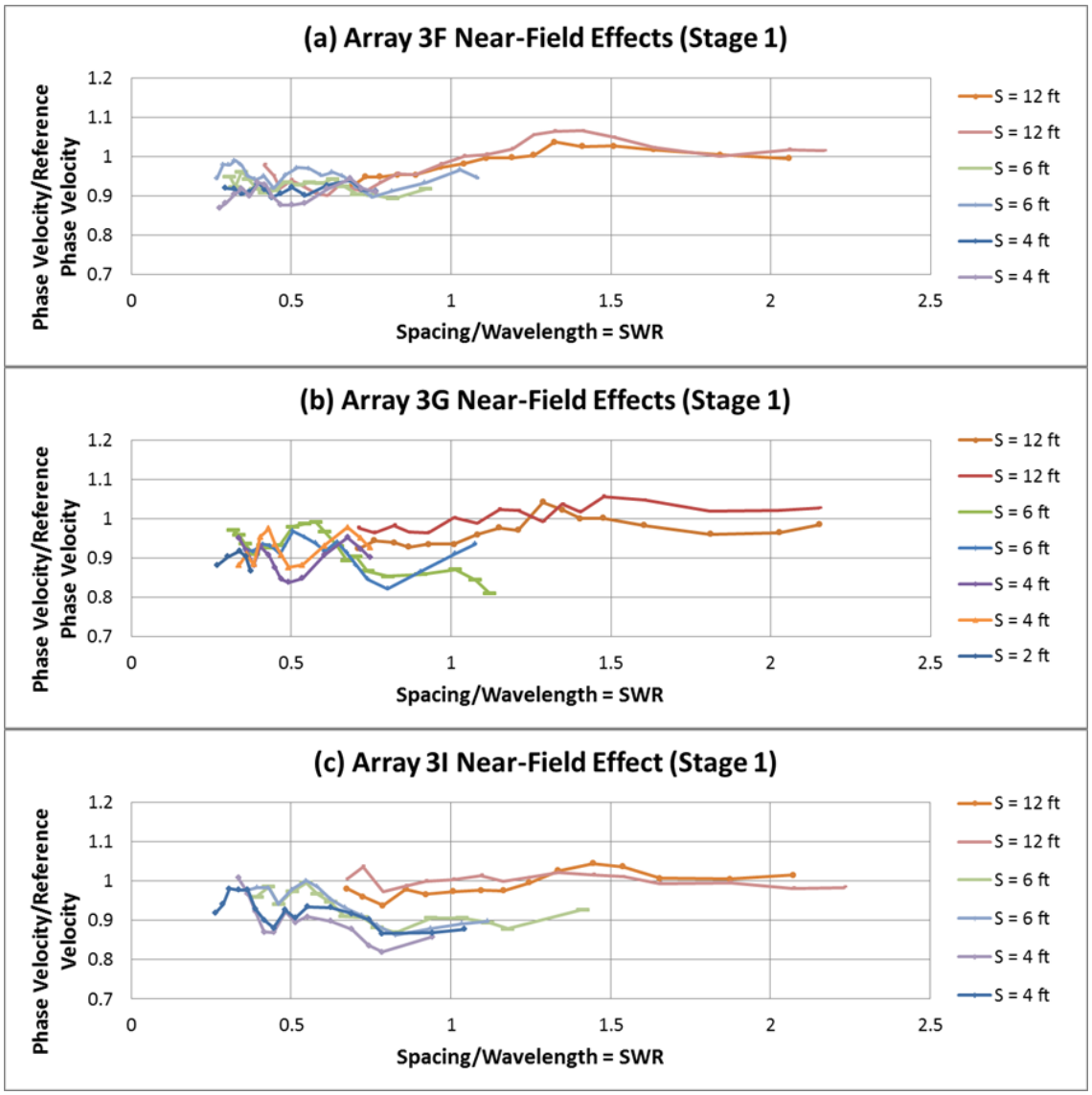

Figure 4.15 Near-Field Effects in the Stage 1 Fill Captured in Normalized Phase Velocity vs SWR at Array 3F, 3G and 3I with Short Receiver Spacing

At the SWR value of 1 where the phase velocity calculate with 360º phase difference (1 λ) from each receiver spacings already underestimate the phase velocity. This could be due to the near-field effect mainly at 2-, 4- and 6-ft receiver spacings. Therefore, cases C-2 or C-3 filtering criteria should be used to eliminate the near-filed effect in terms of short receiver spacings.

4.3.2 ANALYSIS OF SASW DISPERSION DATA COLLECTED IN THE BBM LAYER IN STAGE 1

To correlate the near-field effect with the contrast of V_s profile, the analysis is extended to the BBM layer below the normally dispersive V_s profile (25-ft backfill). Normalized phase velocity versus wavelength plots or normalized phase velocity versus normalized spacing plots are generated with maximum of 100-ft wavelength.

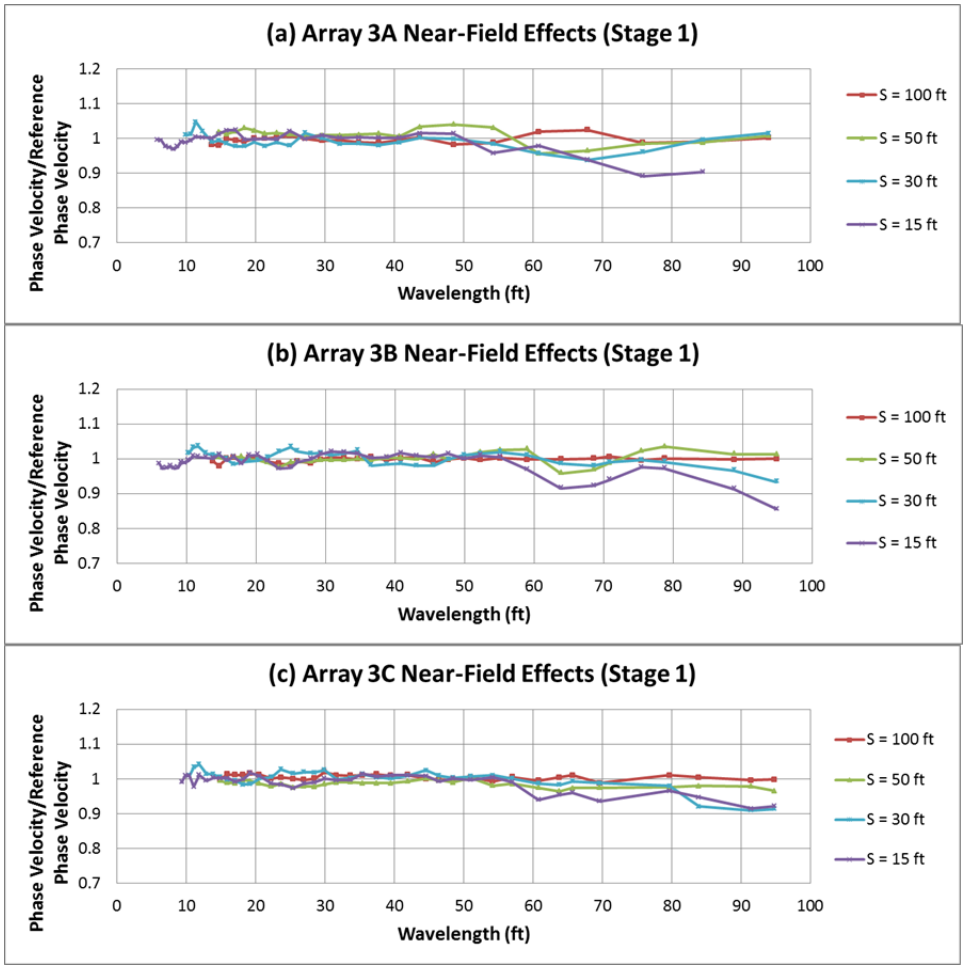

Figure 4.16 Near-Field Effects in the Stage 1 Fill Captured in Normalized Phase Velocity vs Wavelength Data at Array 3A, 3B and 3C

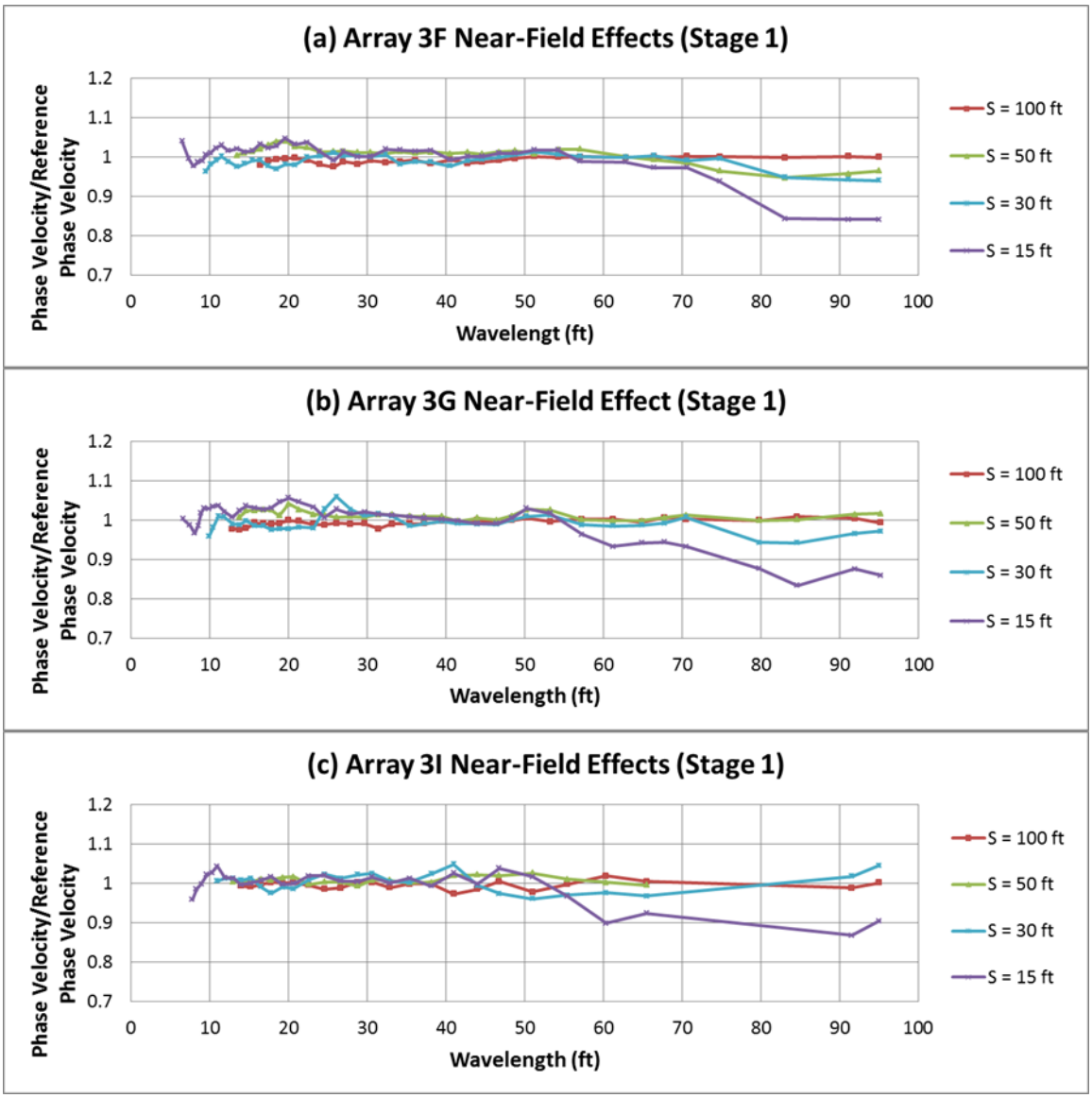

Figure 4.17 Near-Field Effects in the Stage 1 Fill Captured in Normalized Phase Velocity vs Wavelength Data at Array 3F, 3G and 3I

All results show the similar tendency. There are no influences of near-field effects at the 100 and 50-ft receiver spacing. The 30-ft receiver spacing begins to underestimate the phase velocity at the range of 50- to 70-ft wavelength. The 15-ft receiver spacing underestimates the phase velocity at 55-ft wavelength where exactly the BBM influences

the dispersion curve. This indicates that the near-field effects occur when the V_s profile have a large contrast. Below the 55-ft wavelength which mainly stresses the 25-ft thick fill, there is no influence of the near-field effect at 15, 30, 50 and 100-ft receiver spacing. However, when the wavelength became longer than the 55-ft the near-field effect begin to underestimate the true phase velocity. Especially when the receiver spacing is shorter than the depth of the stiff material like as the 15-ft receiver spacing, magnitude of error associate with near-field effect increases. In case of 30-ft receiver spacing, it is longer than the depth of the BBM, but still not enough to capture the 50-ft wavelength phase velocity where the BBM influence the dispersion curve. To capture the true phase velocity, the spacing should be at least longer than the two times the depth of the stiff material. As a suggestion, receiver spacing should be calculated as following;

$$\text{Receiver spacing} = \text{depth to stiffer} \times 2.5$$

If the spacing satisfies the suggestion, phase velocity calculated from 180^{o} phase difference ($0.5\ \lambda$) can be used as an estimation of the Vs profile which will be still in 10% range of error. It is easier to evaluate the magnitude of error associated with near-field effect by looking at Figures 4.18 and 4.19. For the spacing to wavelength ratio (SWR) < 1, indicates the interference of the near-field effects, wavelength is longer than the receiver spacing. All receiver spacings exhibit the magnitude of error associated with near-field effect less than 10%, except for 15-ft receiver spacing as shown in Figure 4.18.

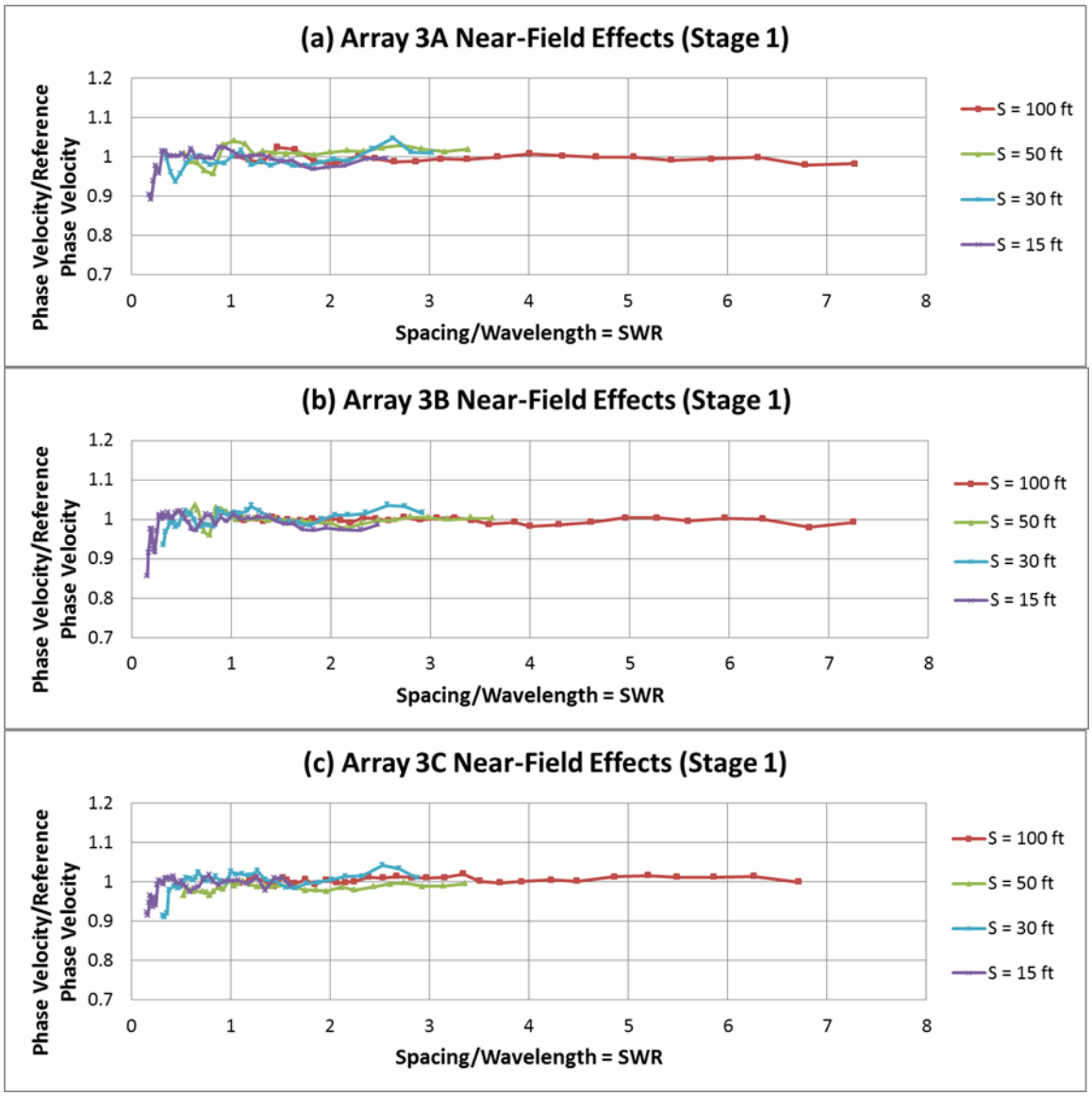

Figure 4.18 Near-Field Effects in the Stage 1 Fill Captured in Normalized Phase Velocity vs SWR at Array 3A, 3B and 3C with 100, 50, 30 and 15-ft Receiver Spacing

As shown in Figure 4.19, as same as Figure 4.18, all receiver spacing exhibit the magnitude of error associated with near-field effect less than 10%, except for 15-ft receiver spacing.

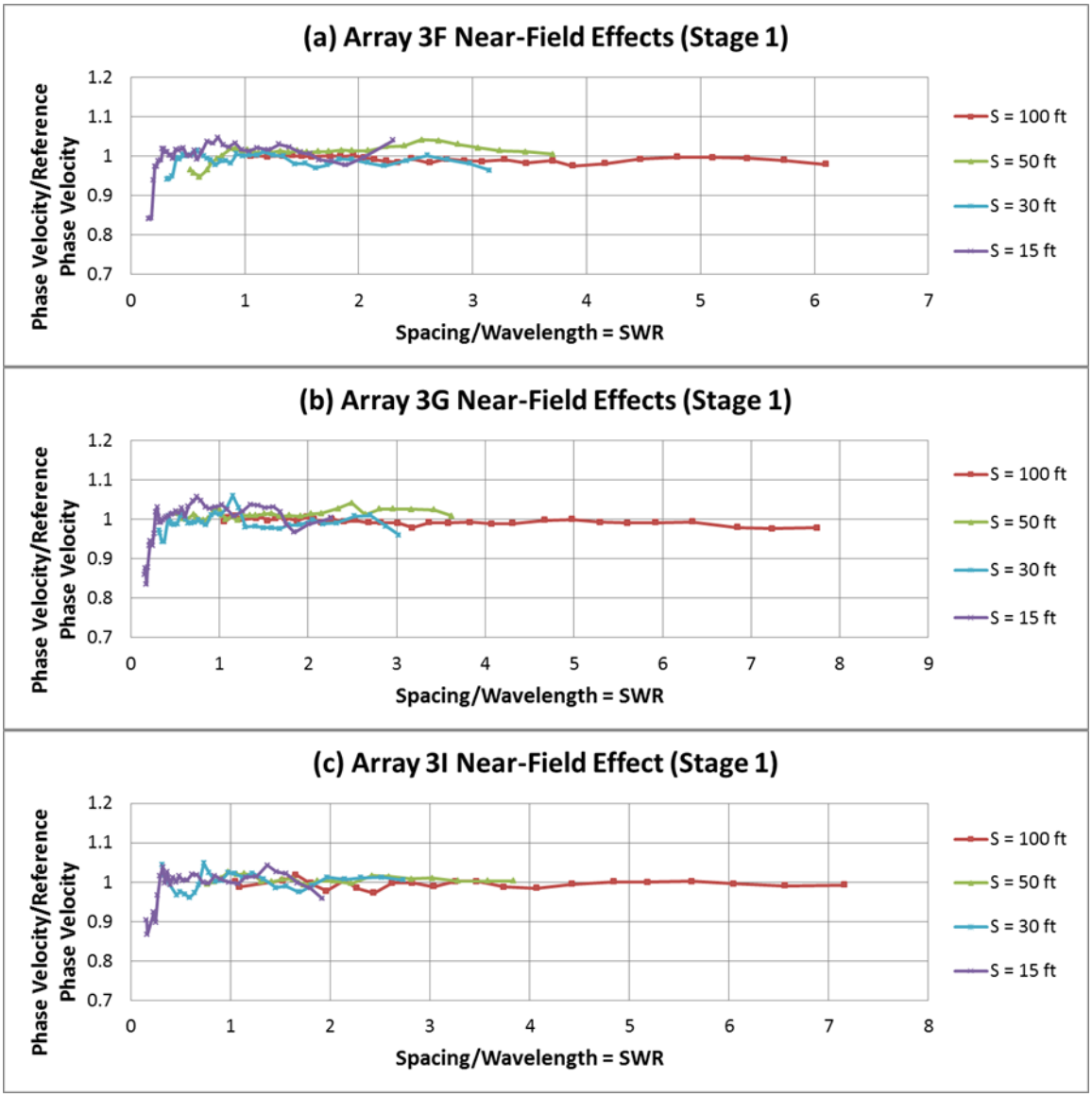

Figure 4.19 Near-Field Effects in the Stage 1 Fill Captured in Normalized Phase Velocity vs SWR at Array 3F, 3G and 3I with 100, 50, 30 and 15-ft Receiver Spacing

4.4 SUMMARY

SASW test data from Stage 1 (25-ft thick fill) at VEGP Site is analyzed in terms of near-field effects. Two types of soil profiles can be studied in this site; (1) the normally dispersive soil profile above the BBM and (2) the "soft backfill" layer on the top of the BBM layer. There is no influence of the near-field effects when the receiver spacing is longer than the twice of the depth of BBM. This indicates the near-field effects influence significantly when the wavelength longer than the receiver spacing reach at the layer with the large contrast of shear wave velocity. Below this layer (normally dispersive soil profile), there is no influence of near-field effect. In case of shorter receiver spacing, case C-1 filtering criteria cannot be used due to the large gradient of shear wave velocity in shallow layer. Therefore, the magnitude associate with near-field effects increases where the shear wave velocity have a large contrast.

CHAPTER 5 : STAGE 2 IN UNIT 3 AT VOGTLE ELECTRIC GENERATING PLANT (VEGP) SITE

5.1 SASW TESTING AT STAGE 2

Ten SASW test arrays were performed in Stage 2 (45-ft thick backfill) at Unit 3. As in Stage 2, the clearness of the data was excellent so six SASW arrays (3A, 3B, 3C, 3F, 3G, 3H) from Stage 2 at Unit 3 were selected to use in this study of near-field effects simply to save time. Also, in the case of Arrays 3D, 3E and 3J, each array was located near the edge of the fill. Therefore, any influence of the near-by material was removed from this study by simply not considering these arrays. The locations of the arrays in Stage 2 at Unit 3 are shown in Figure 5.1.

General receiver spacings in this stage were 2, 4, 6, 12, 20, 40, 60 and 120 ft. These spacings allowed reliable field dispersion curves to be developed due to extensive overlapping in the individual dispersion curves for the different receiver spacing. For the shorter-wavelength measurements, shorter than the 20-ft receiver spacing, a hand-held hammer was used for the impact source. For the longer-wavelength measurements, equal to or longer than the 20-ft spacing, a Caterpillar D9 Bulldozer was used as the active source.

As same with Stage 1, this site exhibits a normally dispersive shear wave velocity profile above the depth of the BBM. At the top of the BBM, there is a significant jump in the shear wave velocity profile (a factor of 1.5 to 1.7 times the V_s) as shown in the Figure 5.2. However, with the exceptions of small inversion at top of SASW arrays, the general trend in the Vs profile is still normally dispersive.

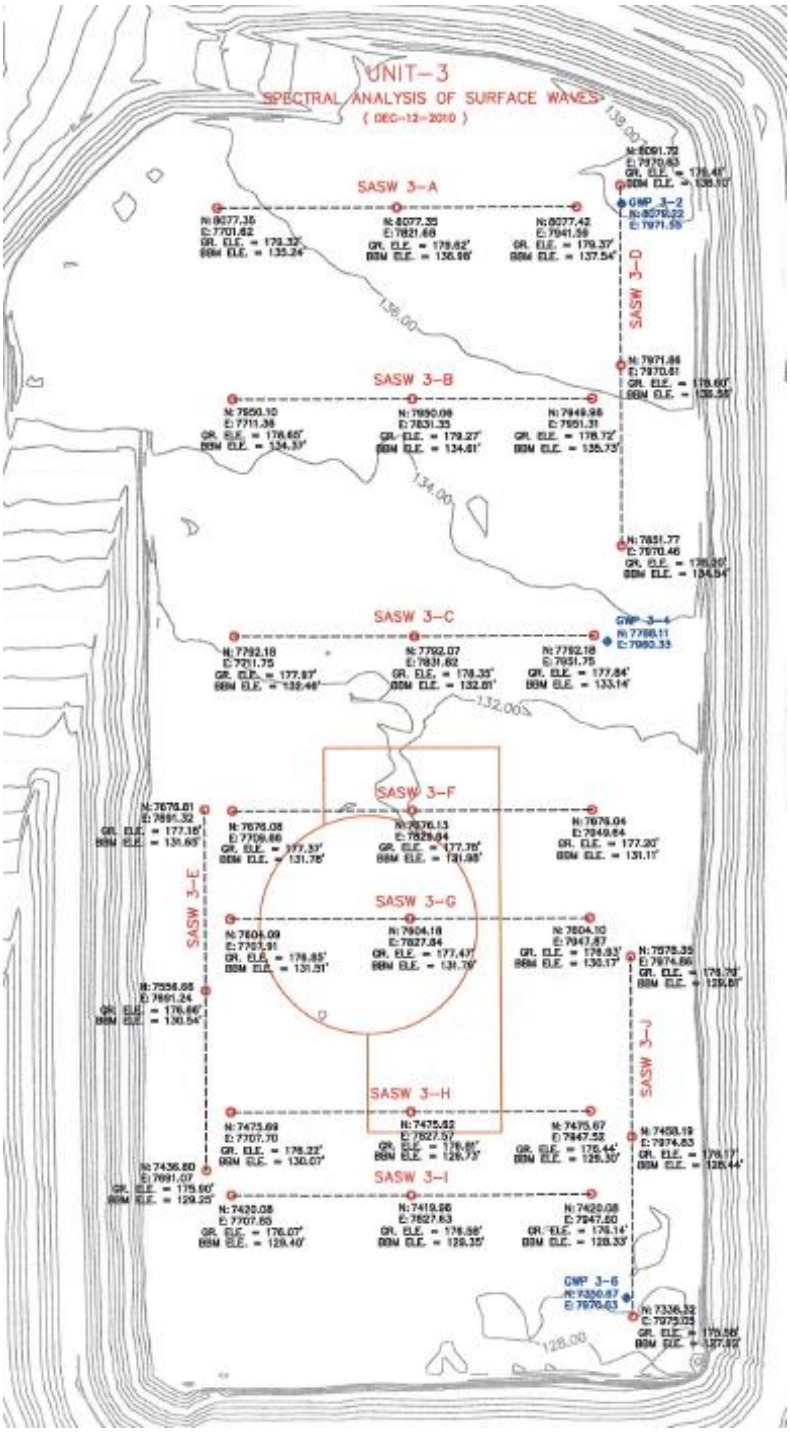

Figure 5.1 SASW Test Arrays in the Unit 3 Backfill at the Vogtle Electric Generating Plant Site in Stage 2 (Fill Thickness ≅ 45ft)

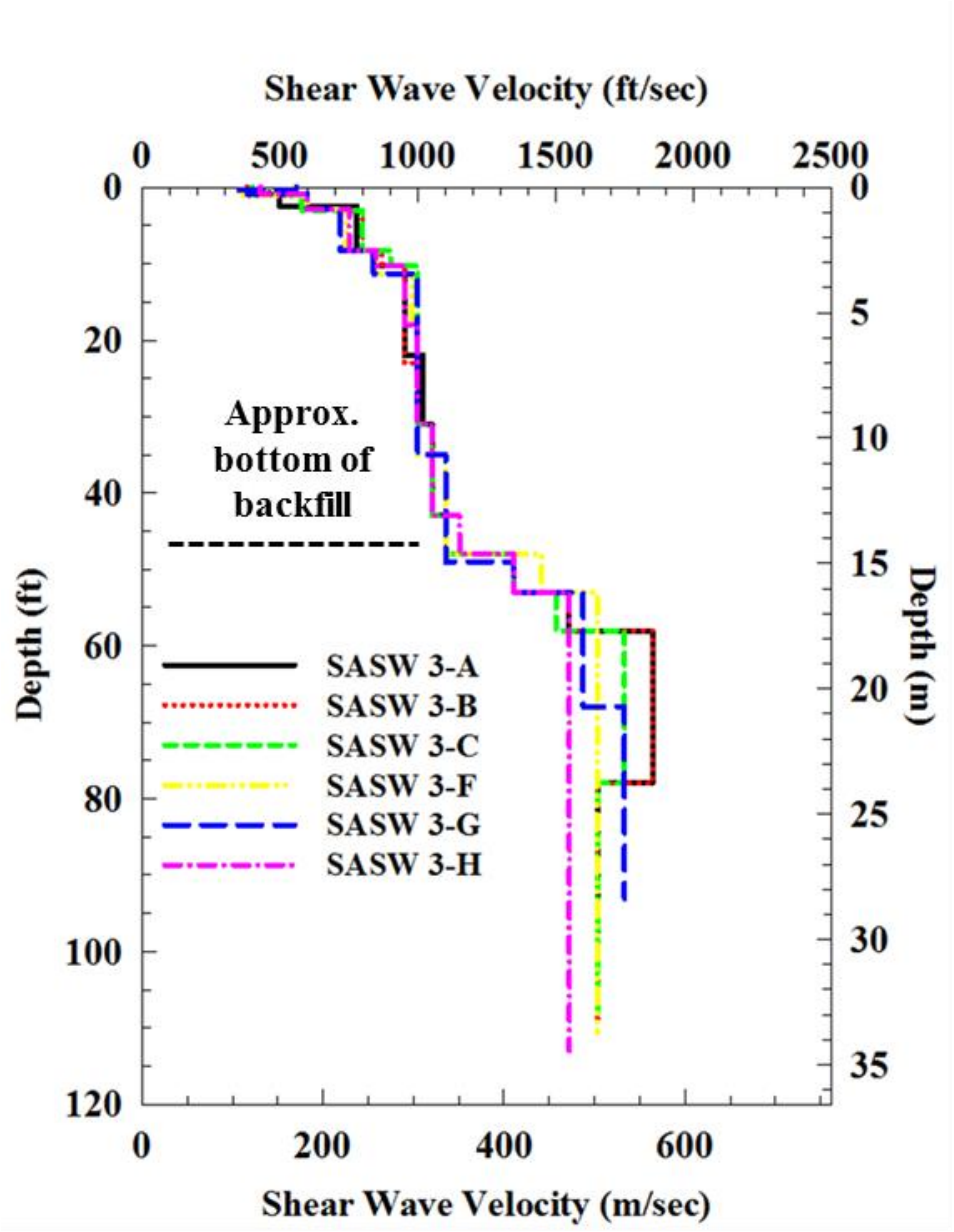

Figure 5.2 Six V_s Profiles from SASW Testing in Stage 2; Unit 3 at the Vogtle Electric Generating Plant Site

To identify the location of the BBM, the shear wave velocity profiles from SASW testing and Vs profiles determined by dynamic laboratory data from resonant column (RC) testing reconstituted specimens of the backfill are compared in Figure 5.3.

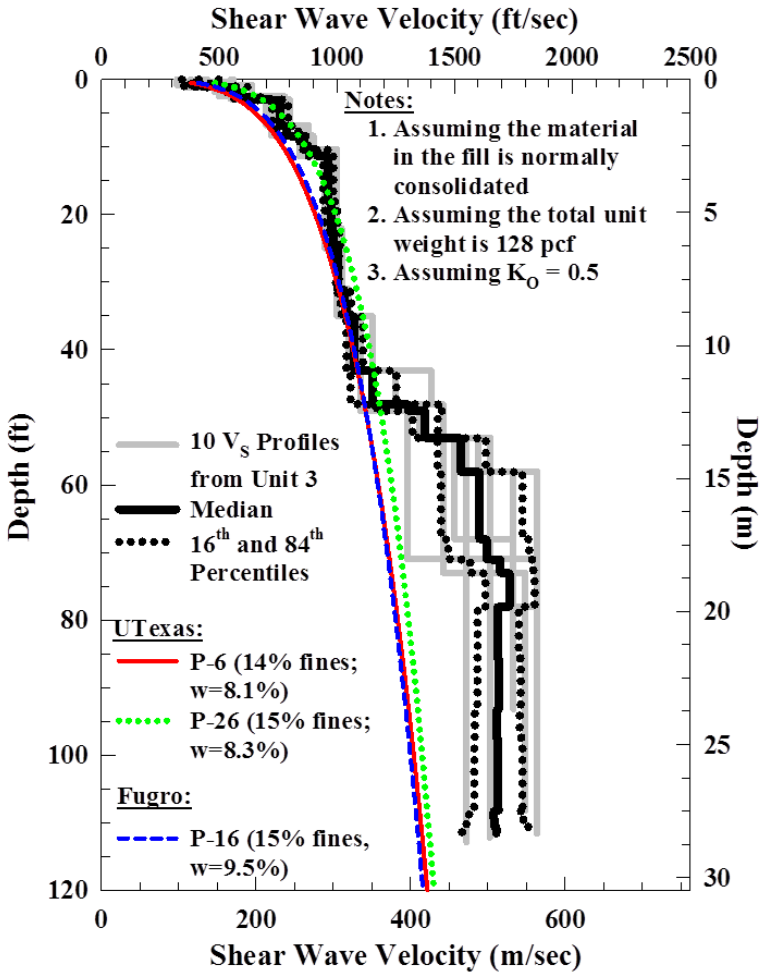

Figure 5.3 Comparison of V_s Values Determined by Laboratory Resonant Column Tests with Backfill Material and V_s Profiles Determined from SASW Tests at Stage 2 (from Stokoe et al, 2013)

The shear wave velocities from SASW testing begin to deviate from the laboratory curve supporting depth of BBM that is known to be approximately 45-ft below the testing surface at this time. Another feature shown in the Vs profile at this stage is that a shallow layer in the range of 3 to 32-ft was over-compacted by the contractor due to a possible material-type concern. This over-compaction should have little of any influence on the magnitude of error associated with near-field effects at shallow layer.

5.2 ANALYSIS OF DISPERSION DATA COLLECTED IN STAGE 2

Reference averaged phase velocity versus wavelength curves (V_R vs λ) were generated using a moving average over the field case C-R dispersion curve. As discussed in Section 4.3, there is a possibility of influence of near-field effects at phase velocity calculated with 360º phase difference (1 λ) from shorter receiver spacings due zone of rapidly increasing V_s near surface. To verify this concept, the case C-R dispersion curve at Stage 2 is generated with receiver spacing longer than 6 ft as shown in Figure 5.4. Due to the over-compaction in Stage 2, there are larger inversion compare to Stage 1 at the top of SASW array, but general trend in the Vs profiles is still normally dispersive. This curve is compared with the field cases C-1 through C-5 dispersion curve to be validated as a reference value. All reference averaged phase velocity versus λ curve and comparisons with field cases C-1 through C-5 dispersion curves at each Array in Stage 2 are attached in the Appendix B.

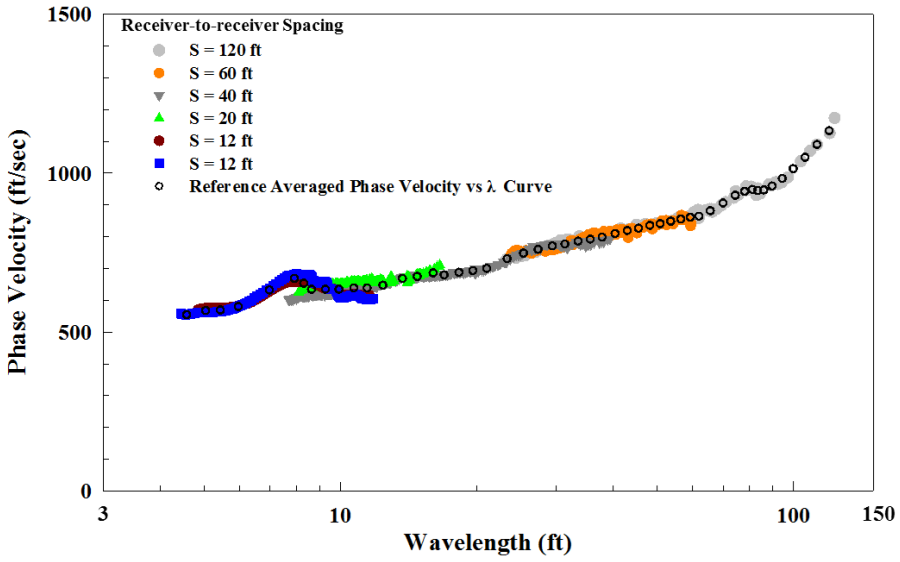

Figure 5.4 Comparison of the Field C-R Dispersion Curves and the Reference Averaged Phase Velocity versus λ Curve at Array 3A in Stage 2

In Stage 2, the depth to the BBM was approximately 45 ft below the surface of the backfill in Stage 2. As shown in Section 4.3, near-field effects due to a significant step increase in the V_s profile influence the dispersion curve when the wavelength is about twice the depth to the step increase. In the case of the V_s increase due to the BBM, the depth is about 45 ft and the wavelength will be about 90 ft. To verify this concept, the field C-R dispersion curves at Stage 2 and the theoretical dispersion curve generated with shear wave velocities from the Resonant Column test (P-26) are compared in Figure 5.5.

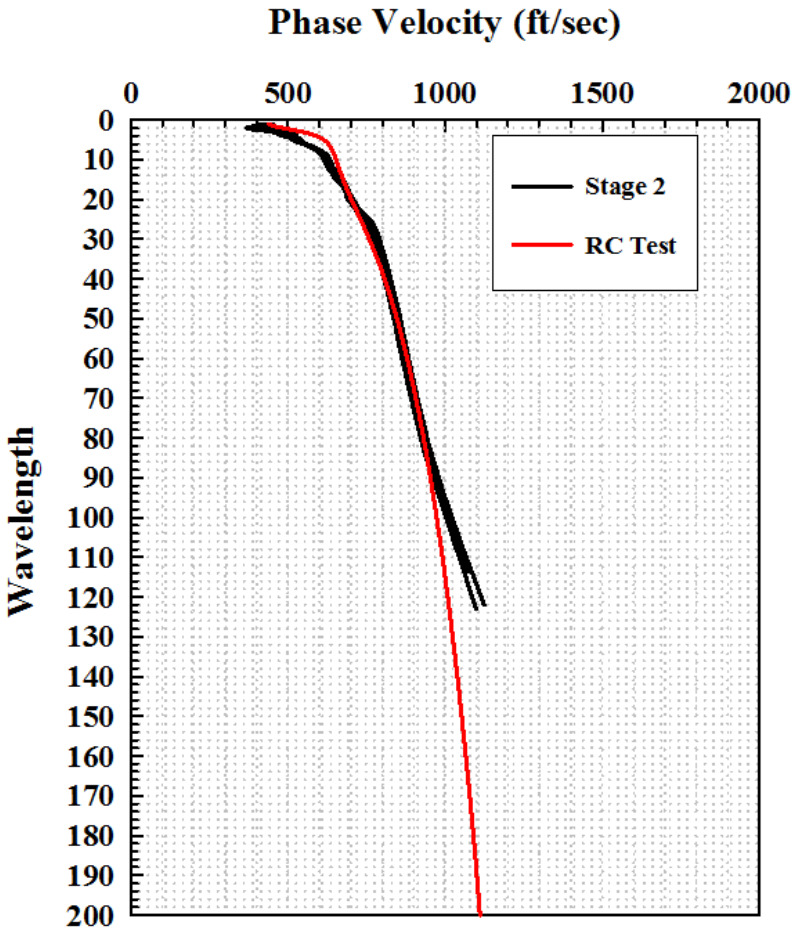

Figure 5.5 Comparison of the Stage 2 Field C-R Dispersion Curves and the Theoretical Dispersion Curve Generated Using SASW with the Shear Wave Velocities from Resonant Column Tests on Reconstituted Backfill Material

As seen in the figure, the depth of about 45 ft to the BBM at Stage 2 was captured in the zone where field wavelengths around 90 ft have phase velocities that begin to exceed the predicted dispersion curve using the resonant-column predicted V_s profiles.

5.2.1 ANALYSIS OF SASW DISPERSION DATA COLLECTED IN THE BACKFILL LAYER IN STAGE 2

As shown in Figure 5.5, wavelengths in SASW dispersion curve that are less than about 90 ft show no effect of the BBM. Therefore, to study near-field effects in the normally dispersive Vs profile of the backfill, only wavelength data with $\lambda \leq 85$ ft were used. These figures, in terms of normalized phase velocity versus wavelength, are presented in Figures 5.6 and 5.7.

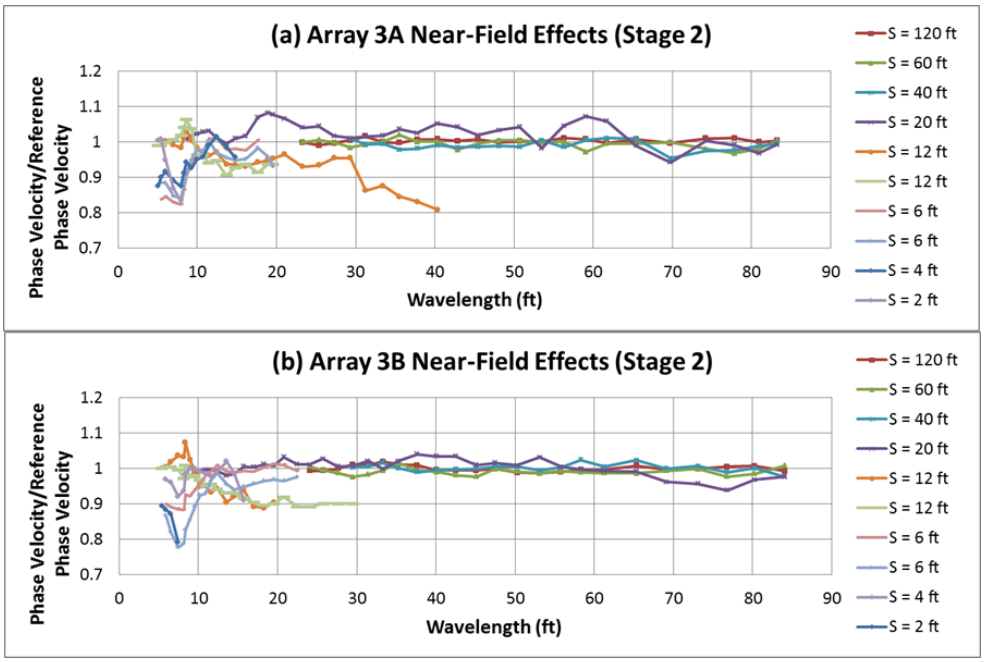

Figure 5.6 Near-Field Effects in the Stage 2 Fill Captured in Normalized Phase Velocity vs Wavelength Data at Array 3A and 3B

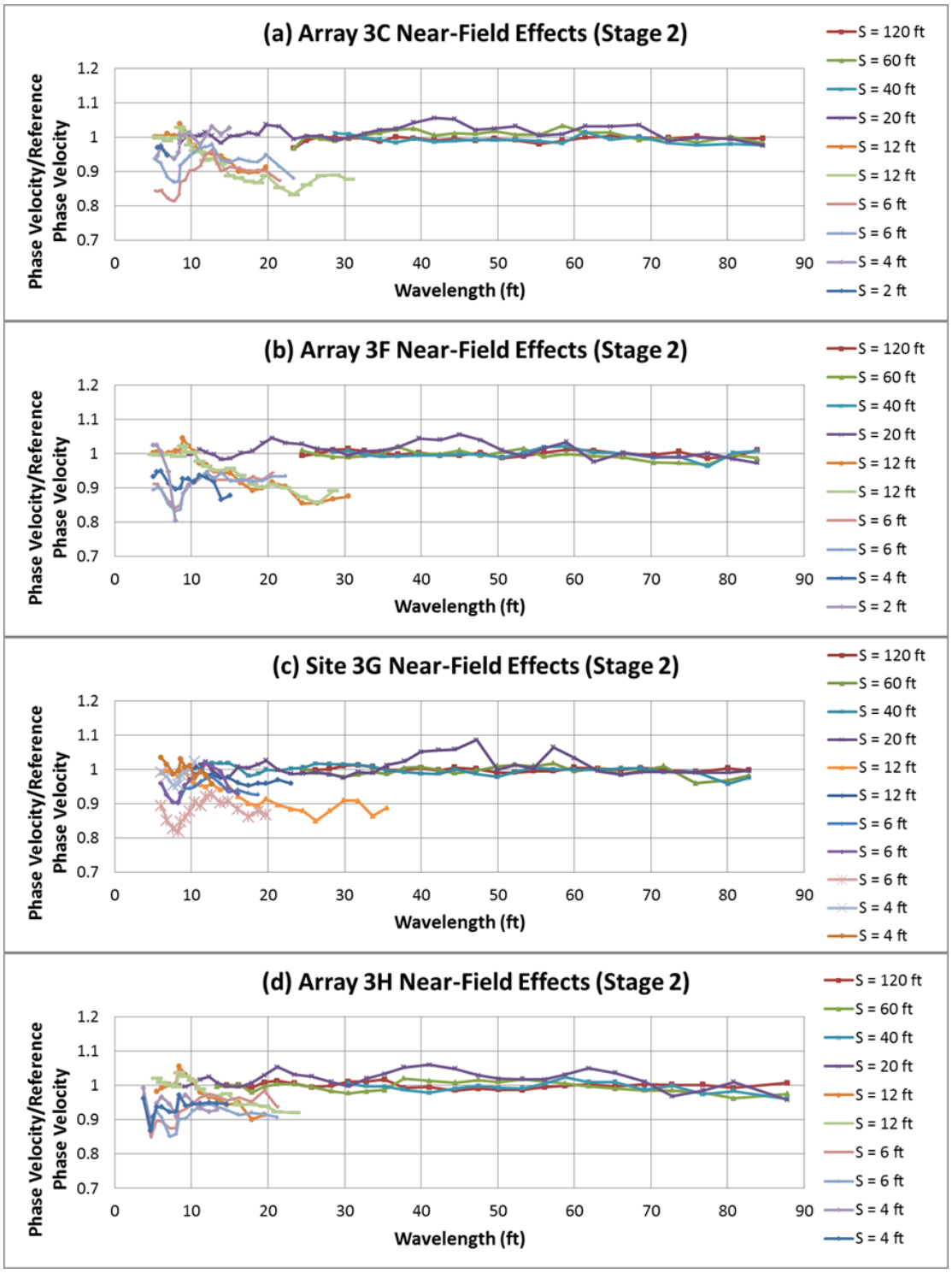

Figure 5.7 Near-Field Effects in the Stage 2 Fill Captured in Normalized Phase Velocity vs Wavelength Data at Array 3C, 3F, 3G and 3I

All results in the two figures for S = 20 to 120-ft receiver spacings show the same tendency with Stage 1 results. Shorter than 90-ft wavelength phase velocity which mainly stresses the 45-ft thick backfill, there are no influences of near-field effects at the S = 20- to 120-ft receiver spacing. Higher phase velocity from the 20-ft receiver spacing is due to the clearness of the data not by the influence of the near-field effect. These results draw a same conclusion that there is no significant influence of near-field effects where the stiffness of layer gradually increased with depth. (a normally dispersive soil.)

It is easier to evaluate the magnitude of error associated with near-field effect at receiver spacing 20, 40, 60 and 120-ft by looking at Figures 5.8 and 5.9. For the spacing to wavelength ratio (SWR) < 1, indicates the interference of the near-field effects, wavelength is longer than the receiver spacing.

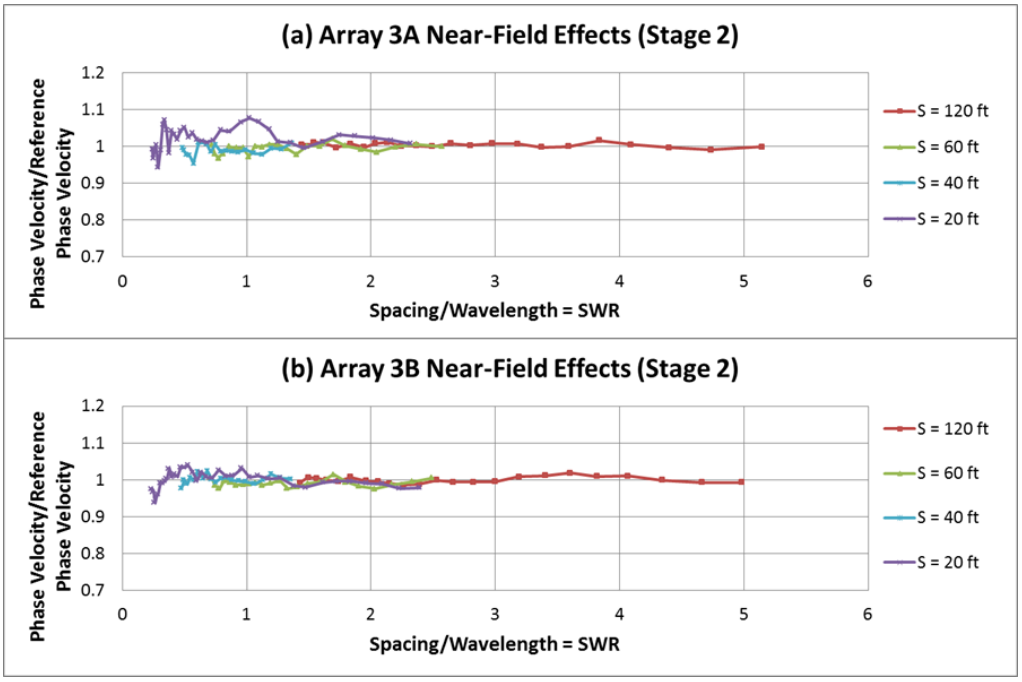

Figure 5.8 Near-Field Effects in the Stage 2 Fill Captured in Normalized Phase Velocity vs SWR at Array 3A and 3B with 120, 60, 40 and 20-ft Receiver Spacing

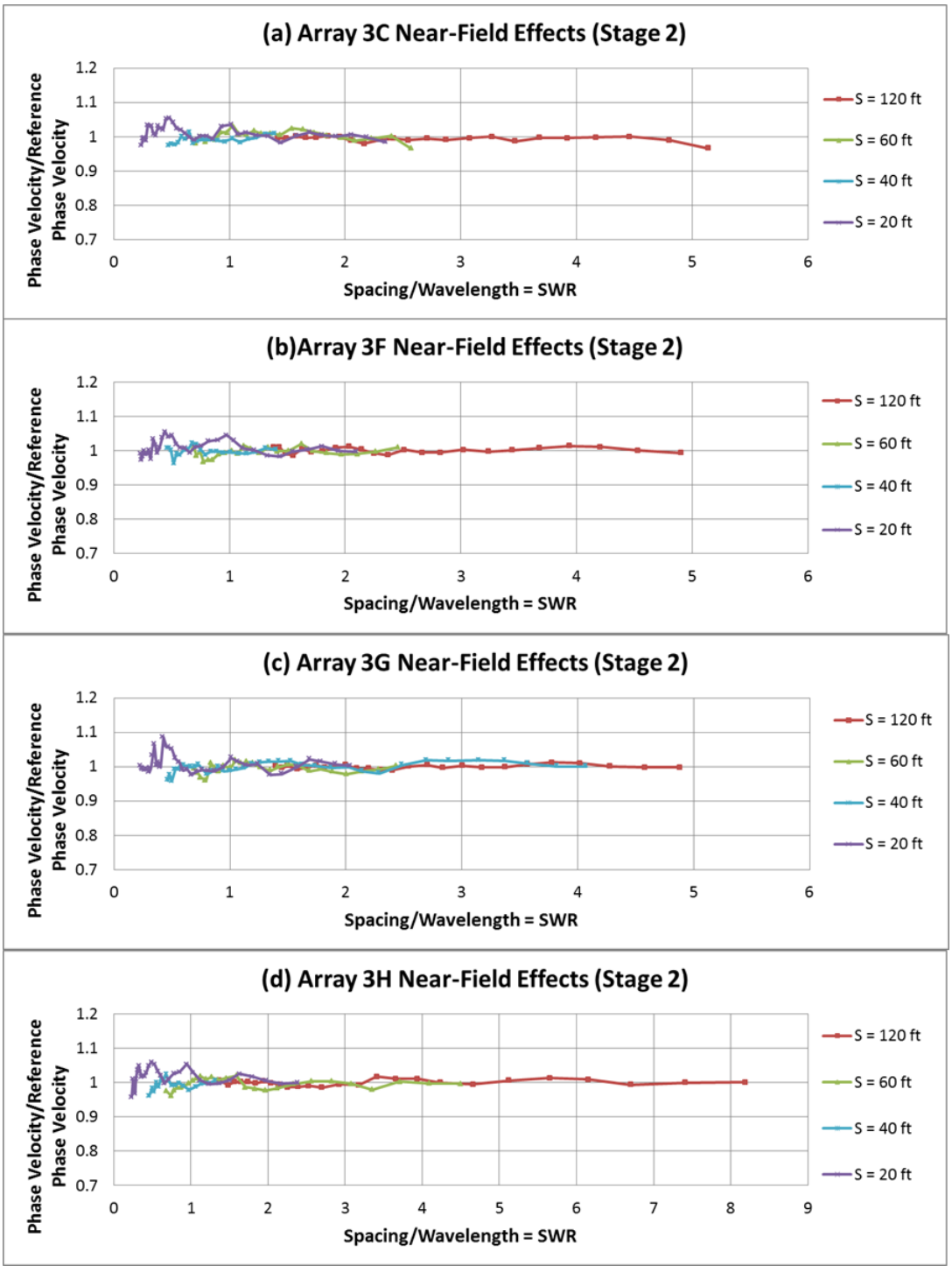

Figure 5.9 Near-Field Effects in the Stage 2 Fill Captured in Normalized Phase Velocity vs SWR at Array 3C, 3F, 3G and 3I with 120, 60, 40 and 20-ft Receiver Spacing

To study the near-field effect at short spacing, Figures 5.10 and 5.11 are created.

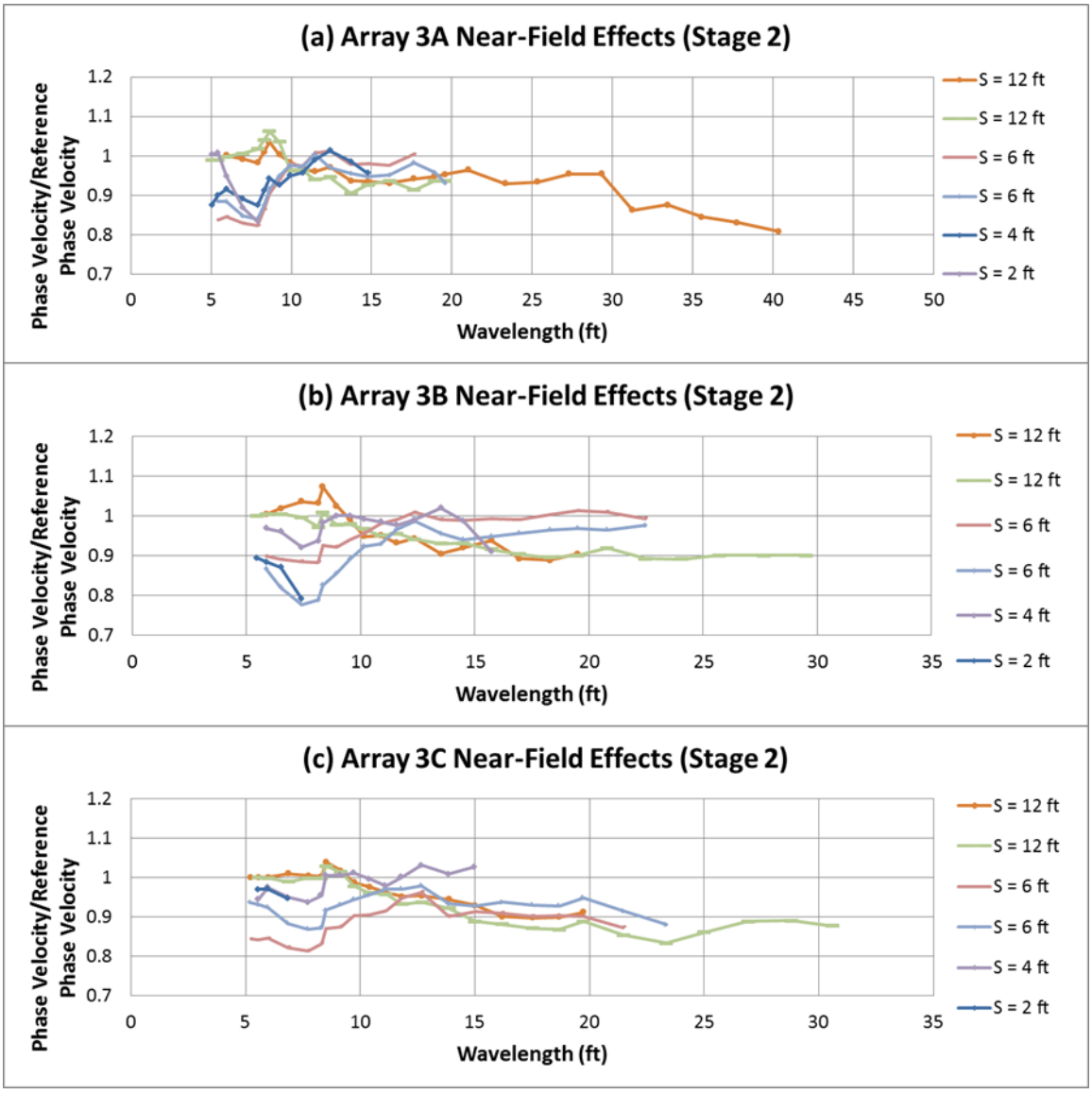

Figure 5.10 Near-Field Effects in the Stage 2 Fill Captured in Normalized Phase Velocity vs Wavelength Data at Array 3A, 3B and 3C with Short Receiver Spacings

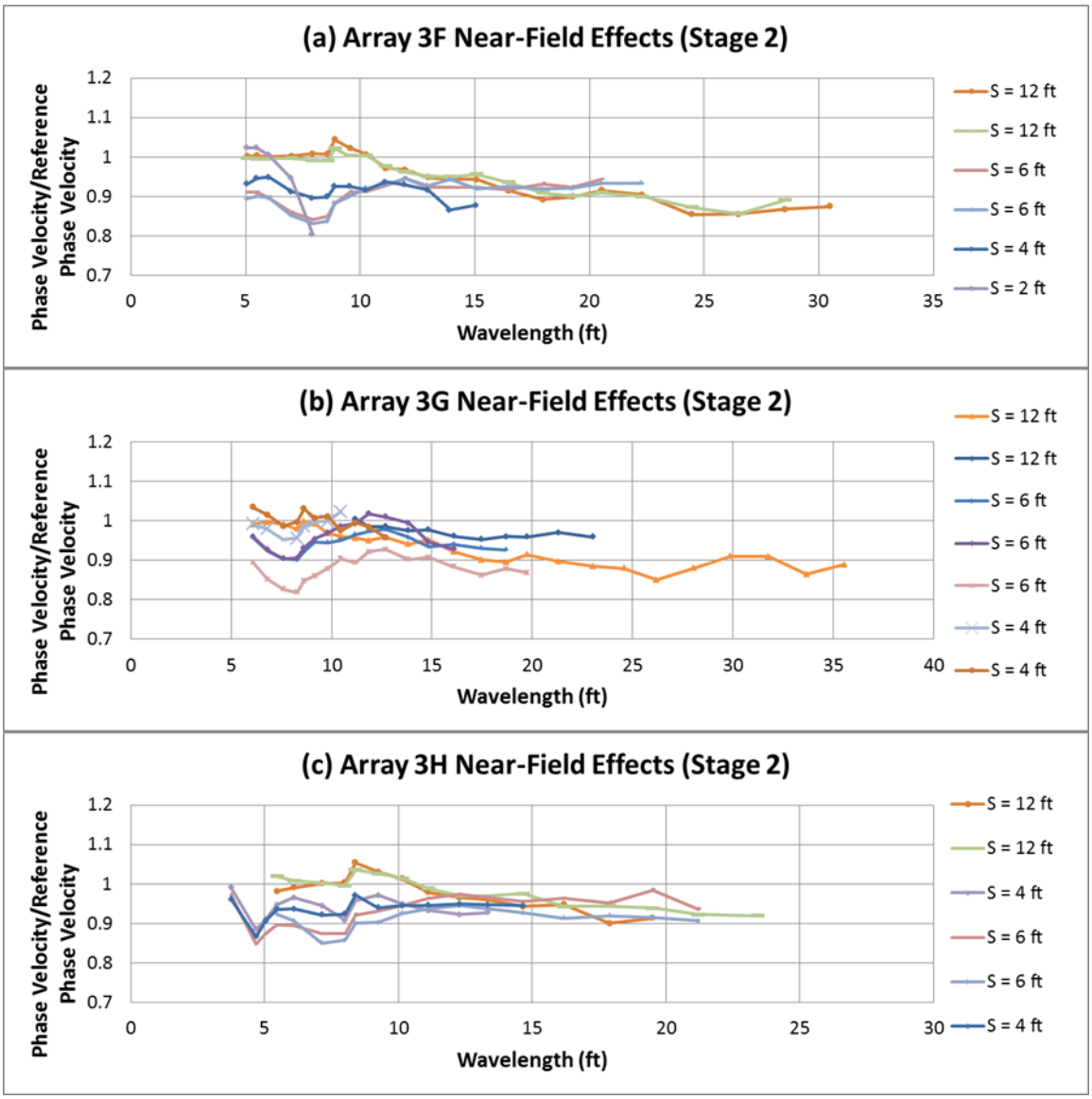

Figure 5.11 Near-Field Effects in the Stage 2 Fill Captured in Normalized Phase Velocity vs Wavelength Data at Array 3F, 3G and 3H with Short Receiver Spacings

As shown in Figures 5.10 and 5.11, the magnitude of error is more than 10%, even by as much as 20%. These figures show the same tendency with Stage 1 due to the large contrast of the shear wave velocity profile of shallow layer. Different with Stage 1 results is that the 12-ft receiver spacing from Stage 2 underestimate the phase velocity

close to 20% while 12-ft receiver spacing from Stage 1 only underestimate within 10%. This is caused by the over-compaction of Stage 2 as shown in Figure 5.12.

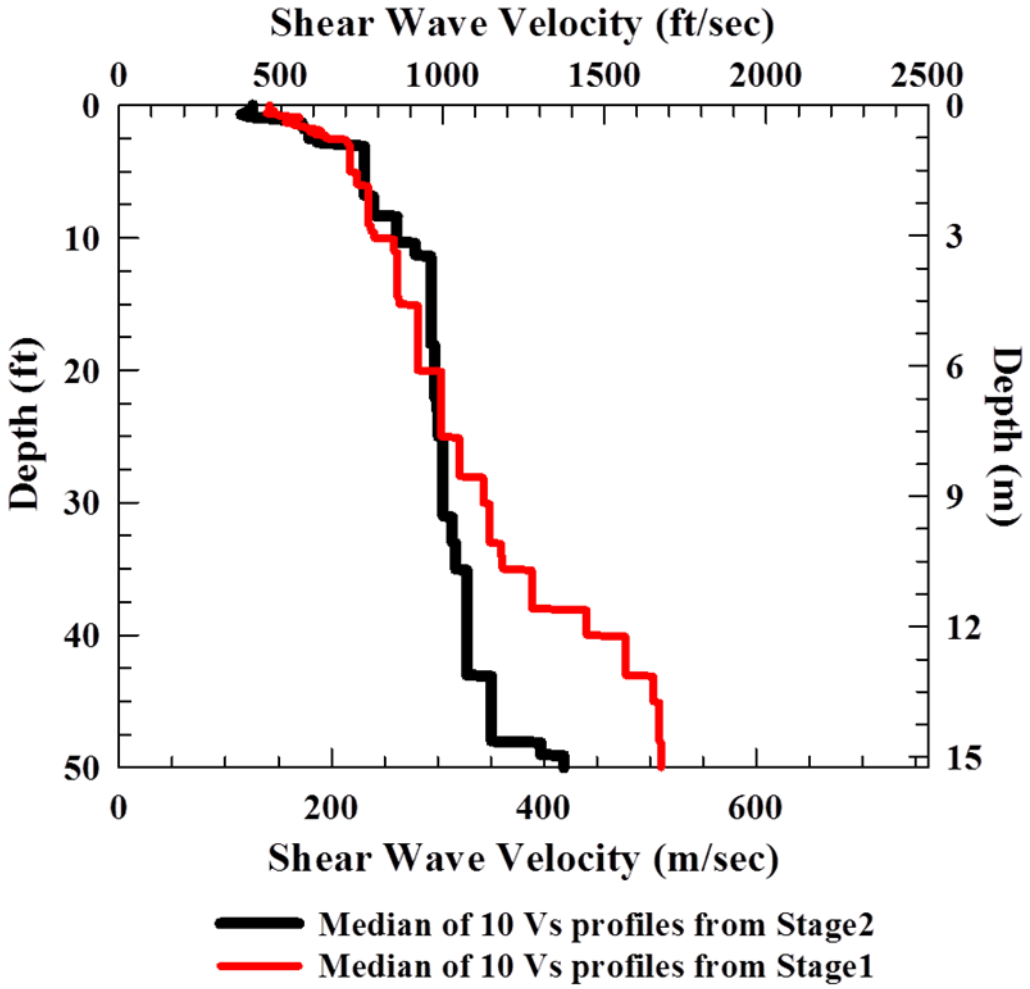

Figure 5.12 Comparison between Median of 10 Vs Profiles from Stage 1 and 2

Shear wave velocity ratio from surface to the depth of 10 ft is approximately 1.84 in Stage 1 and 2.22 in Stage 2. Based on this result, same conclusion was drawn that the larger shear wave velocity contrast result in increasing of the error associate with near-field effect.

It is easier to evaluate the magnitude of error associated with near-field effect at receiver short spacing by looking at Figures 5.13 and 5.14 where less than SWR value 1 indicates the interference of the near-field effects.

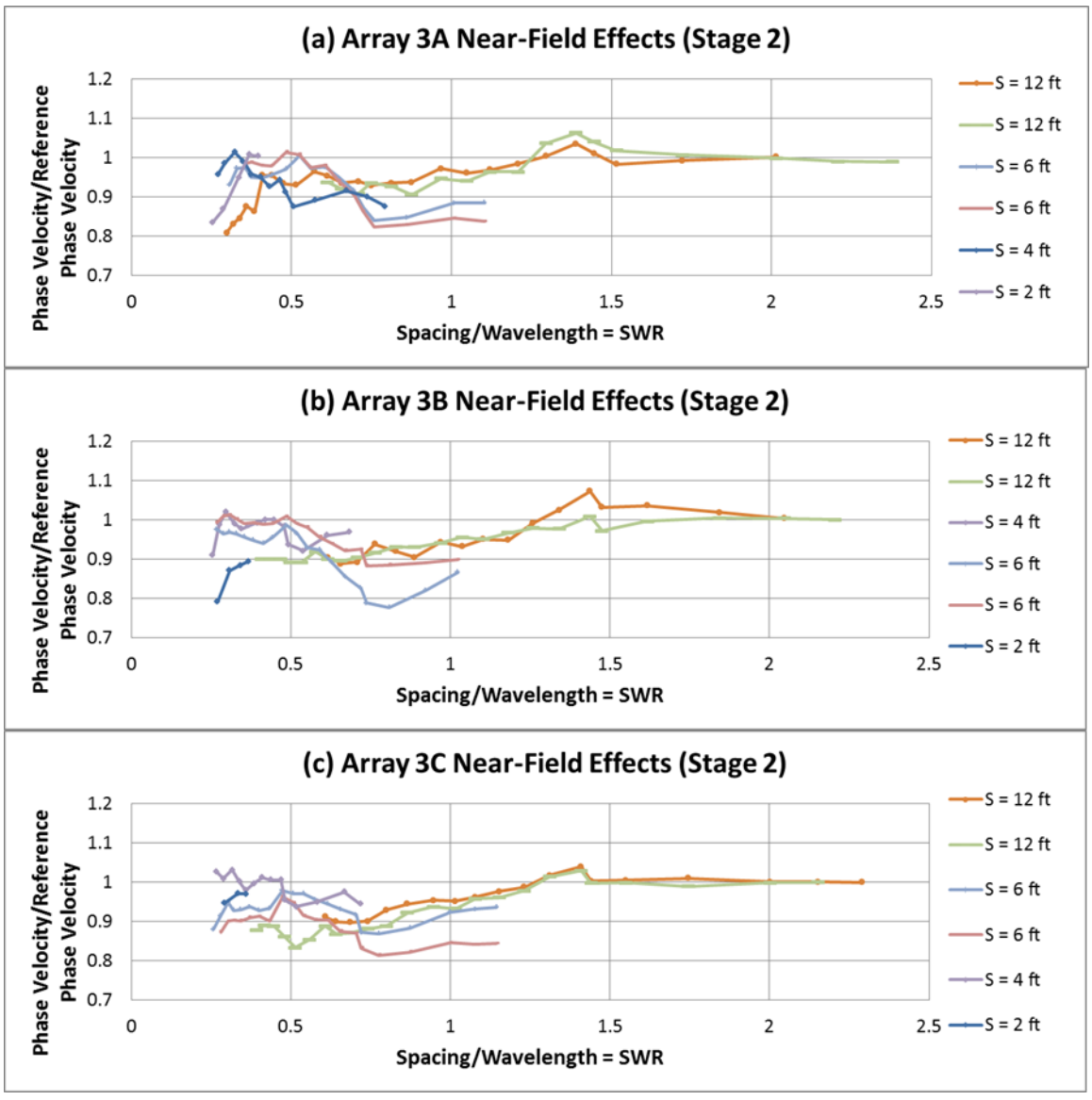

Figure 5.13 Near-Field Effects in the Stage 2 Fill Captured in Normalized Phase Velocity vs SWR at Array 3A, 3B and 3C with Short Receiver Spacing

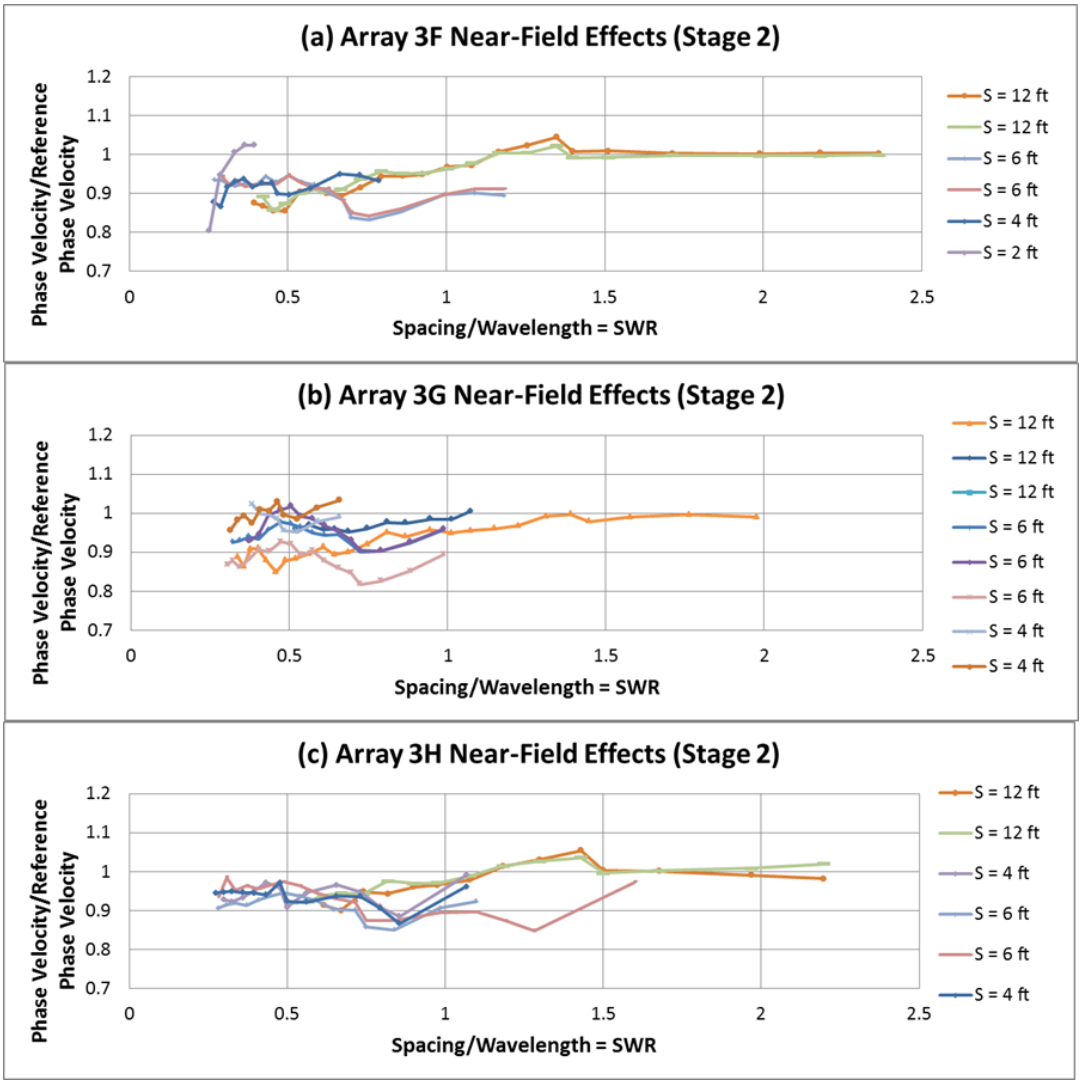

Figure 5.14 Near-Field Effects in the Stage 2 Fill Captured in Normalized Phase Velocity vs SWR at Array 3F, 3G and 3H with Short Receiver Spacing

At the SWR value of 1 where the phase velocity calculate with 360º phase difference (1 λ) from each receiver spacings already underestimate the phase velocity, same with the Stage 1 results. This could be due to the near-field effects especially when the receiver spacing became shorter. Therefore, in terms of short spacing, cases C-2 or C-3 filtering criteria should be used to eliminate the near-filed effect. Also the magnitude of error associated with near-field effects increase as the receiver spacing decrease.

5.2.2 ANALYSIS OF SASW DISPERSION DATA COLLECTED IN THE BBM LAYER IN STAGE 2

To correlate the near-field effect with the contrast of V_s profile, the analysis is extended to the BBM layer below the normally dispersive V_s profile (45-ft backfill). Normalized phase velocity versus wavelength plots or normalized phase velocity versus normalized spacing plots are generated with maximum of 120-ft wavelength.

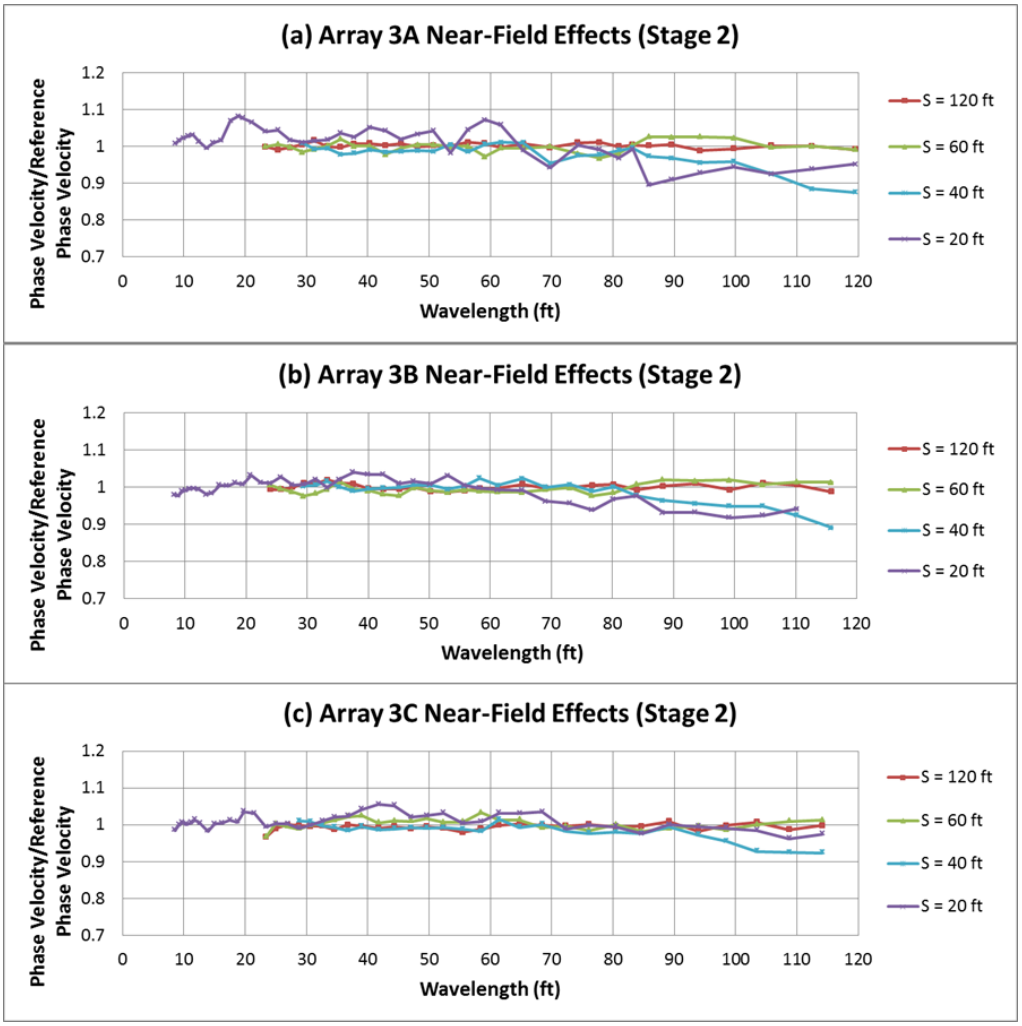

Figure 5.15 Near-Field Effects in the Stage 2 Fill Captured in Normalized Phase Velocity vs Wavelength Data at Array 3A, 3B and 3C

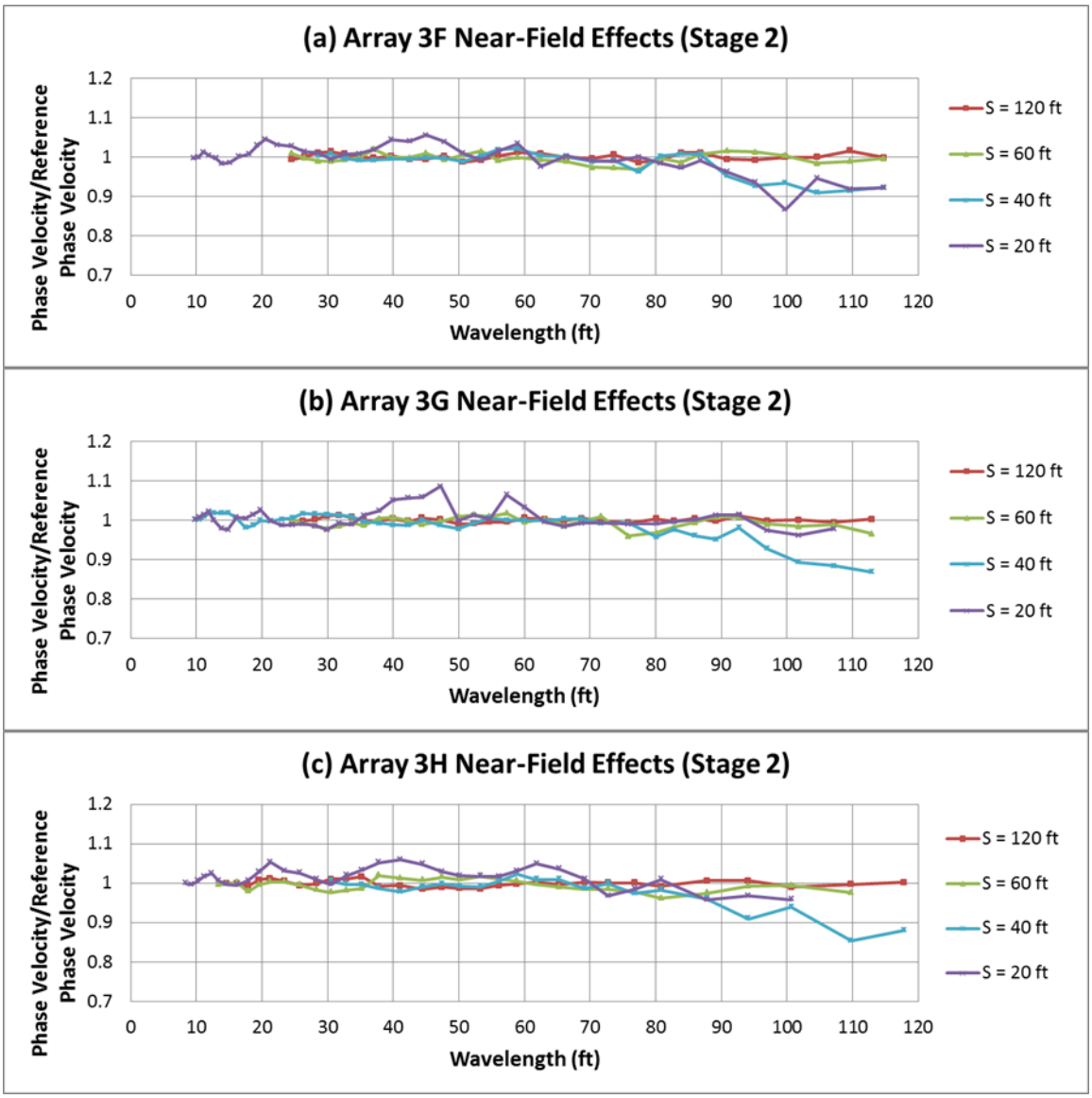

Figure 5.16 Near-Field Effects in the Stage 2 Fill Captured in Normalized Phase Velocity vs Wavelength Data at Array 3F, 3G and 3H

All results for S = 20 to 120-ft show the same tendency with Stage 1. There are no influences of near-field effects at the 60 and 120-ft receiver spacing and the 40- and 20-ft receiver spacing begins to underestimate the phase velocity approximately at the 85-ft wavelength. Below the 85-ft wavelength which mainly averages the 45-ft thick fill, there

is no influence of the near-field effect at 20, 40, 60 and 120-ft receiver spacing. Above the 85-ft wavelength which influence by the BBM, 20- and 40-ft receiver spacing underestimate the phase velocity. These results draw a same conclusion. Near-field effects underestimate the phase velocity when the V_s profiles have a large contrast and magnitude of error associate with near-field effect increases especially when the receiver spacing is short than the depth of the stiff material

It is easier to evaluate the magnitude of error associated with near-field effect at receiver spacing of 20, 40, 60 and 120-ft by looking at the Figures 5.17 and 5.18. For the spacing to wavelength ratio (SWR) < 1, indicates the interference of the near-field effects, wavelength is longer than the receiver spacing.

The 60- and 120-ft receiver spacings exhibit the magnitude of error associated with near-field effect less than 10%. In case of 20- and 40-ft receiver spacing, magnitude of error associated with near-field effects is slightly over 10% after 100-ft wavelength phase velocity as shown in Figures 5.17 and 5.18.

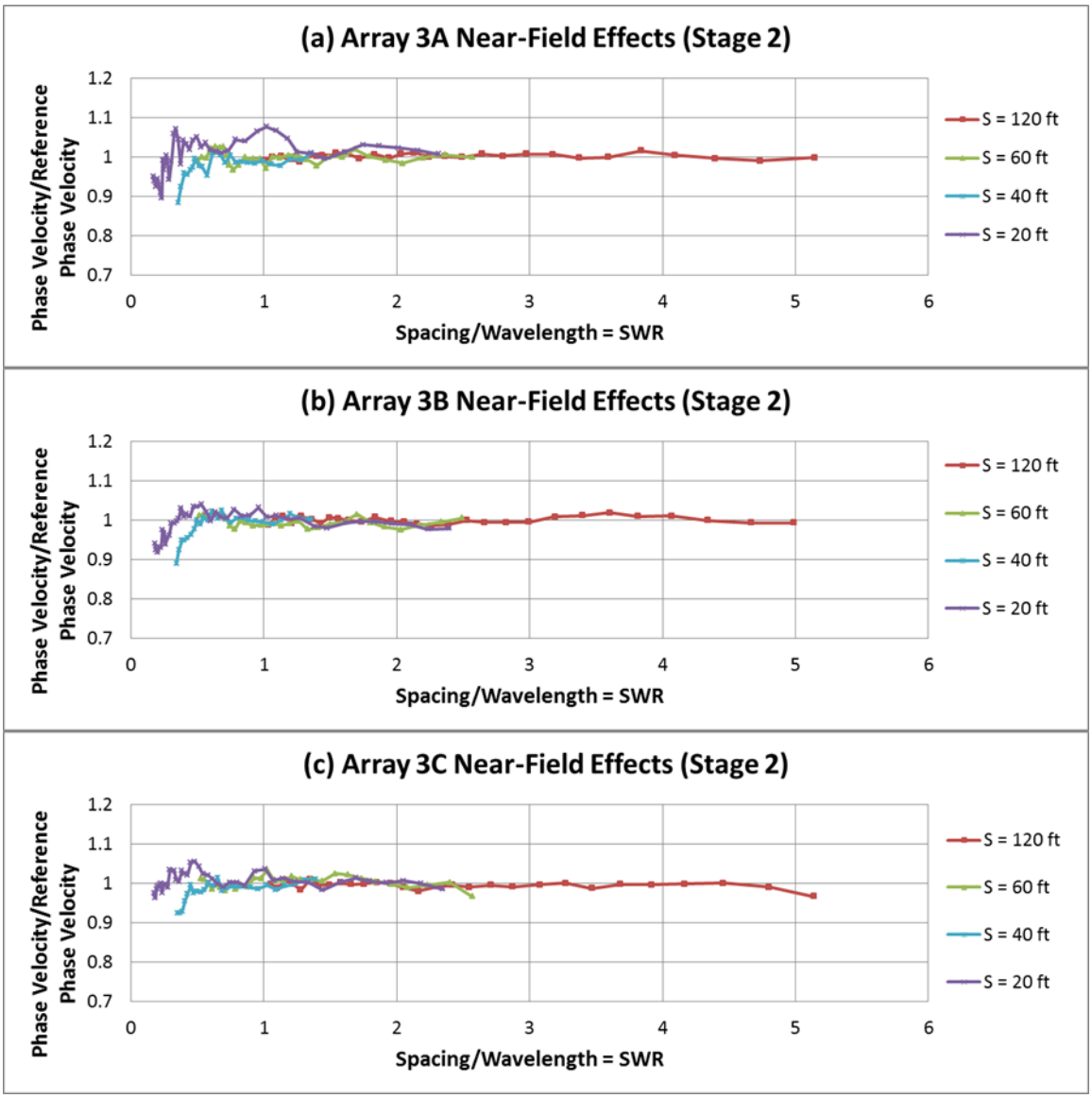

Figure 5.17 Near-Field Effects in the Stage 2 Fill Captured in Normalized Phase Velocity vs SWR at Array 3A, 3B and 3C with 120, 60, 40 and 20-ft Receiver Spacing

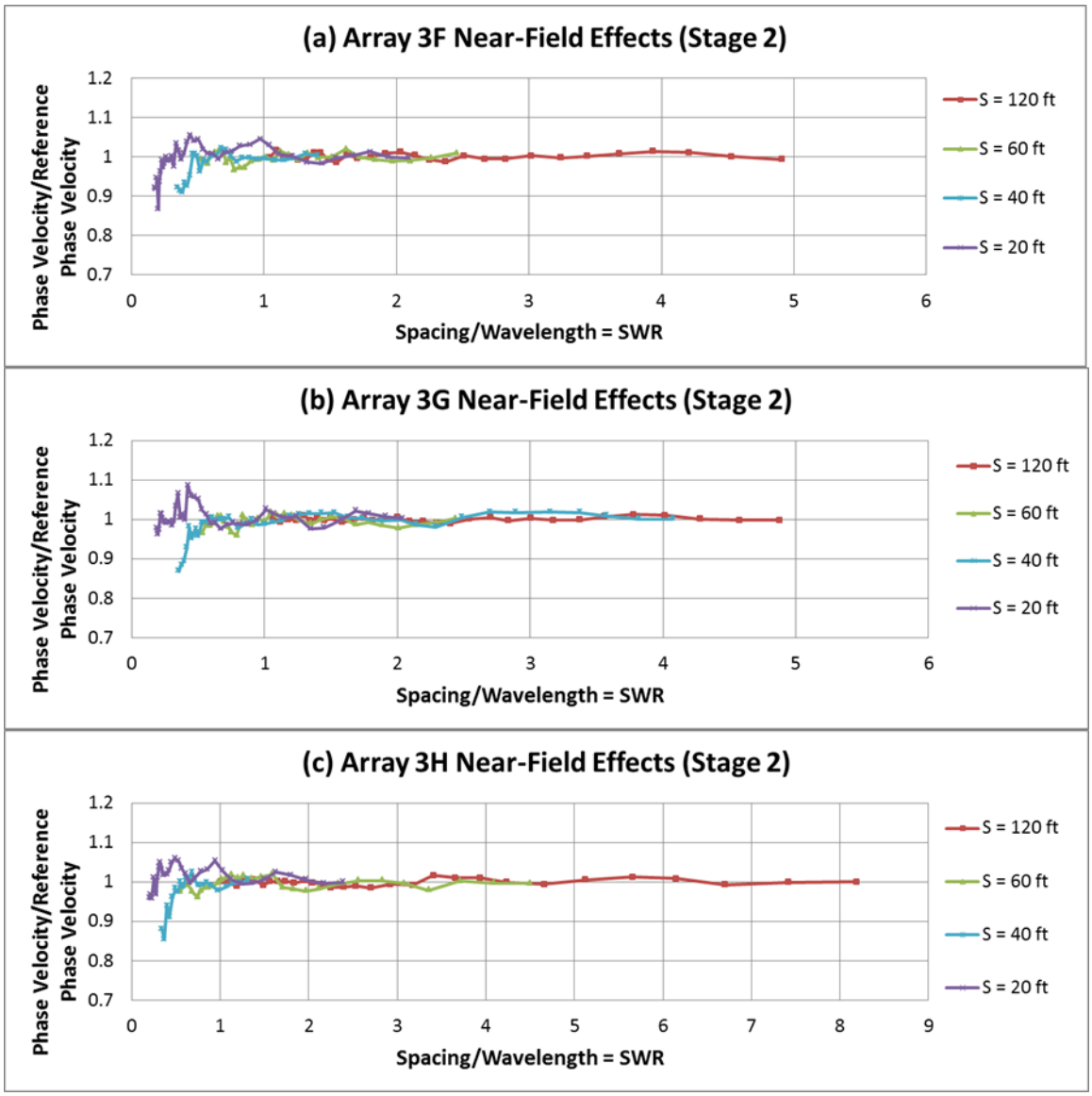

Figure 5.18 Near-Field Effects in the Stage 2 Fill Captured in Normalized Phase Velocity vs SWR at Array 3F, 3G and 3H with 120, 60, 40 and 20-ft Receiver Spacing

5.3 SUMMARY

SASW test data from Stage 2 (45-ft thick fill) at VEGP Site is analyzed in terms of near-field effects. The same tendency with Stage 1 is seen at Stage 2 results. One different feature of this Stage 2 is over-compaction of the surface layer. This result in the increase of the magnitude of error associated with near-field effect at 12-ft spacing. This result draws the same conclusion that the magnitude associate with near-field effects increases where the shear wave velocities have a larger contrast.

CHAPTER 6 : SUMMARY, CONCLUSIONS, AND RECOMMENDATIONS

6.1 SUMMARY

A limitation of prior studies of near-field effects is that most of them were based on either numerical simulations with simple velocity profile or small-scale experimental investigations. In this study, full-scale field test data using the Spectral-Analysis-of-Surface-Waves (SASW) method were used to investigate near-field effects.

Two types of soil profiles were studied in terms of near-field effects as follows: (1) a normally dispersive velocity profile in the upper portion of the geotechnical profile and (2) a stiffer layer beneath this normally dispersive material. Both layers composed the same sites in this investigation which involved a 90-ft deep backfill that was constructed at the Vogtle Electric Generating Plant near Augusta, GA. For the quantitative comparisons in terms of dispersion curves, reference averaged phase velocity was necessary. These values were taken from reference averaged phase velocity versus wavelength curves which were generated using a moving average over the field reference case dispersion curve (dispersion curve generated with phase differences from 1 λ to Min-Useable λ phase difference) that is named the C-R dispersion Curve.

To evaluate the magnitude of error associate with near-field effects, comparisons between the reference averaged velocity and the field dispersion curve including near-field effects were conducted and plotted in terms of: (1) normalized phase velocity versus wavelength and (2) normalized phase velocity versus normalized spacing.

6.2 CONCLUSIONS

From the results of the experimental investigation of near-field effects on the SASW dispersion curves, the following conclusions can be made.

1. Generally, near-field effects underestimate the phase velocity of soil layer in the zone of rapidly increasing V_s near surface and at depth where there was significant jump in V_s below the backfill, depending on the receiver spacing.
2. In terms of the normally dispersive upper backfill layer, there is no significant error associated with near-field effect (error less than 5%) at longer receiver spacings (receiver spacings longer than 12 ft).
3. In terms of shorter receiver spacings (receiver spacing shorter than 12 ft), as the receiver spacing became shorter, the error associated with near-field effects increased.
4. In terms of shorter receiver spacing, case C-1 dispersion curve (dispersion curve generated with 0.5 λ-to-0.33 λ phase difference) already underestimated the phase velocity, even by as much as 20%. Therefore, cases C-2 (dispersion curve generated with phase difference from 0.33 λ-to-0.25 λ) or C-3 (dispersion curve generated phase difference from 0.25 λ to Min-Useable λ phase difference) filtering criteria should be used to eliminate the error associated with near-field effects.
5. There is a significant influence in terms of near-field effects when the receiver spacing is shorter than the depth of the stiffer layer (in this case the Blue Bluff Marl). To minimize the near-field effect, the receiver spacing should be calculated as following;

Receiver spacing = depth to stiffer ×2.5

If the receiver spacing satisfies this recommendation, the phase velocity calculated from the 180° phase difference (0.5 λ) can be used to develop a good estimation of the Vs profile which may be on the order of 10% low.

6. The magnitude of the error associated with near-field effects increases as the contrast of in shear wave velocities between layers at depth increases.

6.3 RECOMMENDATIONS

The results from this study were developed from SASW field measurements at a rather simple, normally dispersive V_s profile. In this case, the V_s profile increased rapidly near the surface (about doubling in the top 10 ft) and then again exhibited a rapid increase (factor about 1.5 to 1.7) just below the bottom of the backfill. However, it is common to perform measurements at site with more complexity. Therefore, other studies of near-field effects need to be performed at field site with, irregular V_s profiles where a soft layer is trapped between two stiffer layers or a stiff layer trapped between two soft layers and so forth.

In this study, the spacing used in the receiver pair always equaled to the source-to-first-receiver-spacing. These spacings can be too close to the source for full waveform development in some cases, resulting in sampling shallower depth than estimated by the wavelengths. Therefore, various ratio of source-to-first-receiver-spacing to receiver-to-receiver-spacing are necessary in further investigation of near-field effects. Also, significant advances have occurred in numerical models of seismic wave fields. These newer numerical models should be used in comprehensive studies of nonintrusive surface wave measurements.

Appendix A

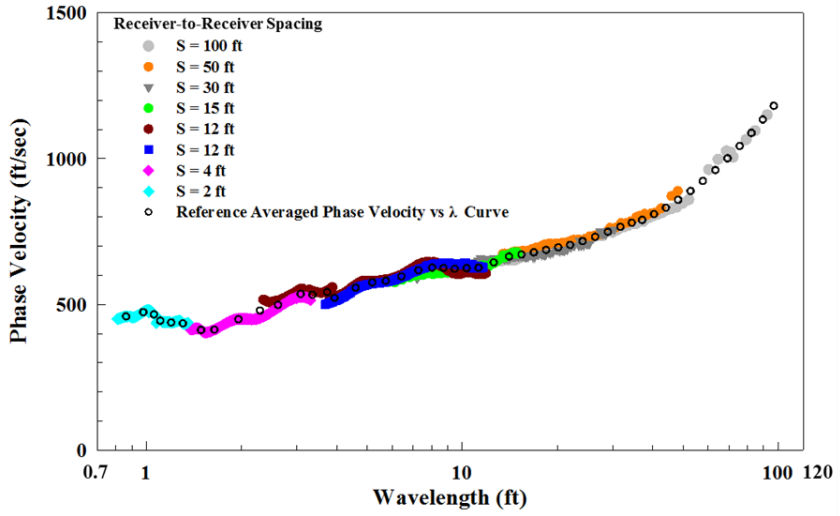

Figure A.1 All Field Dispersion Data Used to Create the C-R Field Dispersion Curve and Reference Averaged Phase Velocity versus λ Curve for the 1 λ to Min-Useable λ Data at Array 3A; Stage 1 at VEGP Site

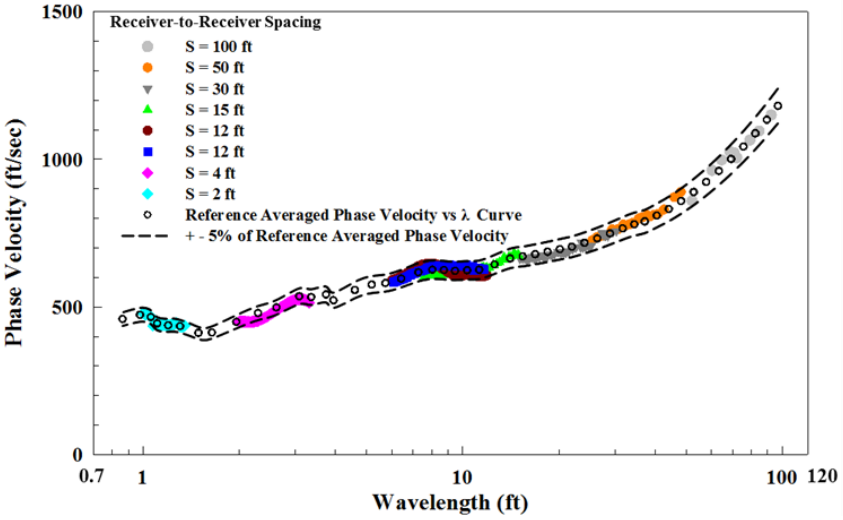

Figure A.2 Comparison of the Reference Averaged Phase Velocity versus λ Curve (Case C-R) and Field C-1 Dispersion Curve at Array 3A; Stage 1 at VEGP Site

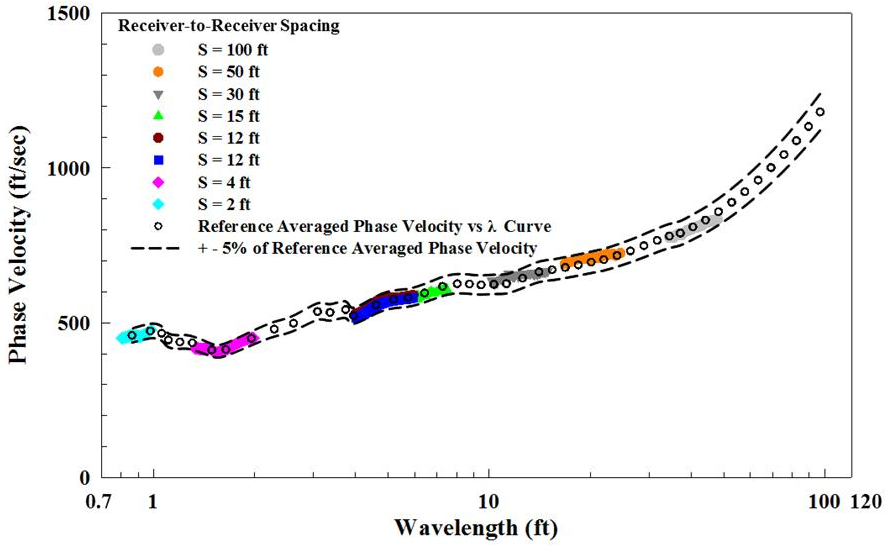

Figure A.3 Comparison of the Reference Averaged Phase Velocity versus λ Curve (Case C-R) and Field C-2 Dispersion Curve at Array 3A; Stage 1 at VEGP Site

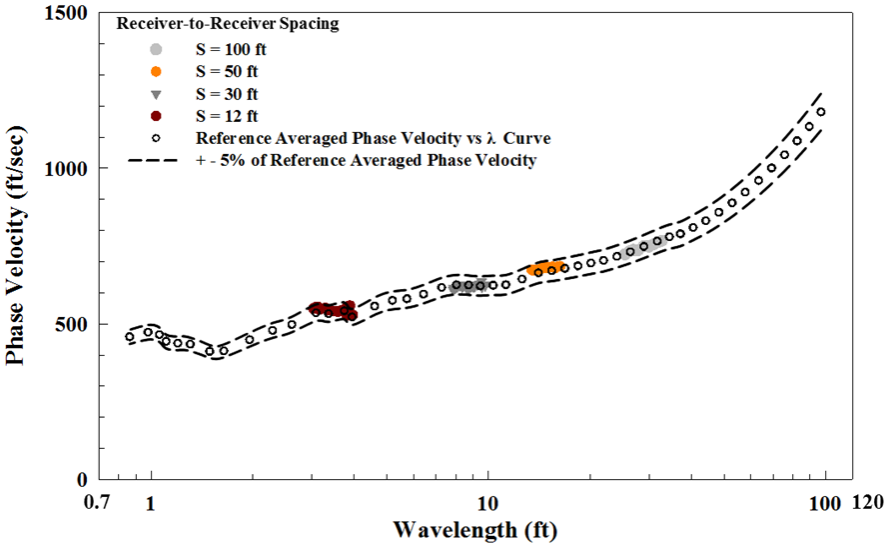

Figure A.4 Comparison of the Reference Averaged Phase Velocity versus λ Curve (Case C-R) and Field C-3 Dispersion Curve at Array 3A; Stage 1 at VEGP Site

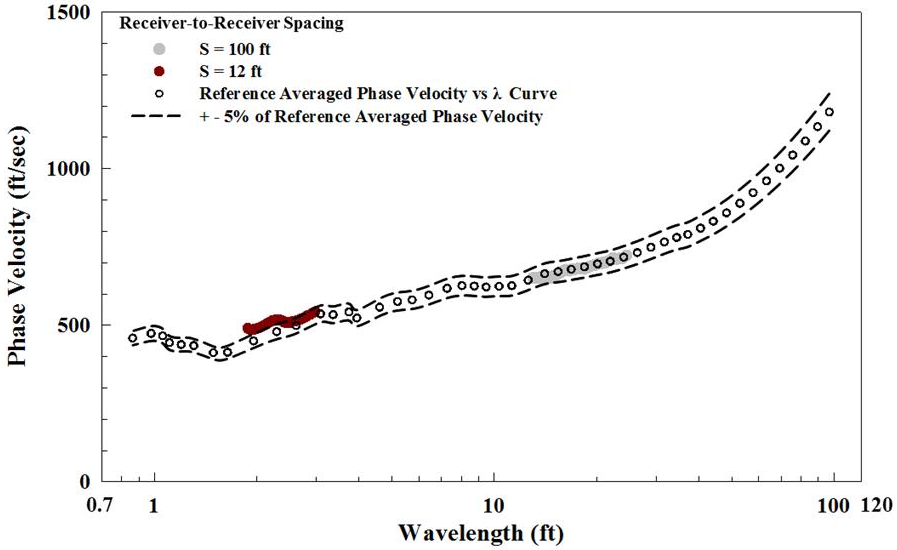

Figure A.5 Comparison of the Reference Averaged Phase Velocity versus λ Curve (Case C-R) and Field C-4 Dispersion Curve at Array 3A; Stage 1 at VEGP Site

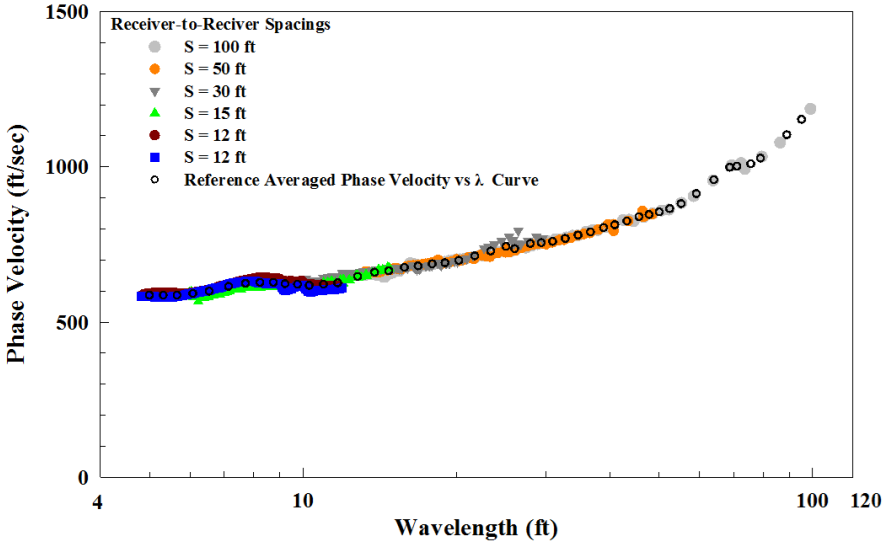

Figure A.6 All Field Dispersion Data Used to Create the C-R Field Dispersion Curve and Reference Averaged Phase Velocity versus λ Curve for the 1 λ to Min-Useable λ Data at Array 3B; Stage 1 at VEGP Site

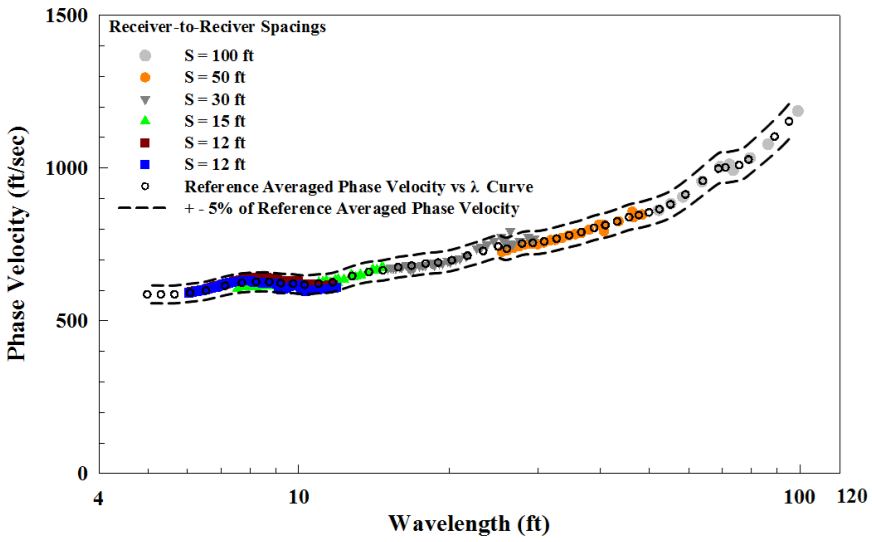

Figure A.7 Comparison of the Reference Averaged Phase Velocity versus λ Curve (Case C-R) and Field C-1 Dispersion Curve at Array 3B; Stage 1 at VEGP Site

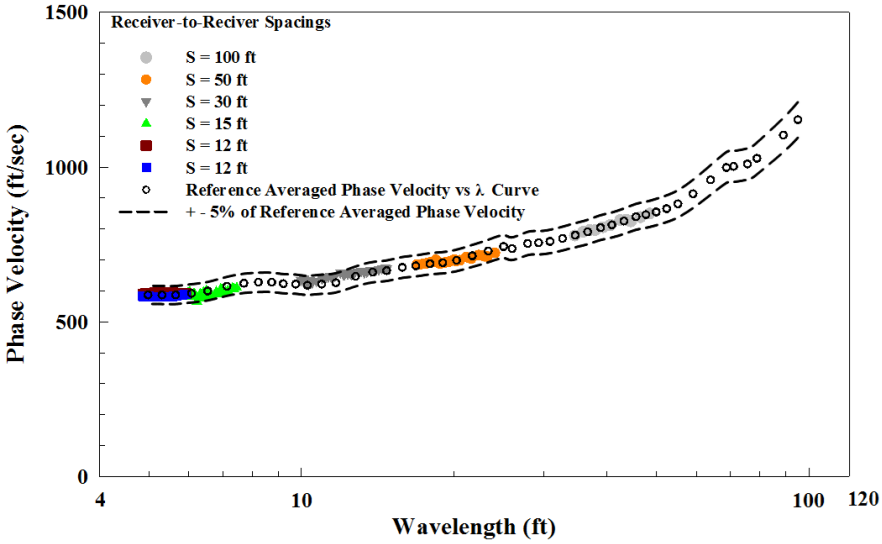

Figure A.8 Comparison of the Reference Averaged Phase Velocity versus λ Curve (Case C-R) and Field C-2 Dispersion Curve at Array 3B; Stage 1 at VEGP Site

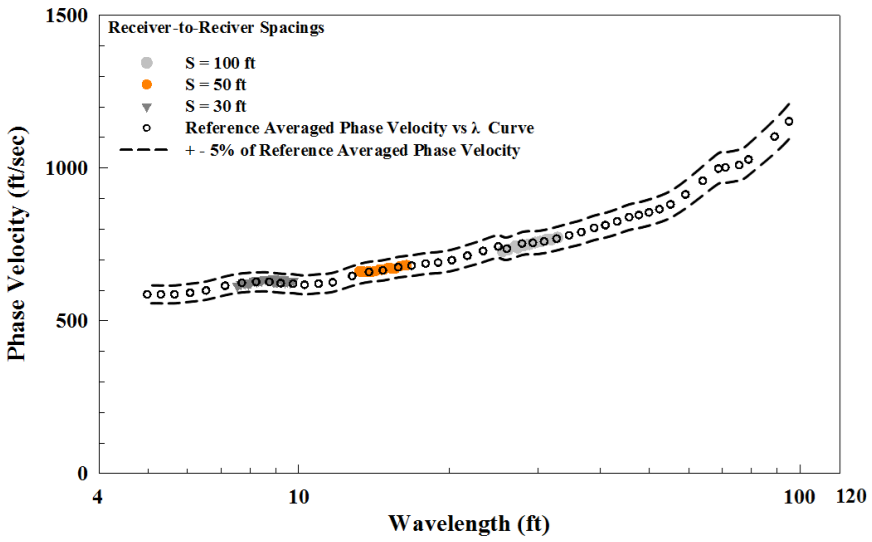

Figure A.9 Comparison of the Reference Averaged Phase Velocity versus λ Curve (Case C-R) and Field C-3 Dispersion Curve at Array 3B; Stage 1 at VEGP Site

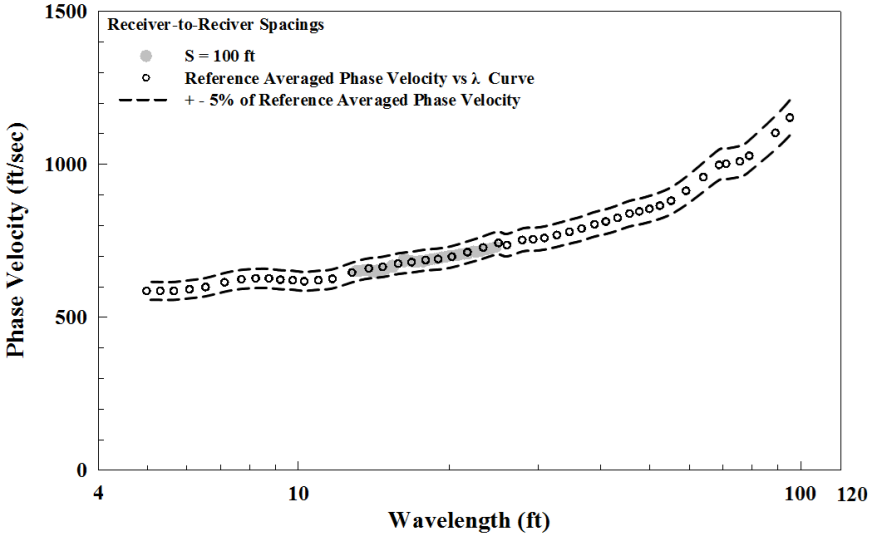

Figure A.10 Comparison of the Reference Averaged Phase Velocity versus λ Curve (Case C-R) and Field C-4 Dispersion Curve at Array 3B; Stage 1 at VEGP Site

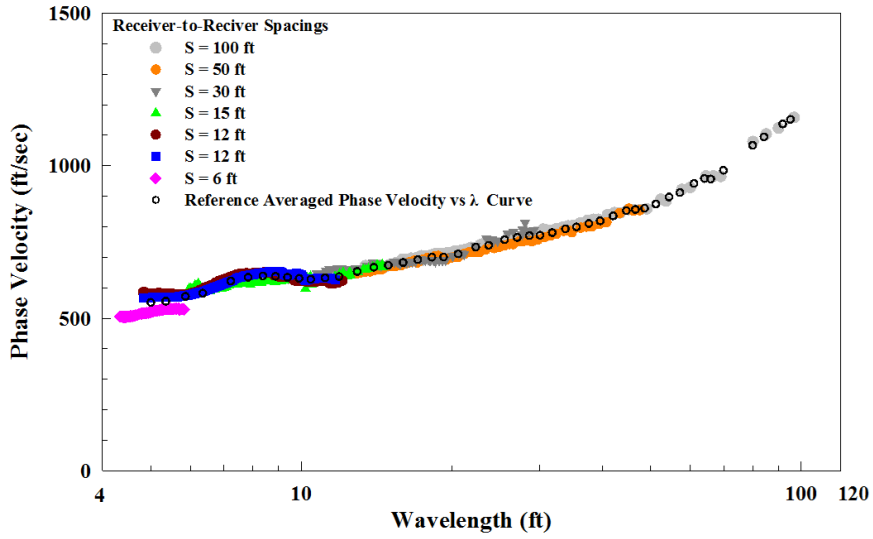

Figure A.11 All Field Dispersion Data Used to Create the C-R Field Dispersion Curve and Reference Averaged Phase Velocity versus λ Curve for the 1 λ to Min-Useable λ Data at Array 3C; Stage 1 at VEGP Site

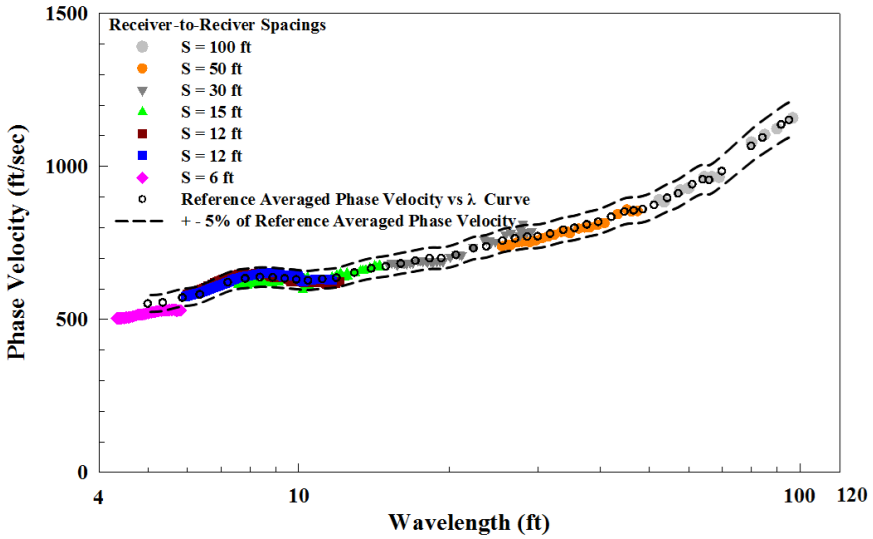

Figure A.12 Comparison of the Reference Averaged Phase Velocity versus λ Curve (Case C-R) and Field C-1 Dispersion Curve at Array 3C; Stage 1 at VEGP Site

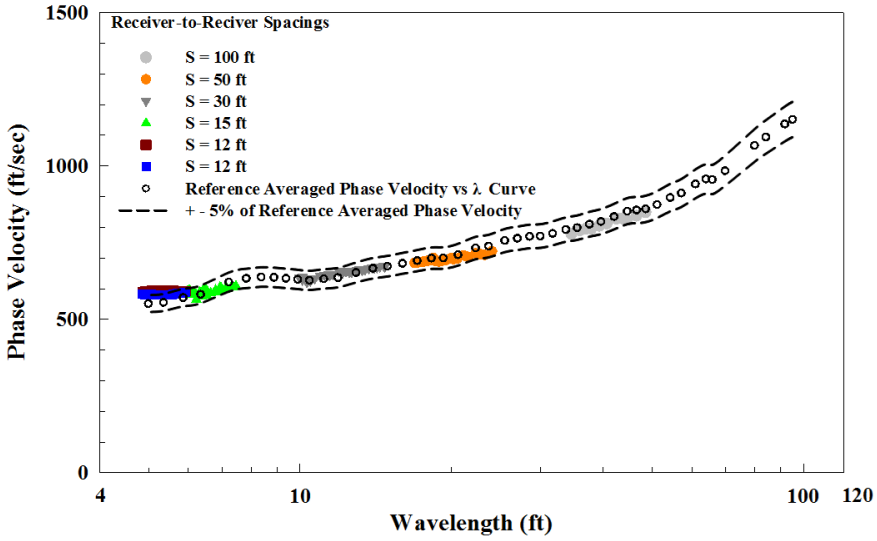

Figure A.13 Comparison of the Reference Averaged Phase Velocity versus λ Curve (Case C-R) and Field C-2 Dispersion Curve at Array 3C; Stage 1 at VEGP Site

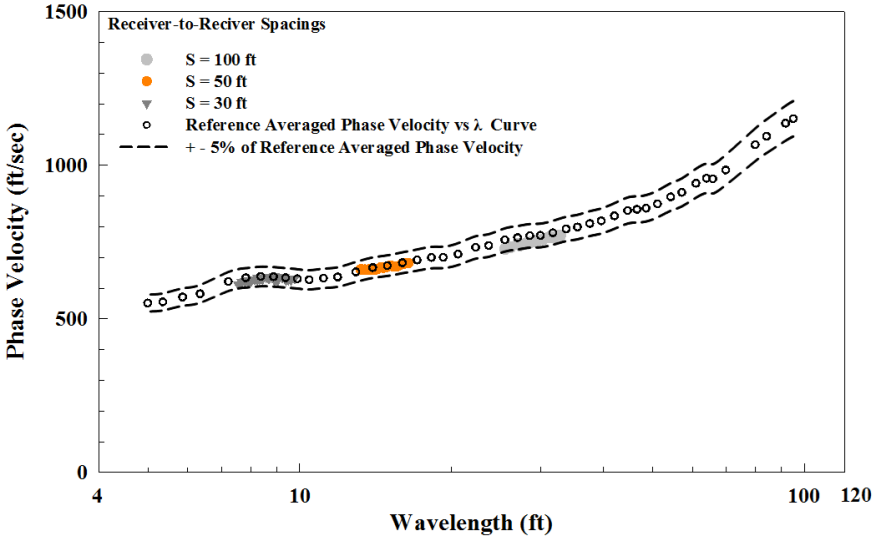

Figure A.14 Comparison of the Reference Averaged Phase Velocity versus λ Curve (Case C-R) and Field C-3 Dispersion Curve at Array 3C; Stage 1 at VEGP Site

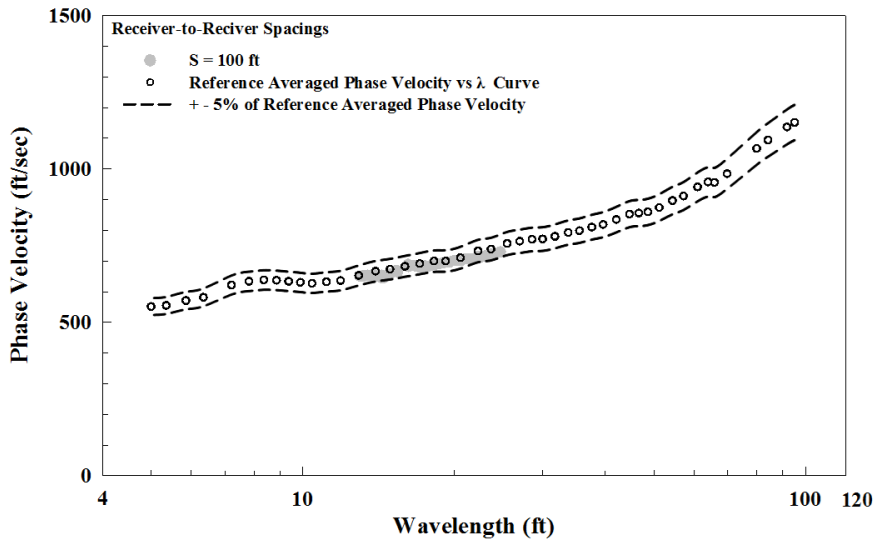

Figure A.15 Comparison of the Reference Averaged Phase Velocity versus λ Curve (Case C-R) and Field C-4 Dispersion Curve at Array 3C; Stage 1 at VEGP Site

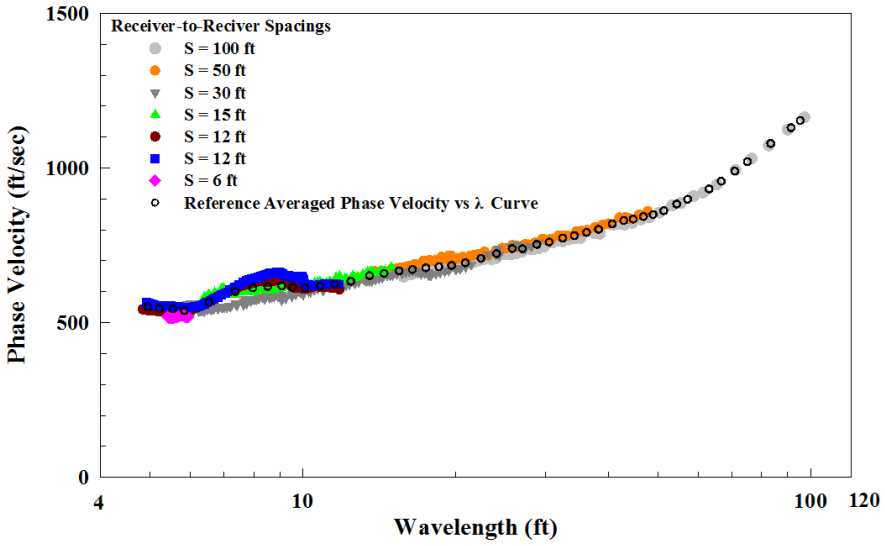

Figure A.16 All Field Dispersion Data Used to Create the C-R Field Dispersion Curve and Reference Averaged Phase Velocity versus λ Curve for the 1 λ to Min-Useable λ Data at Array 3F; Stage 1 at VEGP Site

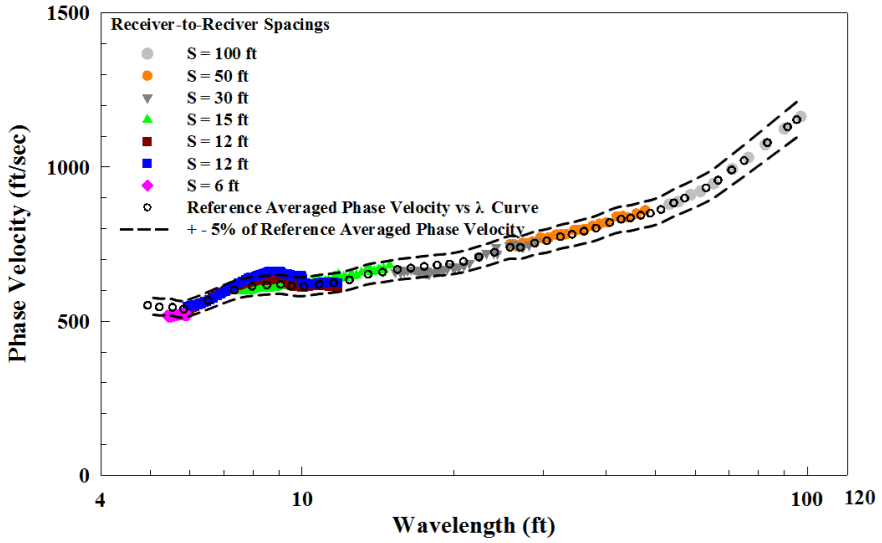

Figure A.17 Comparison of the Reference Averaged Phase Velocity versus λ Curve (Case C-R) and Field C-1 Dispersion Curve at Array 3F; Stage 1 at VEGP Site

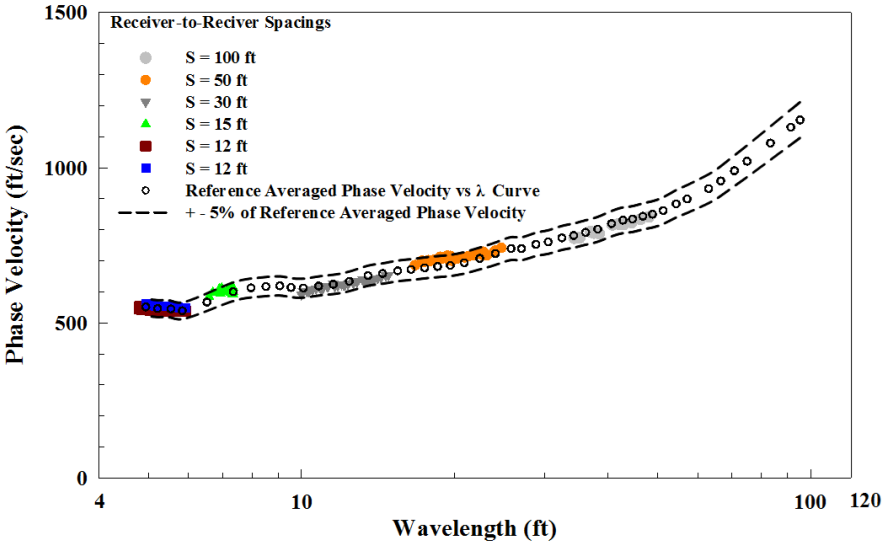

Figure A.18 Comparison of the Reference Averaged Phase Velocity versus λ Curve (Case C-R) and Field C-2 Dispersion Curve at Array 3F; Stage 1 at VEGP Site

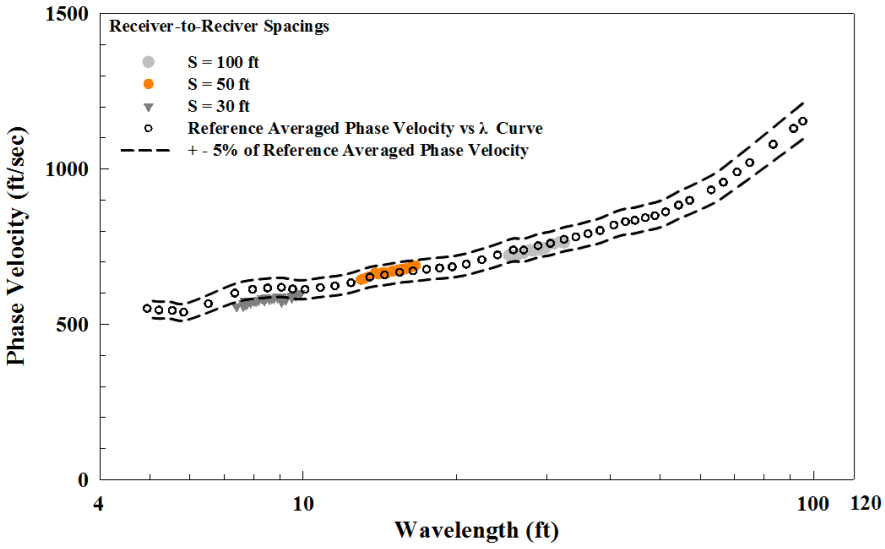

Figure A.19 Comparison of the Reference Averaged Phase Velocity versus λ Curve (Case C-R) and Field C-3 Dispersion Curve at Array 3F; Stage 1 at VEGP Site

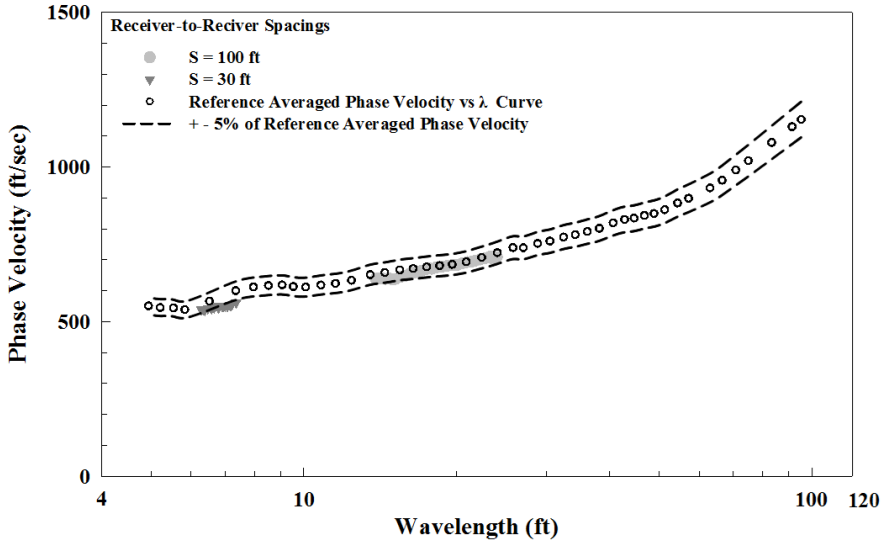

Figure A.20 Comparison of the Reference Averaged Phase Velocity versus λ Curve (Case C-R) and Field C-4 Dispersion Curve at Array 3F; Stage 1 at VEGP Site

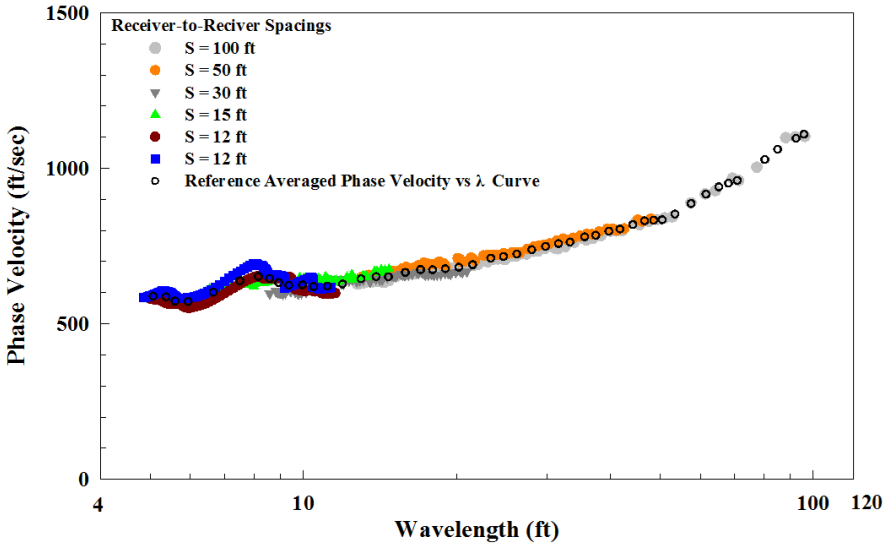

Figure A.21 All Field Dispersion Data Used to Create the C-R Field Dispersion Curve and Reference Averaged Phase Velocity versus λ Curve for the 1 λ to Min-Useable λ Data at Array 3G; Stage 1 at VEGP Site

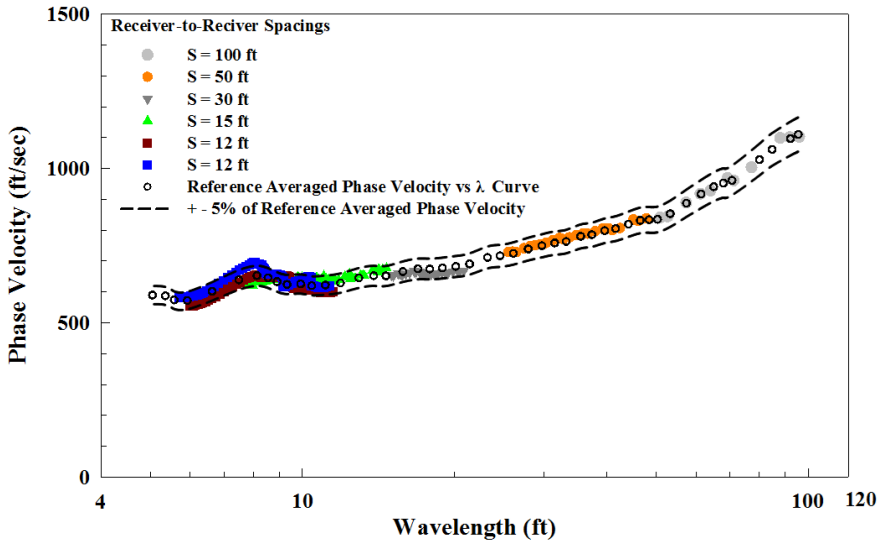

Figure A.22 Comparison of the Reference Averaged Phase Velocity versus λ Curve (Case C-R) and Field C-1 Dispersion Curve at Array 3G; Stage 1 at VEGP Site

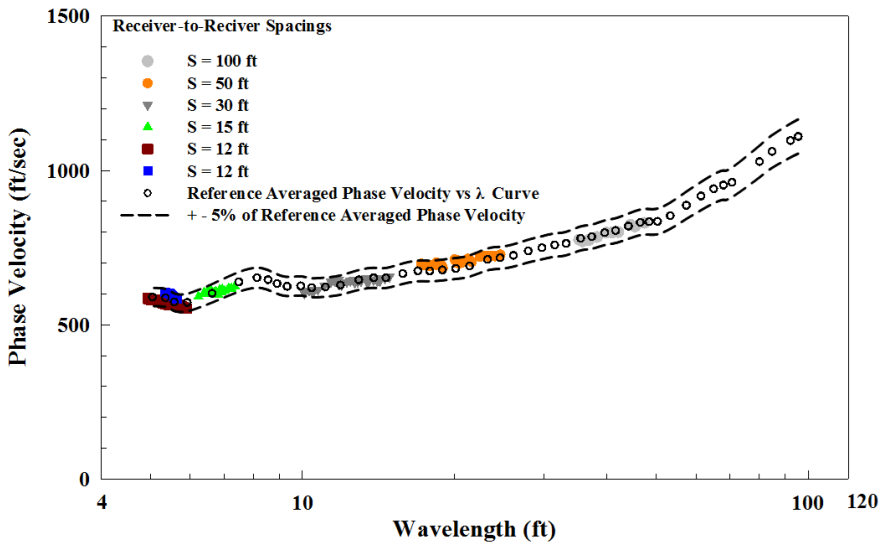

Figure A.23 Comparison of the Reference Averaged Phase Velocity versus λ Curve (Case C-R) and Field C-2 Dispersion Curve at Array 3G; Stage 1 at VEGP Site

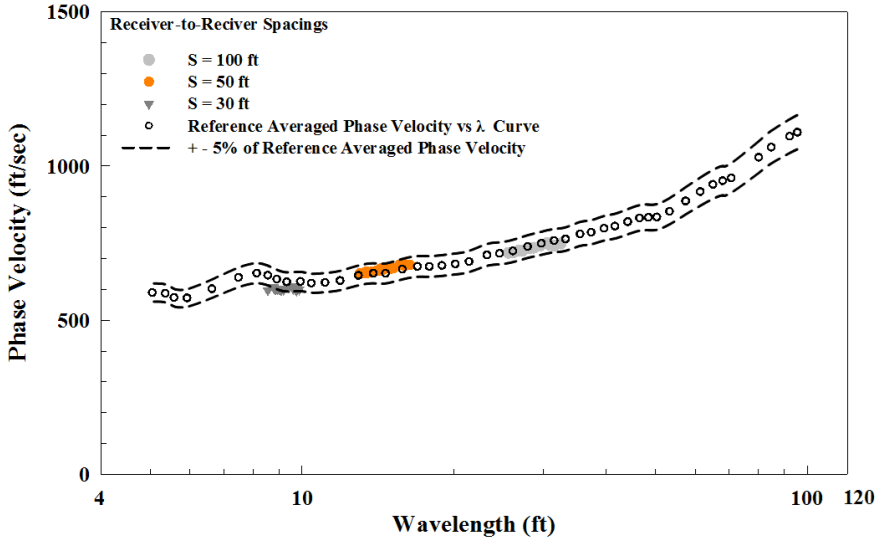

Figure A.24 Comparison of the Reference Averaged Phase Velocity versus λ Curve (Case C-R) and Field C-3 Dispersion Curve at Array 3G; Stage 1 at VEGP Site

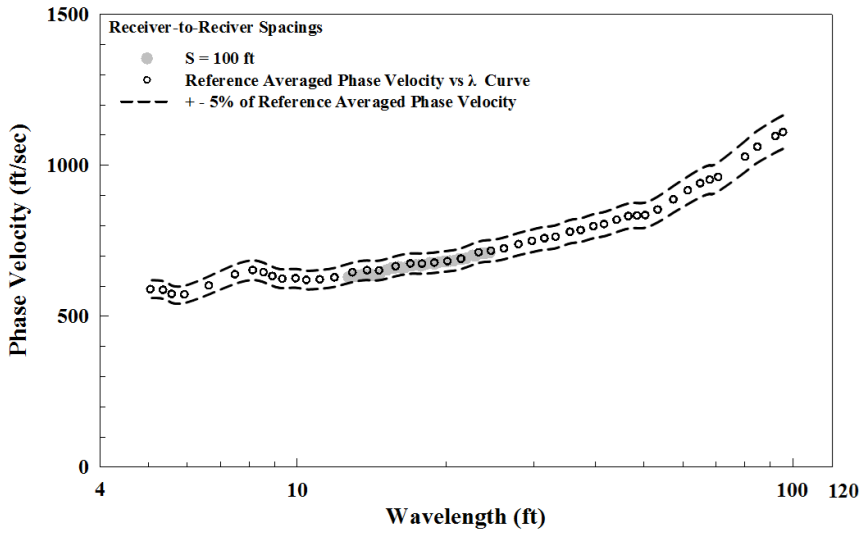

Figure A.25 Comparison of the Reference Averaged Phase Velocity versus λ Curve (Case C-R) and Field C-4 Dispersion Curve at Array 3G; Stage 1 at VEGP Site

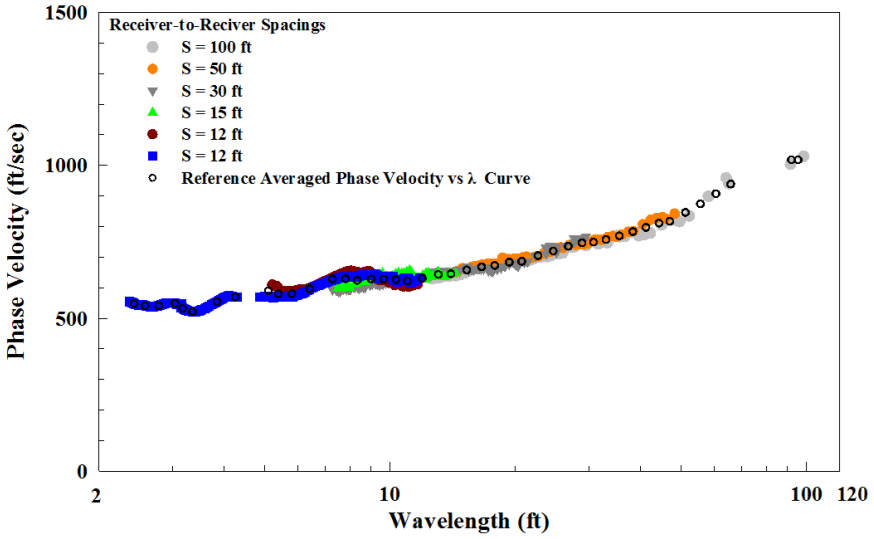

Figure A.26 All Field Dispersion Data Used to Create the C-R Field Dispersion Curve and Reference Averaged Phase Velocity versus λ Curve for the 1 λ to Min-Useable λ Data at Array 3I; Stage 1 at VEGP Site

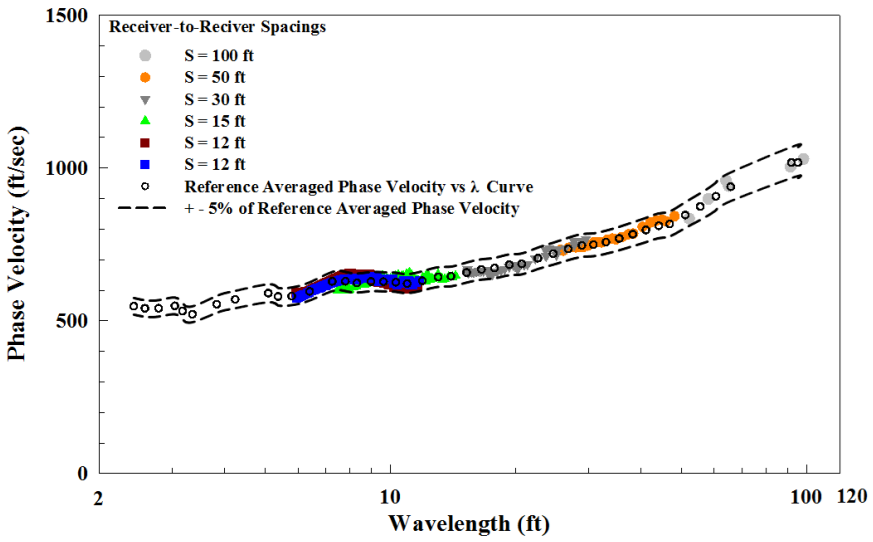

Figure A.27 Comparison of the Reference Averaged Phase Velocity versus λ Curve (Case C-R) and Field C-1 Dispersion Curve at Array 3I; Stage 1 at VEGP Site

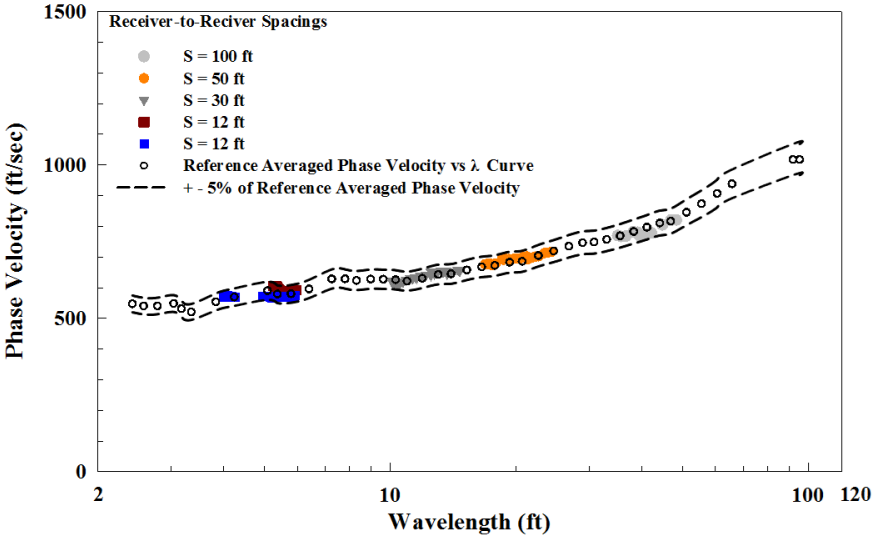

Figure A.28 Comparison of the Reference Averaged Phase Velocity versus λ Curve (Case C-R) and Field C-2 Dispersion Curve at Array 3I; Stage 1 at VEGP Site

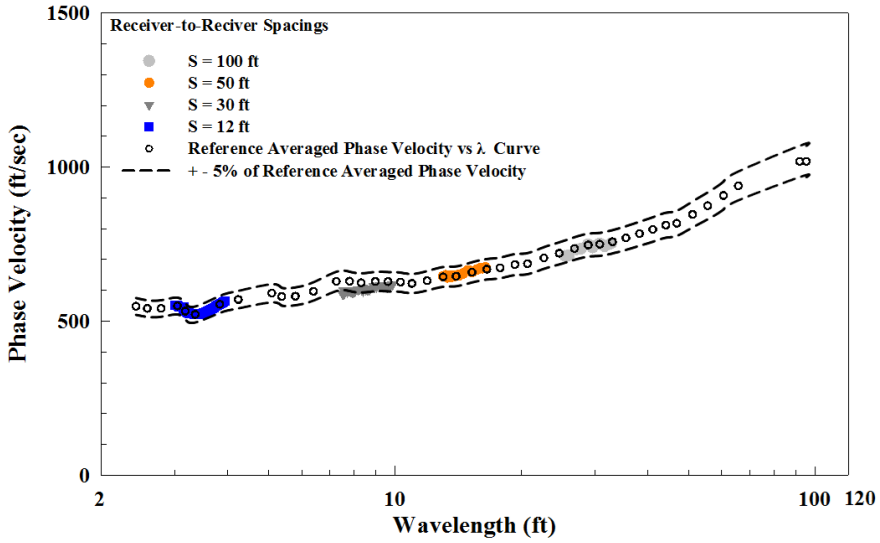

Figure A.29 Comparison of the Reference Averaged Phase Velocity versus λ Curve (Case C-R) and Field C-3 Dispersion Curve at Array 3I; Stage 1 at VEGP Site

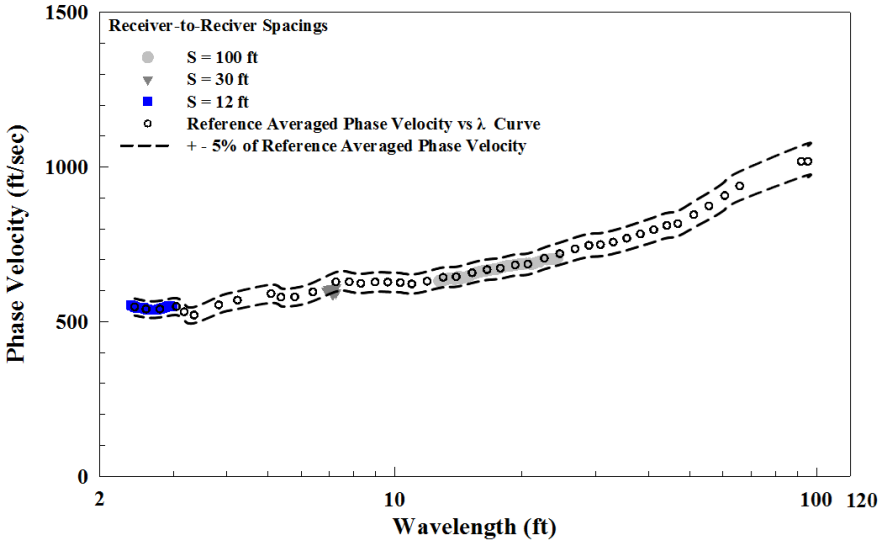

Figure A.30 Comparison of the Reference Averaged Phase Velocity versus λ Curve (Case C-R) and Field C-4 Dispersion Curve at Array 3I; Stage 1 at VEGP Site

Appendix B

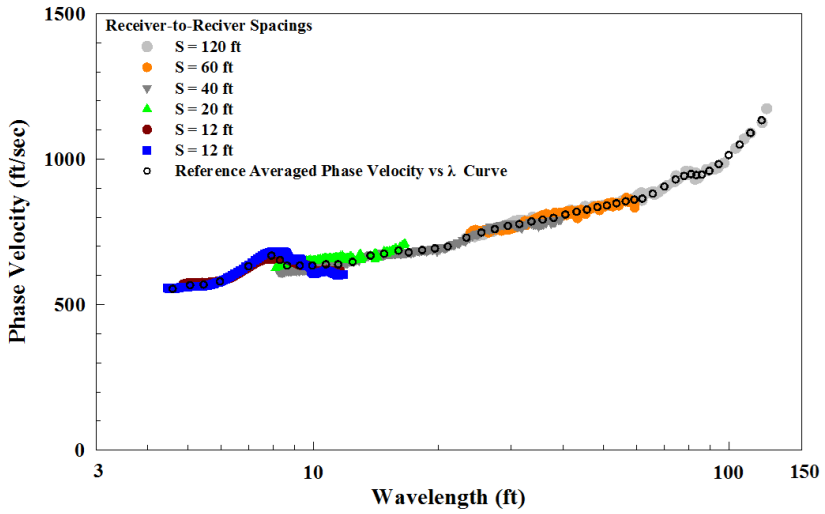

Figure B.1 All Field Dispersion Data Used to Create the C-R Field Dispersion Curve and Reference Averaged Phase Velocity versus λ Curve for the 1 λ to Min-Useable λ Data at Array 3A; Stage 2 at VEGP Site

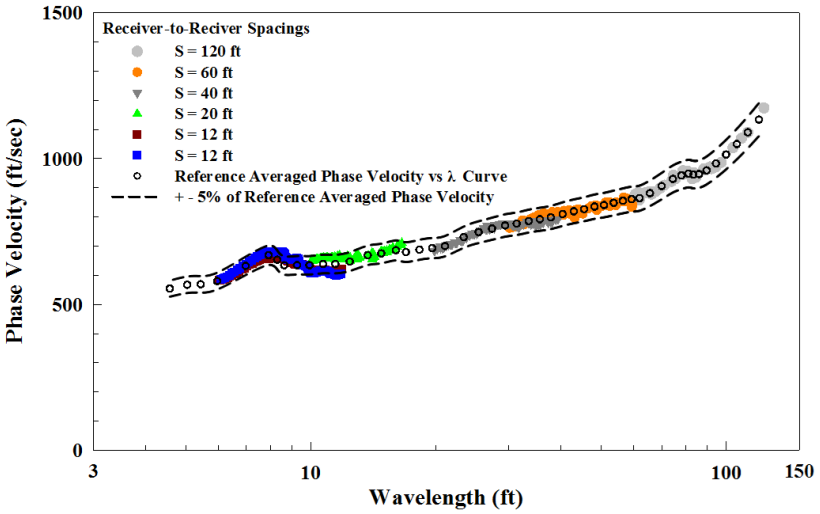

Figure B.2 Comparison of the Reference Averaged Phase Velocity versus λ Curve (Case C-R) and Field C-1 Dispersion Curve at Array 3A; Stage 2 at VEGP Site

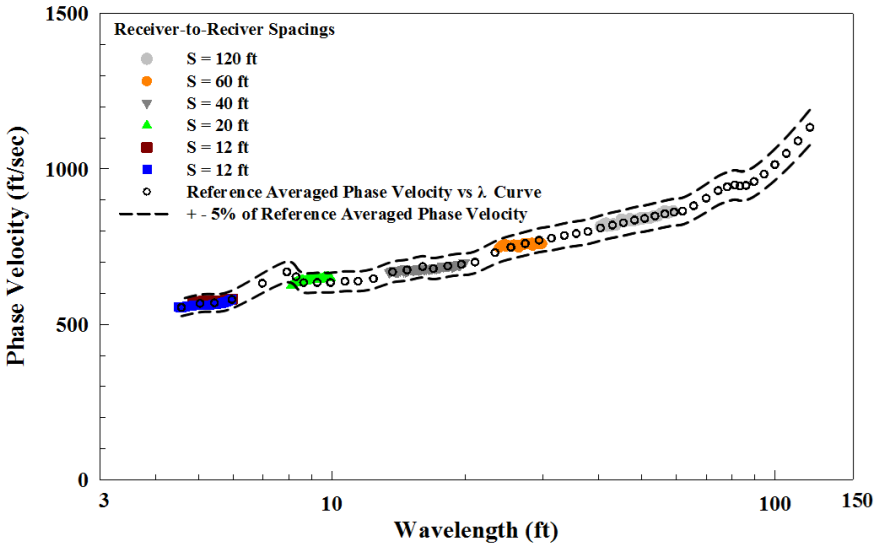

Figure B.3 Comparison of the Reference Averaged Phase Velocity versus λ Curve (Case C-R) and Field C-2 Dispersion Curve at Array 3A; Stage 2 at VEGP Site

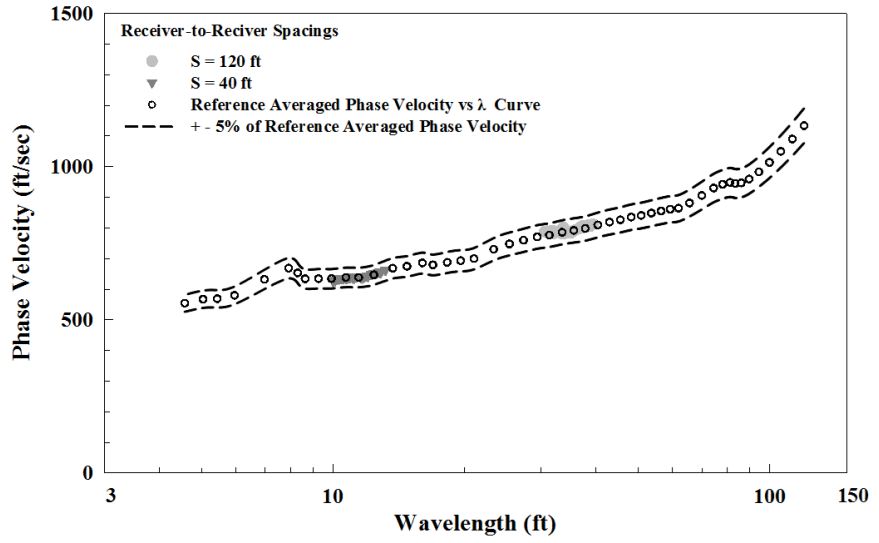

Figure B.4 Comparison of the Reference Averaged Phase Velocity versus λ Curve (Case C-R) and Field C-3 Dispersion Curve at Array 3A; Stage 2 at VEGP Site

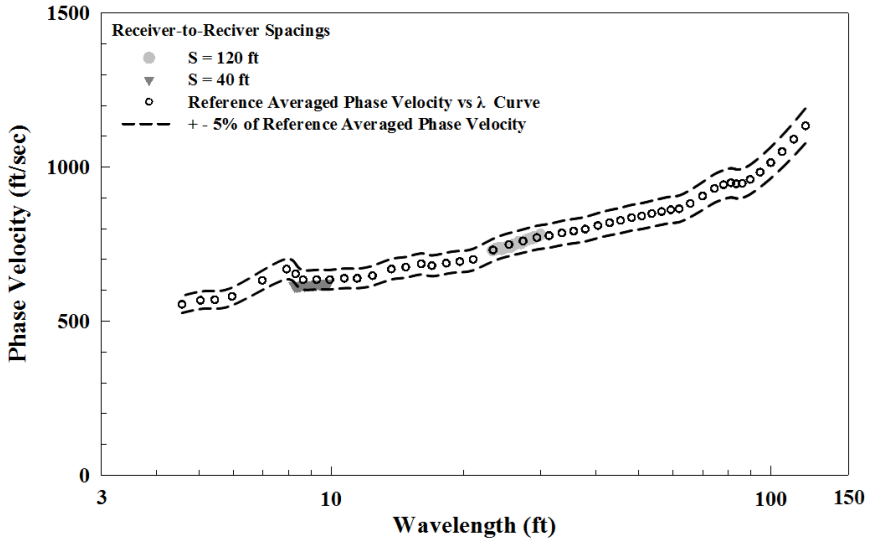

Figure B.5 Comparison of the Reference Averaged Phase Velocity versus λ Curve (Case C-R) and Field C-4 Dispersion Curve at Array 3A; Stage 2 at VEGP Site

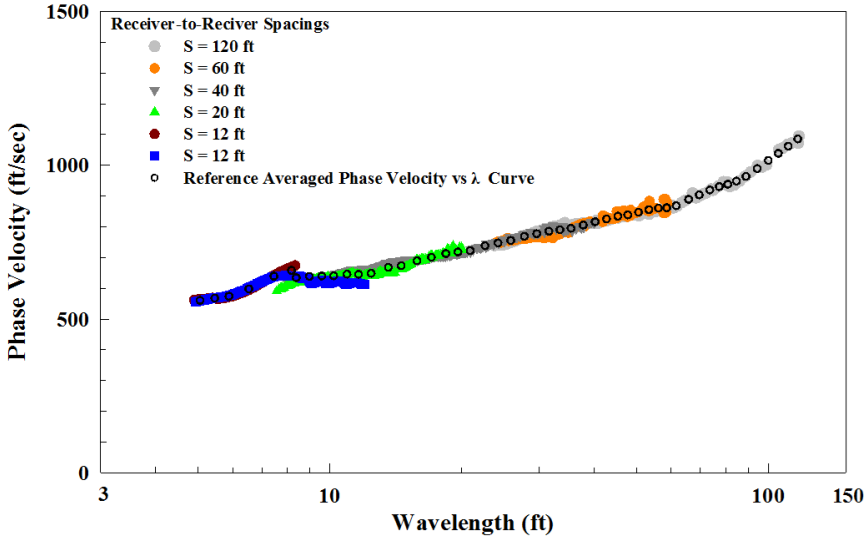

Figure B.6 All Field Dispersion Data Used to Create the C-R Field Dispersion Curve and Reference Averaged Phase Velocity versus λ Curve for the 1 λ to Min-Useable λ Data at Array 3B; Stage 2 at VEGP Site

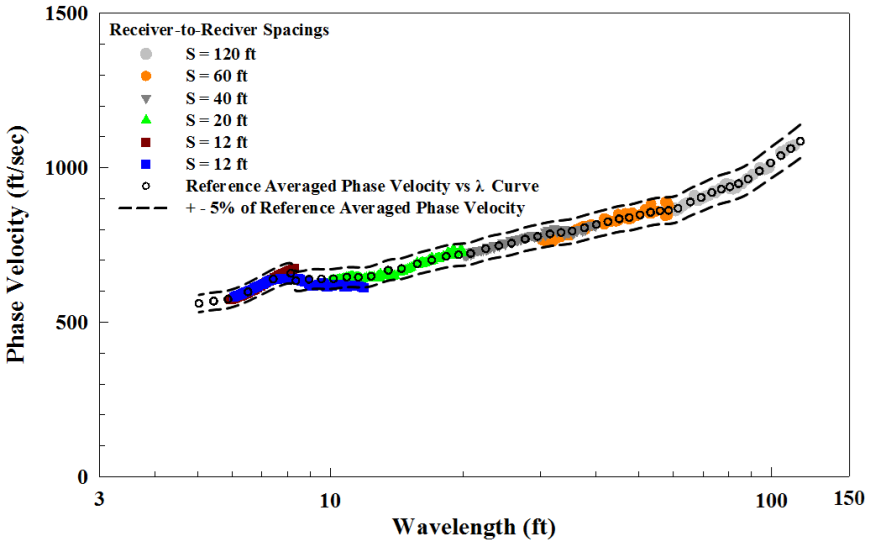

Figure B.7 Comparison of the Reference Averaged Phase Velocity versus λ Curve (Case C-R) and Field C-1 Dispersion Curve at Array 3B; Stage 2 at VEGP Site

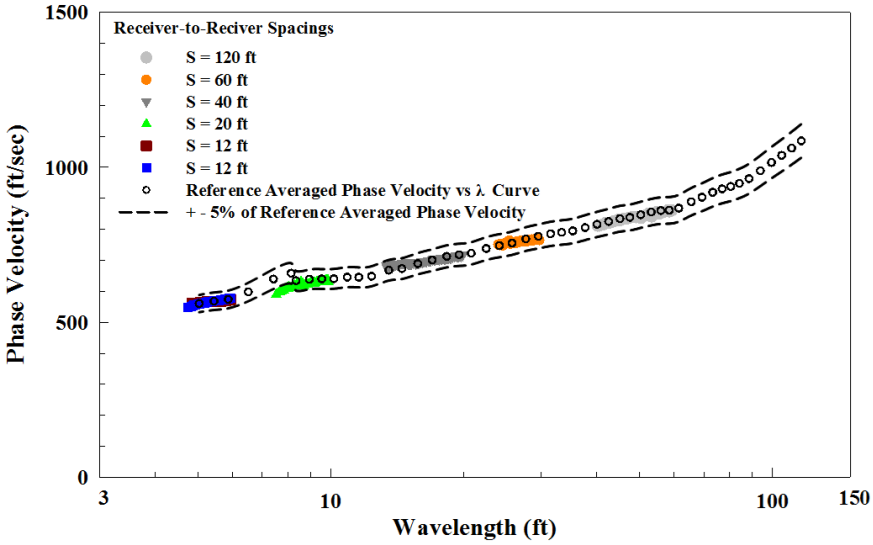

Figure B.8 Comparison of the Reference Averaged Phase Velocity versus λ Curve (Case C-R) and Field C-2 Dispersion Curve at Array 3B; Stage 2 at VEGP Site

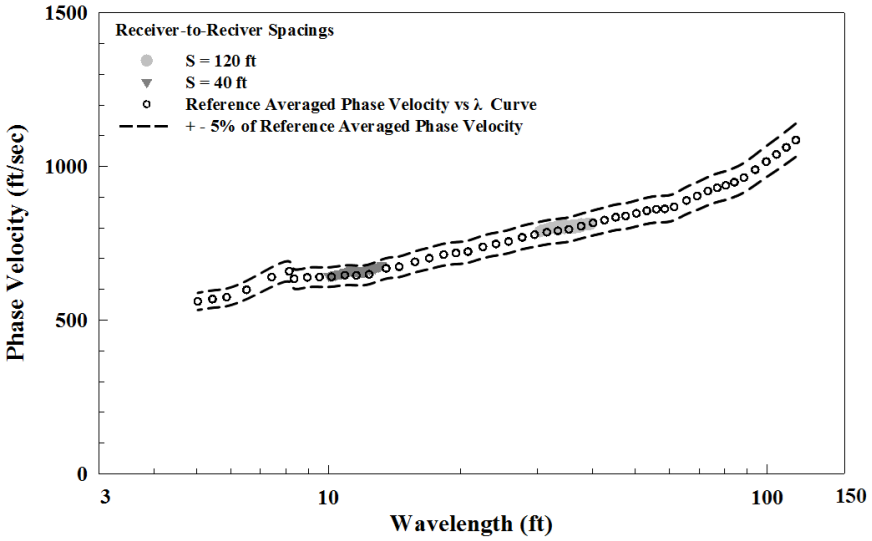

Figure B.9 Comparison of the Reference Averaged Phase Velocity versus λ Curve (Case C-R) and Field C-3 Dispersion Curve at Array 3B; Stage 2 at VEGP Site

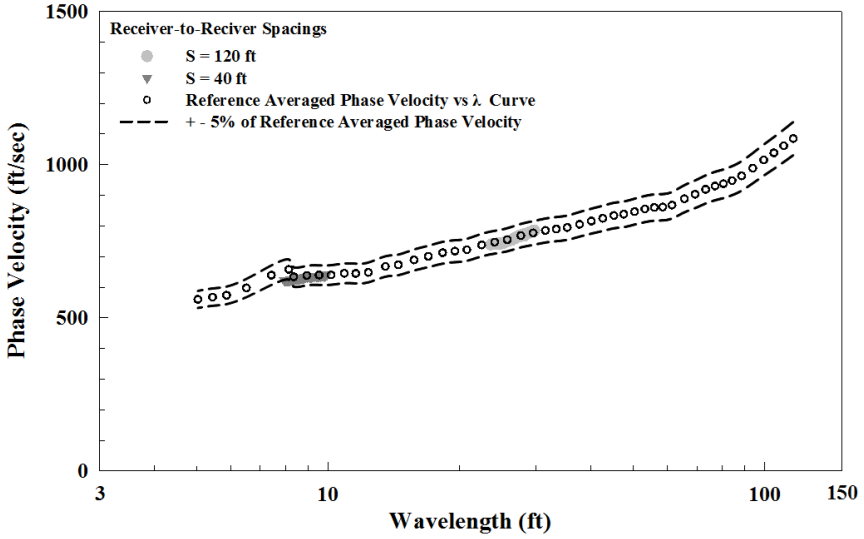

Figure B.10 Comparison of the Reference Averaged Phase Velocity versus λ Curve (Case C-R) and Field C-4 Dispersion Curve at Array 3B; Stage 2 at VEGP Site

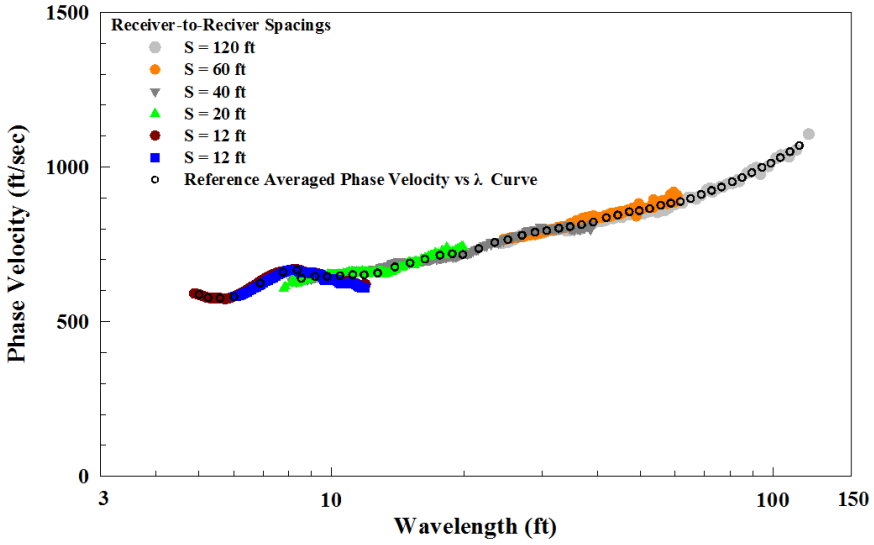

Figure B.11 All Field Dispersion Data Used to Create the C-R Field Dispersion Curve and Reference Averaged Phase Velocity versus λ Curve for the 1 λ to Min-Useable λ Data at Array 3C; Stage 2 at VEGP Site

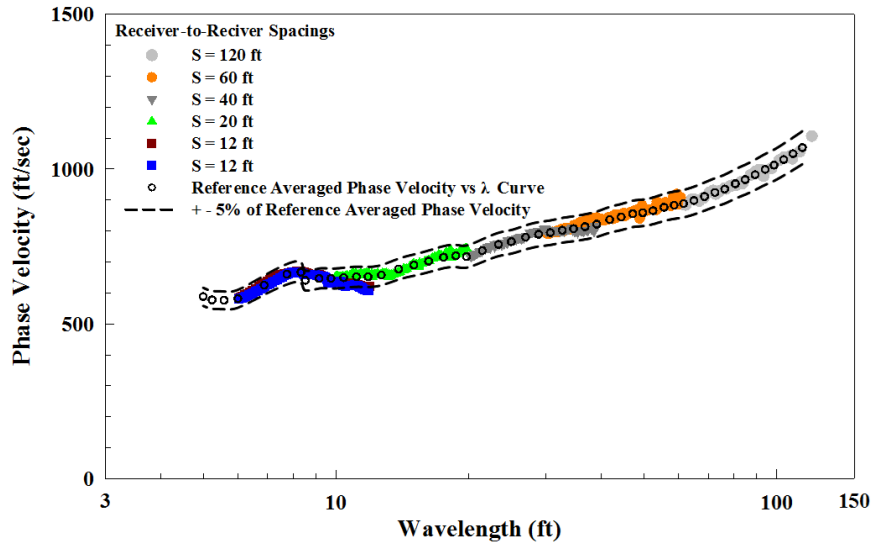

Figure B.12 Comparison of the Reference Averaged Phase Velocity versus λ Curve (Case C-R) and Field C-1 Dispersion Curve at Array 3C; Stage 2 at VEGP Site

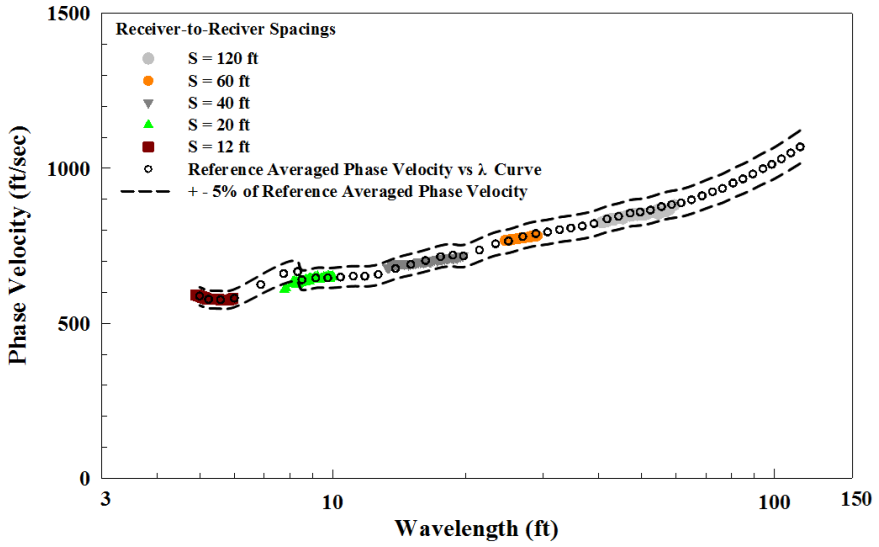

Figure B.13 Comparison of the Reference Averaged Phase Velocity versus λ Curve (Case C-R) and Field C-2 Dispersion Curve at Array 3C; Stage 2 at VEGP Site

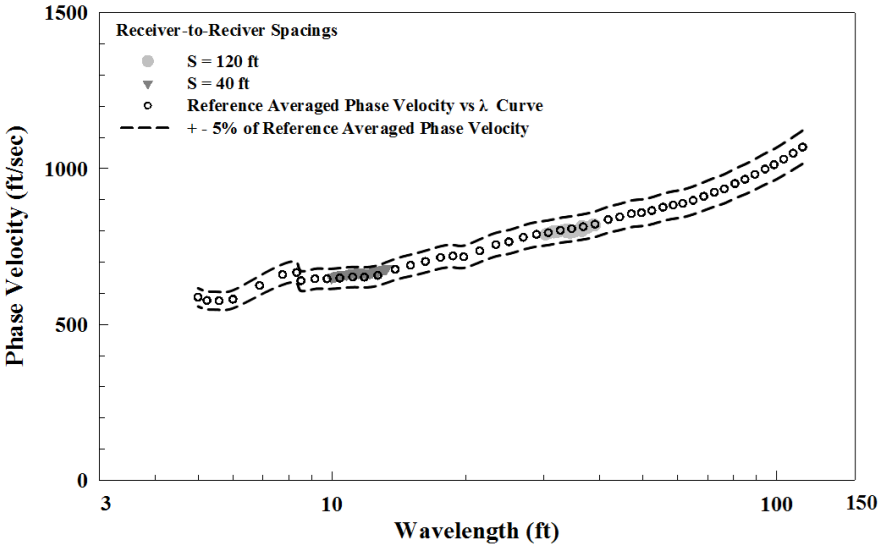

Figure B.14 Comparison of the Reference Averaged Phase Velocity versus λ Curve (Case C-R) and Field C-3 Dispersion Curve at Array 3C; Stage 2 at VEGP Site

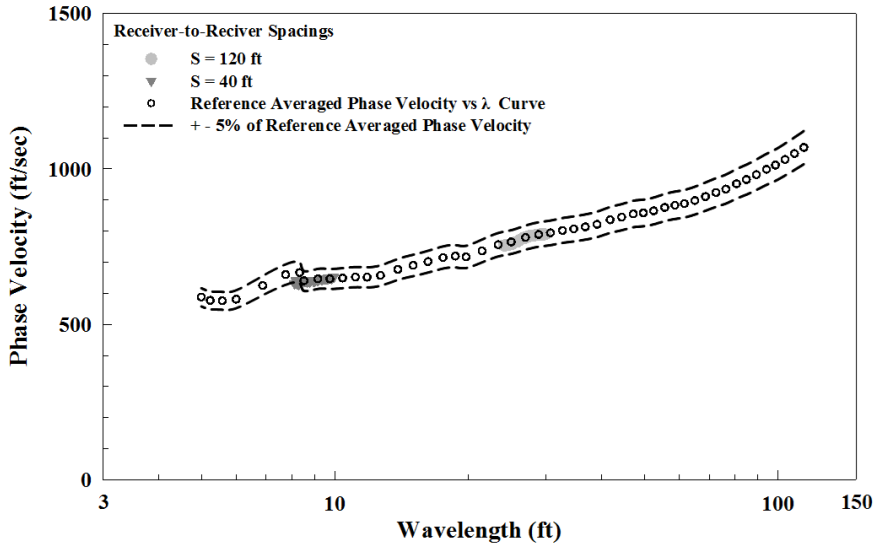

Figure B.15 Comparison of the Reference Averaged Phase Velocity versus λ Curve (Case C-R) and Field C-4 Dispersion Curve at Array 3C; Stage 2 at VEGP Site

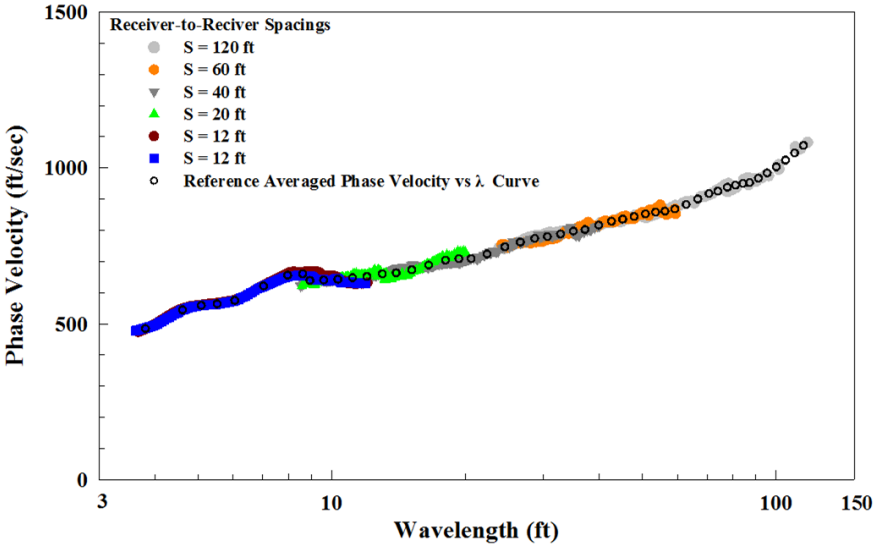

Figure B.16 All Field Dispersion Data Used to Create the C-R Field Dispersion Curve and Reference Averaged Phase Velocity versus λ Curve for the 1 λ to Min-Useable λ Data at Array 3F; Stage 2 at VEGP Site

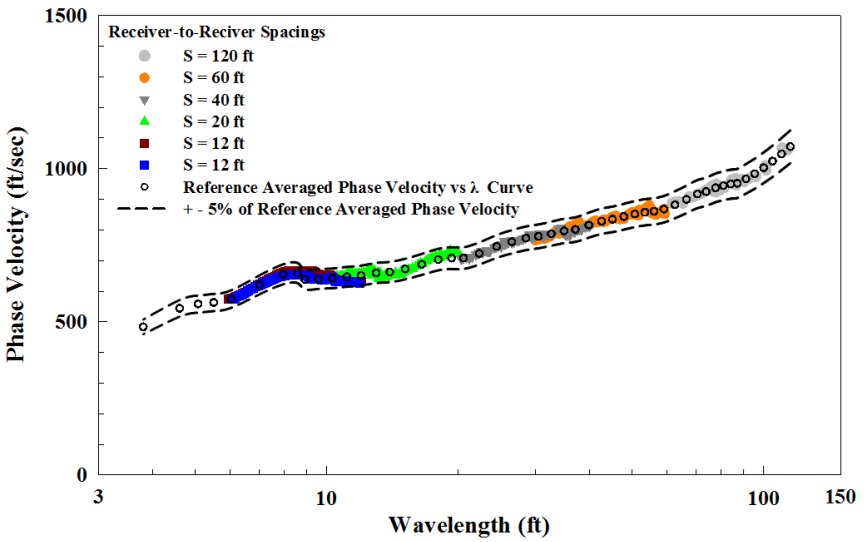

Figure B.17 Comparison of the Reference Averaged Phase Velocity versus λ Curve (Case C-R) and Field C-1 Dispersion Curve at Array 3F; Stage 2 at VEGP Site

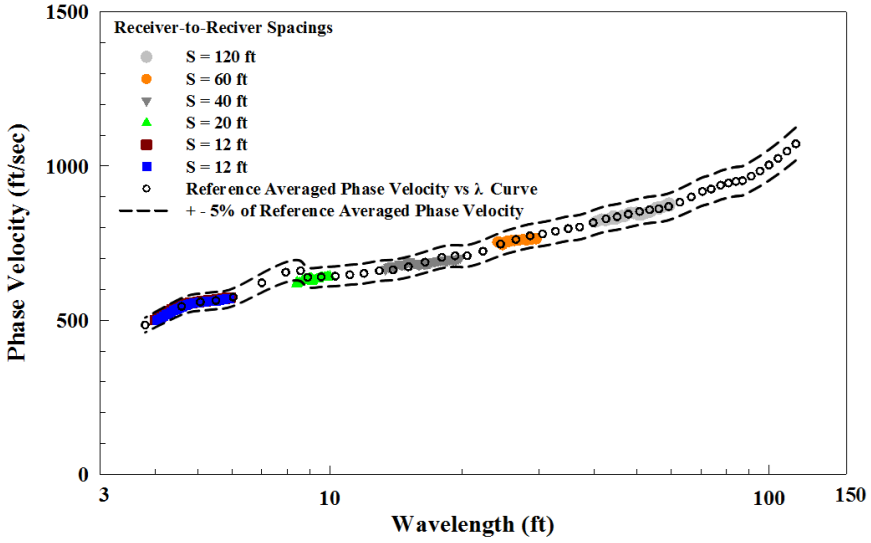

Figure B.18 Comparison of the Reference Averaged Phase Velocity versus λ Curve (Case C-R) and Field C-2 Dispersion Curve at Array 3F; Stage 2 at VEGP Site

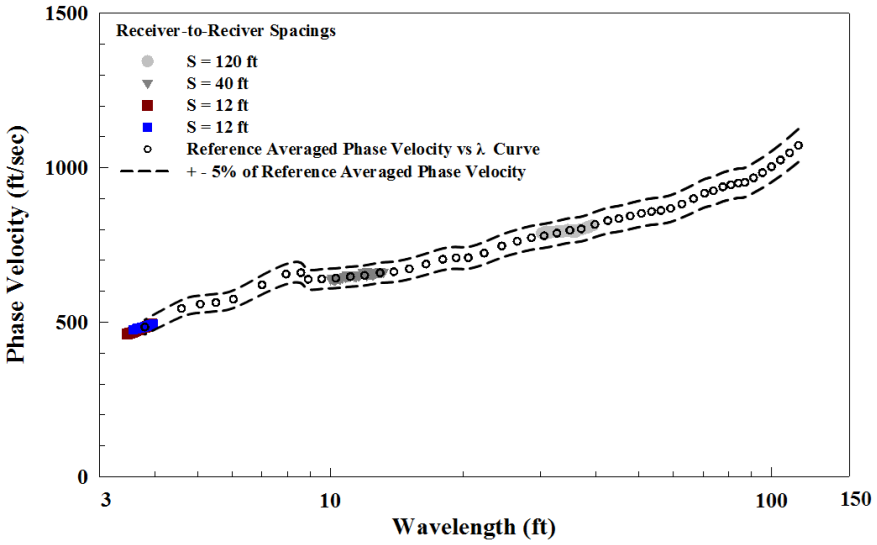

Figure B.19 Comparison of the Reference Averaged Phase Velocity versus λ Curve (Case C-R) and Field C-3 Dispersion Curve at Array 3F; Stage 2 at VEGP Site

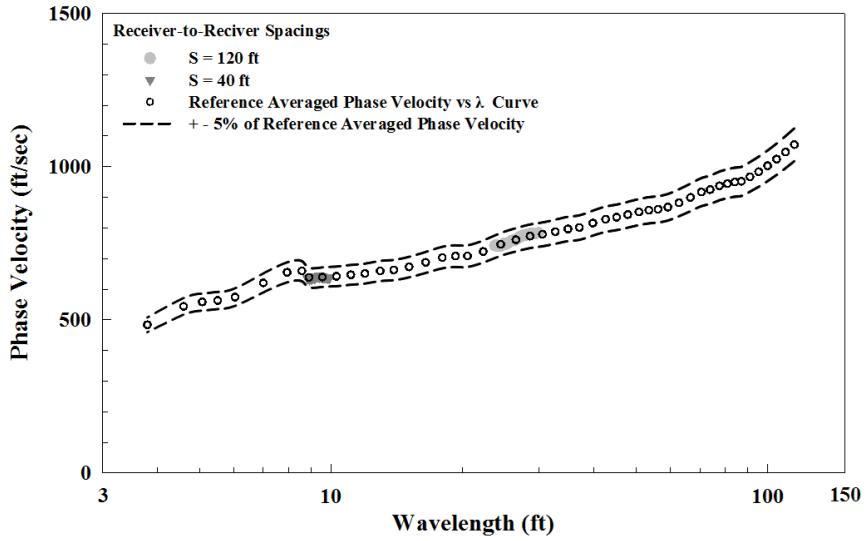

Figure B.20 Comparison of the Reference Averaged Phase Velocity versus λ Curve (Case C-R) and Field C-4 Dispersion Curve at Array 3F; Stage 2 at VEGP Site

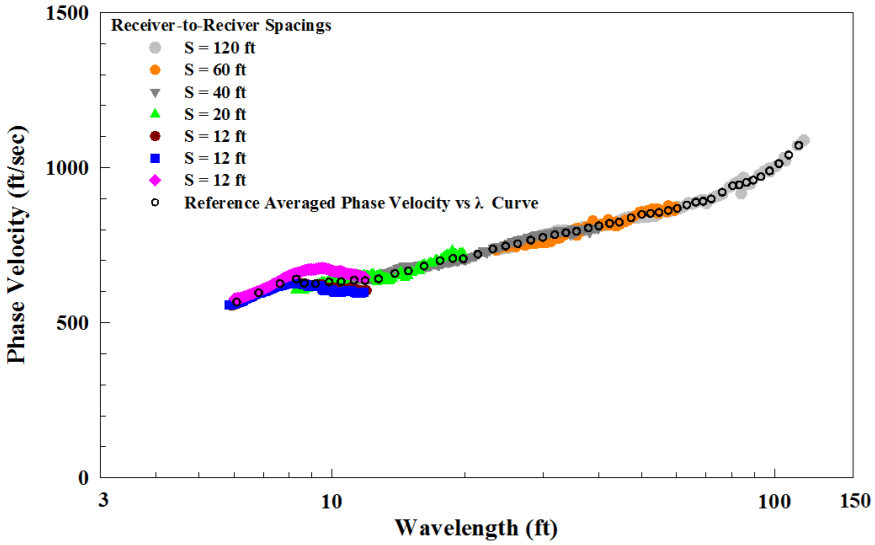

Figure B.21 All Field Dispersion Data Used to Create the C-R Field Dispersion Curve and Reference Averaged Phase Velocity versus λ Curve for the 1 λ to Min-Useable λ Data at Array 3G; Stage 2 at VEGP Site

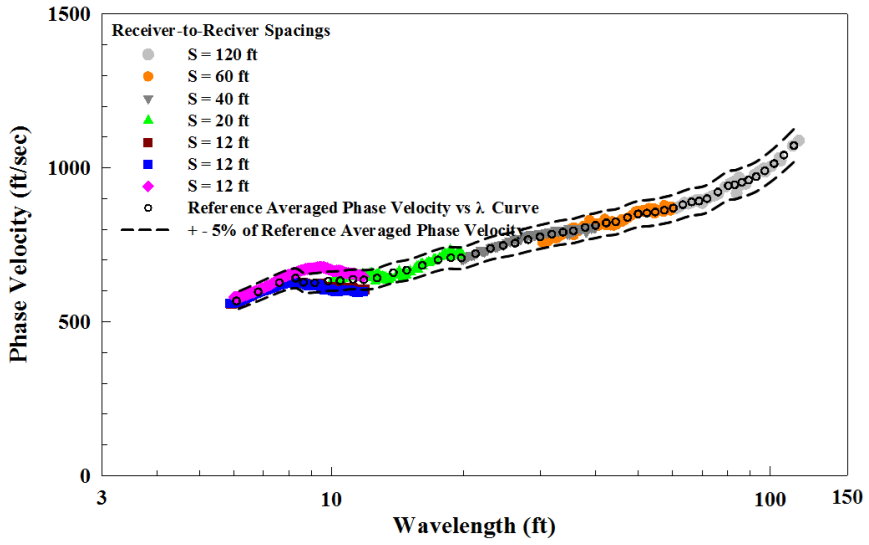

Figure B.22 Comparison of the Reference Averaged Phase Velocity versus λ Curve (Case C-R) and Field C-1 Dispersion Curve at Array 3G; Stage 2 at VEGP Site

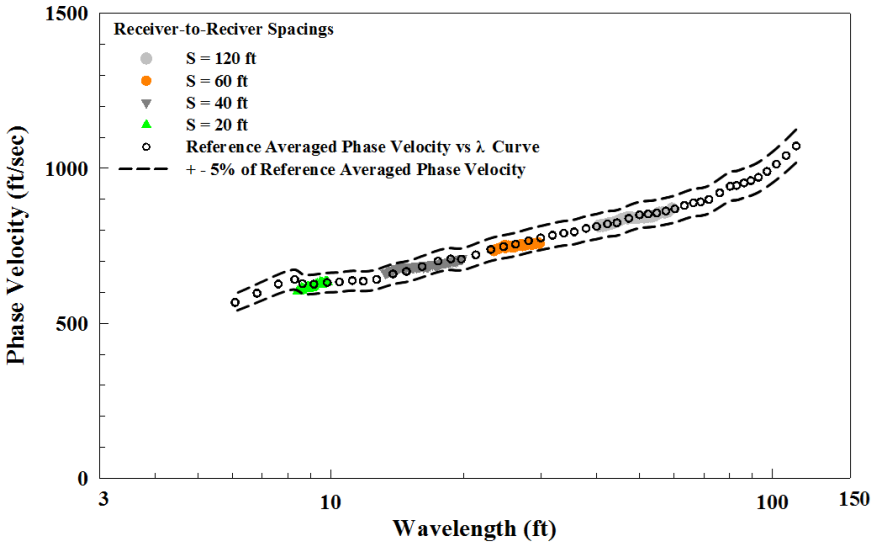

Figure B.23 Comparison of the Reference Averaged Phase Velocity versus λ Curve (Case C-R) and Field C-2 Dispersion Curve at Array 3G; Stage 2 at VEGP Site

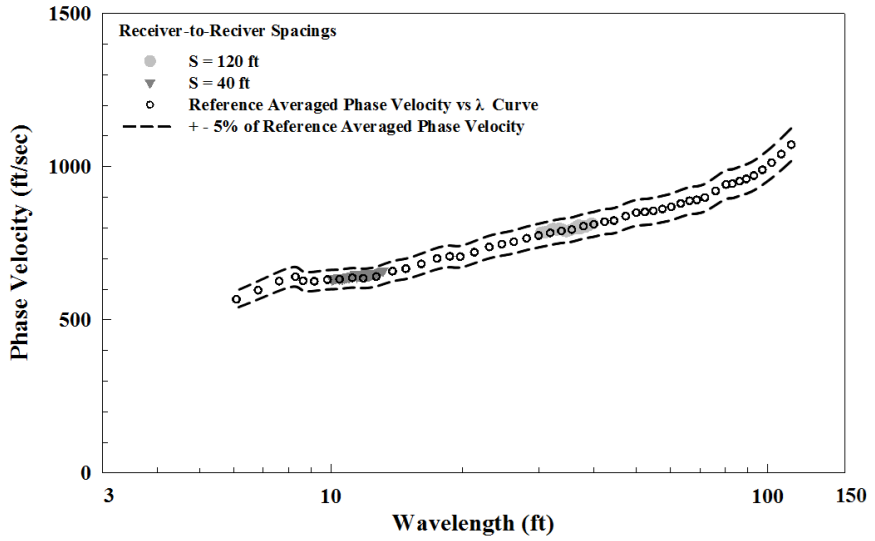

Figure B.24 Comparison of the Reference Averaged Phase Velocity versus λ Curve (Case C-R) and Field C-3 Dispersion Curve at Array 3G; Stage 2 at VEGP Site

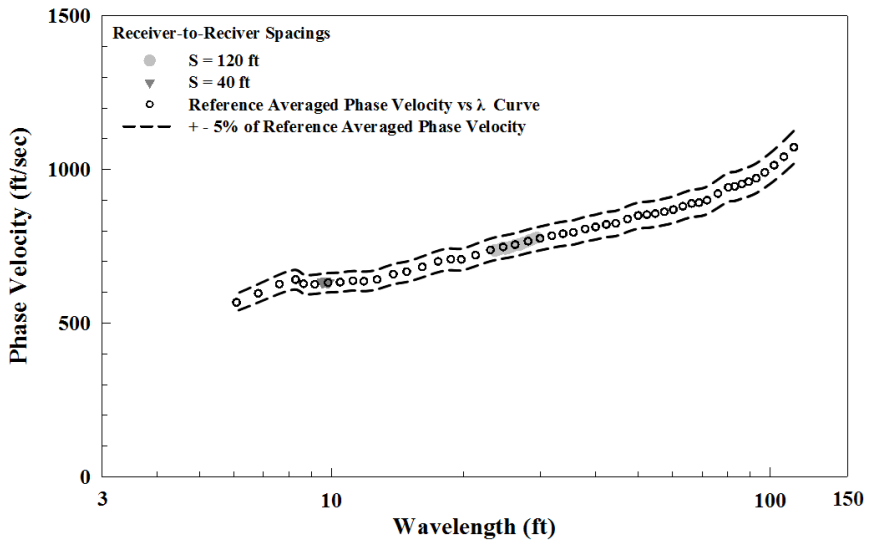

Figure B.25 Comparison of the Reference Averaged Phase Velocity versus λ Curve (Case C-R) and Field C-4 Dispersion Curve at Array 3G; Stage 2 at VEGP Site

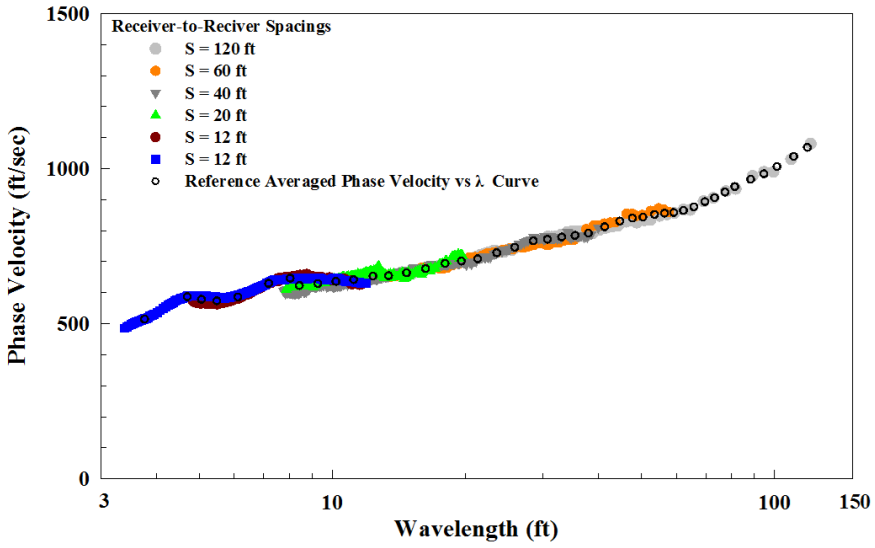

Figure B.26 All Field Dispersion Data Used to Create the C-R Field Dispersion Curve and Reference Averaged Phase Velocity versus λ Curve for the 1 λ to Min-Useable λ Data at Array 3H; Stage 2 at VEGP Site

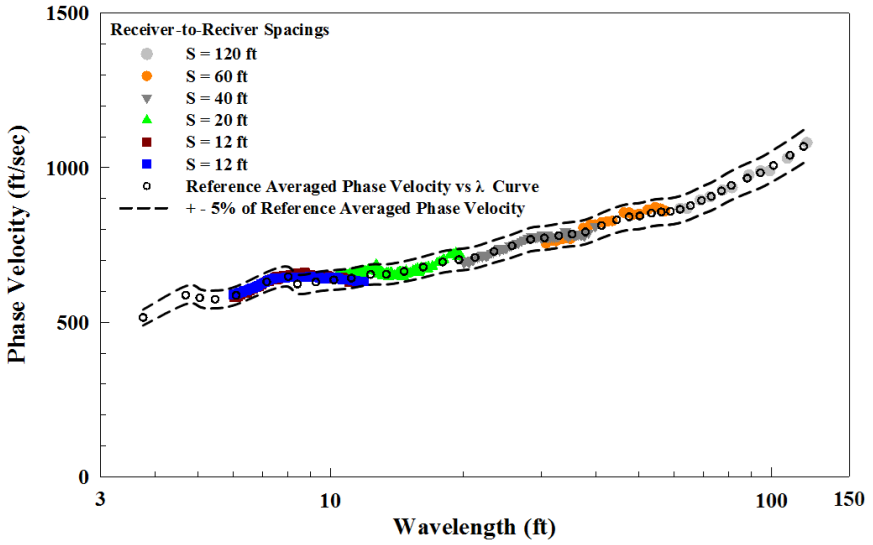

Figure B.27 Comparison of the Reference Averaged Phase Velocity versus λ Curve (Case C-R) and Field C-1 Dispersion Curve at Array 3H; Stage 2 at VEGP Site

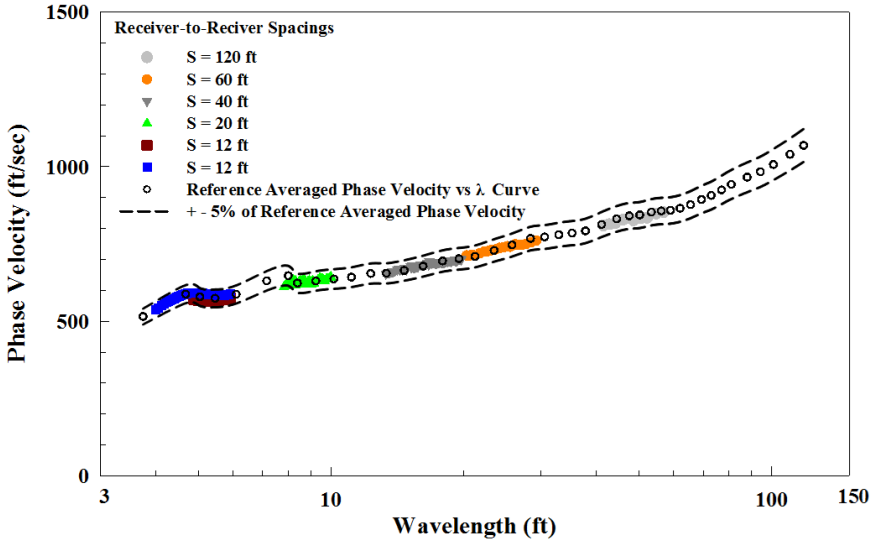

Figure B.28 Comparison of the Reference Averaged Phase Velocity versus λ Curve (Case C-R) and Field C-2 Dispersion Curve at Array 3H; Stage 2 at VEGP Site

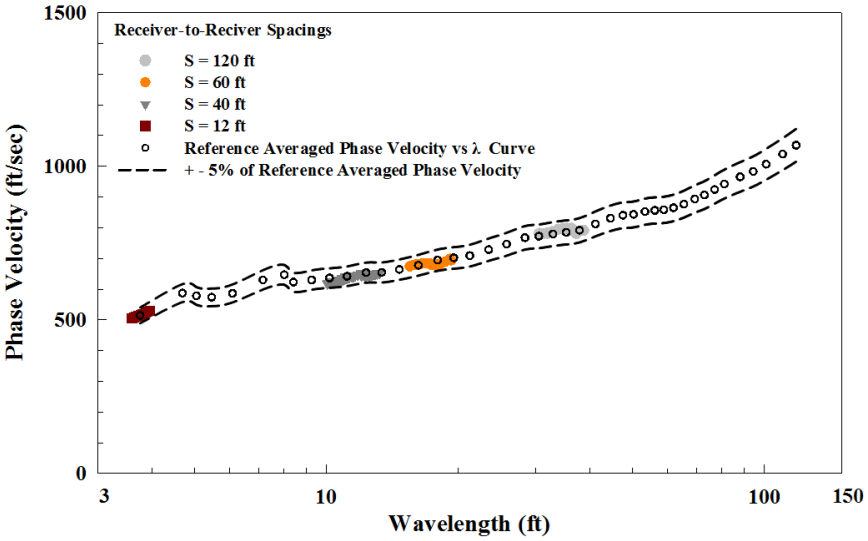

Figure B.29 Comparison of the Reference Averaged Phase Velocity versus λ Curve (Case C-R) and Field C-3 Dispersion Curve at Array 3H; Stage 2 at VEGP Site

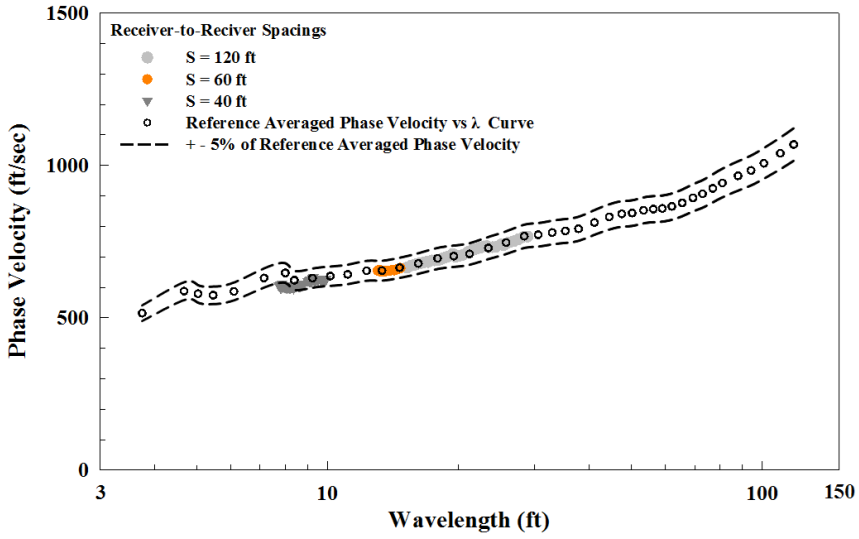

Figure B.30 Comparison of the Reference Averaged Phase Velocity versus λ Curve (Case C-R) and Field C-4 Dispersion Curve at Array 3H; Stage 2 at VEGP Site

References

Aki, K., and Richards, P.G. (1980), *Quantitative Seismology-Theory and Methods*, Vols. I and II, Freeman Company, San Francisco.

Al-Hunaidi, M.O. (1993), "Insights on the SASW Nondestructive Testing Method," *Canadian Geotechnical Journal*, 20, pp. 940-950.

Foinquinos, M.R. (1991), "Analytical Study of Inversion for the Spectral Analysis of Surface Waves Method," *Master's Thesis*, The University of Texas at Austin.

Gucunski, N., and Woods, R. D. (1992), "Numerical Simulation of the SASW Test," *Soil Dynamic and Earthquake Engineering*, 11, pp. 213-277.

Heisey, J. S., Stokoe, K.H., II, Hudson, W. R., and Meyer, A.H. (1982), "Determination of In-situ Shear Wave Velocities from Spectral Analysis of Surface Wave," *Research Report No. 256-2*, Center for Transportation Research, The University of Texas at Austin.

Hiltunen, D. T., and Woods, R. D. (1990), "Variables Affecting the Testing of Pavement by the Surface Wave Method," *Transportation Research Record 1260*, TRB, Washington, D.C., pp. 24-52.

Joh, S.H. (1996), "Advances in the Data Interpretation Technique for Spectral-Analysis-of-Surface-Waves (SASW) Measurements", *Ph.D. Dissertation*, The University of Texas at Austin

Roesset, J.M., Chang W., and Stokoe, K.H., II. (1991), "Comparison of 2D and 3D Models for Analysis of Surface Wave Tests," *Proceedings of the 5th International Conference on Soil Dynamics and Earthquake Engineering*, pp. 111-126.

Roesset, J.M., Chang W., Stokoe, K.H., II and Aouad, M. (1990), "Modulus and Thickness of the Pavement Surface Layer from SASW Tests," *Transportation Research Record 1260*, TRB, Washington, D.C., pp. 53-63.

Sanchez-Salinero, I., Roesset, J. M., Shao, K., Stokoe, K. H., II, and Rix, G.J. (1987), "Analytical Evaluation of Variable Affecting Surface Wave Testing of Pavements," *Transportation Research Record 1136*, TRB, Washington, D.C., pp. 86-95.

Stokoe, II, K.H., Lin, Y.C., Cox, B., Kurtulus, A., and Jung, M.J. (2005), "Shear Wave Profiling at the Waste Treatment Plant Site, Hanford, WA," Vols. I and II, *Geotechnical Engineering Report GR05-1*, The University of Texas at Austin.

Stokoe, II, K.H., Lin, Y.C., Yuan, J., and Jung, M.J. (2013), "Field Seismic Testing : Quantitative and Qualitative Evaluation of Soil and Rock," Presented in the International Conference on Earthquake Geotechnical Engineering, Istanbul, Turkey

Yoon, S., and Rix, G. J. (2009), "Near-Field Effects on Array-Based Surface Wave Methods with Active Sources," *Journal of Geotechnical and Geoenvironmental Engineering*, 135, pp.399-406

Zywicki, D. J. (1999), "Advanced Signal Processing Methods Applied to Engineering Analysis of Seismic Surface Waves," *Ph.D. Dissertation*, Georgia Institute of Technology